Optogenetično praćenje električne aktivnosti neurona primjenom fluorescentnih voltažnih senzora

Trepotec, Željka

Sveučilište u Zagrebu
Prirodoslovno – matematički fakultet
Biološki odsjek

Željka Trepotec

Optogenetic monitoring of neuronal electrical activity using fluorescent protein – based voltage sensors

Master thesis

conducted at the Institute of Complex Systems (ICS-8), Forschungszentrum Jülich

Zagreb, 2015.

Ovaj rad je izrađen u Forschungszentrum Jülich, Njemačka, u laboratoriju na Institutu kompleksnih sustava - bioelektronika, pod vodstvom dr.sc. Vanesse Maybeck. Rad je predan na ocjenu Biološkom odsjeku Prirodoslovno-matematičkog fakulteta Sveučilišta u Zagrebu radi stjecanja zvanja magistar molekularne biologije.

TEMELJNA DOKUMENTACIJSKA KARTICA

Sveučilište u Zagrebu
Prirodoslovno – matematički fakultet
Biološki odsjek Diplomski rad

OPTOGENETIČKO PRAćENJE ELEKTRIČNE AKTIVNOSTI NEURONA PRIMJENOM FLUORESCENTNIH VOLTAŽNIH SENZORA

Željka Trepotec

Rooseveltov trg 6, 10000 Zagreb, Hrvatska

Unatoč dosadašnjim postignućima u neuroznanosti, pitanja koja motiviraju znanstvenike o procesiranju informacija u neuronima još uvijek ostaju nerazjašnjena. Iako je proučavanje pojedinačnih neurona olakšano *in vitro* istraživanjima, ono iziskuje upotrebu neinvazivnih metoda visoke prostorne i vremenske rezolucije. Takva istraživanja omogućena su uvođenjem optogenetike kao novi eksperimentalni alat u neurofiziologiji. U ovom radu opisana je primjena genetički kodiranih fluorescentnih voltažnih senzora kao neinvazivno optogenetičko oruđe za bilježenje elektrofizioloških signala u podražljivim stanicama. U neurone korteksa uneseni su rekombinantni plazmidi hSyn_ArcLight i hSyn_Butterfly transdukcijom adeno – asociranim virusnim vektorima. Nakon ekspresije u neuronima, proteini su evaluirani elektrofiziološkim eksperimentima; električnom stimulacijom uz optičko bilježenje promjene fluorescencije. Time je dokazano da je ArcLight-A242 pogodno oruđe za bilježenje i detekciju pojedinačnih akcijskih potencijala. Iako bez značaja prema ovom istraživanju (zbog ograničenosti uređaja), Butterfly bi trebao biti još pouzdanije oruđe za detekciju, pa čak i promjena u potencijalu ispod praga okidanja. Uz ove rezultate, pretpostavka je da je optogenetika, obogaćena za ove dvije komponente, korak bliže neinvazivnom bilježenju električne aktivnosti neurona.

(94 stranice, 39 slika, 7 tablica, 78 literaturnih navoda, jezik izvornika: engleski)

Rad je pohranjen u Središnjoj biološkoj knjižnici.

Ključne riječi: akcijski potencijal, elektrofiziologija, AAV transdukcija, molekularno kloniranje, patch-clamp, fluorimetrija

Voditelji: doc.dr.sc. Ivana Ivančić – Baće i dr.sc. Vanessa Maybeck
Ocjenitelji: doc.dr.sc. Ivana Ivančić – Baće, izv.prof.dr.sc. Dijana Škorić, doc.dr.sc. Duje Lisičić

Rad prihvaćen: 05/02/2015

BASIC DOCUMENTATION CARD

University of Zagreb
Faculty of Science
Department of Biology

Master Thesis

OPTOGENETIC MONITORING OF NEUONAL ELECTRICAL ACTIVITY USING PROTEIN – BASED VOLTAGE SENSORS

Željka Trepotec

Rooseveltov trg 6, 10000 Zagreb, Croatia

Despite all the recent achievements in the neuroscience, the questions that have motivated scientists about the information processing in individual neurons still remain unanswered. Studying neuronal behaviour *in vitro* facilitates the availability of a single neuron investigation, but requires non-invasiveness with high spatial and temporal resolution. Expansion of the neurophysiologic recording toolbox with the optogenetic stimulation has enabled such recordings. The included work shows the usage of genetically encoded voltage-sensitive fluorescent proteins as a non-invasive optogenetic tool for recording electrophysiological signals in electrogenic cells. The cortical neurons have been transduced with the new constructs, hSyn_ArcLight and hSyn_Butterfly by recombinant adeno-associated viral vectors. These novel constructs, specifically expressed in the neuronal cells, have been evaluated by electrophysiological experiments with electrical stimulations recorded optically. It has been shown that ArcLight A-242 is a valuable tool for recording and detection of single action potentials. Although not successful so far (due to the available equipment), Butterfly should be an even more reliable tool for the detection of even sub-threshold potential changes. Going forward, it might be assumed that the optogenetic toolbox, enriched by those two components, is a step closer to non-invasive, optical monitoring of neural electrical activity.

(94 pages, 39 figures, 7 tables, 78 references, original in: English)

Thesis deposited in the Central Biological Library.

Keywords: action potentials, electrophysiology, AAV transduction, molecular cloning, patch-clamp, Fluorometry

Supervisors: Dr. Ivana Ivančić – Baće, Asst. Prof. and Dr. Vanessa Maybeck
Reviewers: Dr.sc. Ivana Ivančić – Baće, Asst. Prof.; Dr.sc. Dijana Škorić, Assoc. Prof.; Dr.sc. Duje Lisičić, Asst. Prof.

Thesis accepted: 05/02/2015.

Contents

Abbreviations

A	Alanine
Å	Angstrom
AAV	Adeno-Associated Viral Vectors
aqGFP	*Aequorea victoria* Green Fluorescent protein
a.u.	arbitrary units
C	Cytosine
C	Capacitance
c_{in}	Intracellular concentration of ions
Ci-VSP	*Ciona intestinalis* voltage sensor protein
HCMV	Human cytomegalovirus
C_{out}	Extracellular concentration of ions
CT	Computerised tomography
D	Aspartic acid
DMEM	Dulbecco's Minimal Essential Media
DPT	Days post-transfection / post-transduction
ds	double-stranded
E-18	Embryonic day 18
ECM	Extracellular matrix
EDTA	Ethylenediaminetetraacetic acid
EPSP	Excitatory PostSynaptic membrane Potential
FBS	Fetal Bovine Serum
FRET	Förster resonance energy transfer
FRET	*Förster resonance energy transfer*
G	Guanine
GBSS	Gey's Balanced Salt Solution
GEVI	Genetically encoded voltage indicators
GFP	Green fluorescent protein
GFP	Green Fluorescent Protein
HBSS	Hank's Balanced Salt Solution
HEK	Human Embryonic Kidney
HEPES	4-(2-hydroxyethyl)-1-piperazineethanesulfonic acid
hSyn1	human Synapsin
ITR	Inverted Terminal Repeat
k	x1000
kb	kilobase pairs
LB	Luria Broth
MOI	Multiplicity Of Infection
MRI	Magnetic Resonance Imaging

N.A.	Numerical Aperture
NB	Neurobasal medium
PCR	Polymerase Chain Reaction
PDL	Poly–D-Lysine
PET	Positron emission tomography
PIP2	Phosphatidilinositol (4,5) - bisphosphate
PIP3	Phosphatidilinositol (3,4,5) - trisphosphate
PLL	Poly–L-Lysine
R	Resistance
rAAV	recombinant Adeno-Associated Viral Vectors
R_m	Membrane resistance
ROI	Region Of Interest
RT	Room temperature
sc	self-complementary
SE	Standard Error
SNR	Signal - to - Noise Ratio
SOC	Super Optimal broth with Catabolite repression medium
ss	single-stranded
SV40	*Simian virus 40*
TTL	Transistor-Transistor-Logic
UV	Ultraviolet
V	Voltage
V-C	Voltage-clamp
vp/cell	virus particle per cell
VSFP	Voltage Sensitive Fluorescent Protein
YFP	Yellow Fluorescent Protein
Ω	Ohm

1. INTRODUCTION

1.1. Cell anatomy and achieving directionality

When there is a question about the definition of life, one can take a stand from variety of perspectives – scientific, philosophical, or even religious; but the fact they all have in common is that the cells are the major players in the game called life. Cells, as a very first product of evolution 3,5 billion years ago [1], rightly have been called a "fundamental unit of life". In the eras that followed, under the forces of the evolutionary change, they developed from primitive, prokaryotic cells that lack membrane bound organelles to sophisticated, eukaryotic cells. Their defining characteristic is organelle-rich membrane-bounded machinery that provides advantage by separation of functional compartments. Eukaryotic cells can dwell as unicellular organisms (single cell heterotrophic eukaryotes that belong to any of the major lineages of protists) or can be hierarchically embedded in multicellular organisms. Depending on the cell determination and niches where they dwell, every subtype is partially responsible for general homeostasis of the organism.

Due to the vast complexity of thought processes and control actions that the neural system can perform [2], it is not surprising that neurons, as a basic unit of the information conducting system, have sensitive mechanisms of activation, regulation and signal propagation (briefly described in 1.3.2). Despite distinct morphological regions, there is a certain functional anatomy they all follow in order to achieve their specific function (Figure 1.1). As every eukaryotic cell, they contain the nucleus and other organelles necessary for cellular function in the cell body, aka soma. The thin, multiple branched appendages of a neuron, dendrites, are the region where electrochemical signals from other neurons are received. In order to increase the receptive surface area of a neuron, they branch in an iterative form. The key fibre for signal transmission, the axon, extends from the soma, generally opposite the dendrites. The axon ends with the terminals that transmit the electrochemical signal across the gap between cells, the synapse. There, one neuron forms a connection with another one and conveys information through the process of synaptic transmission [3].

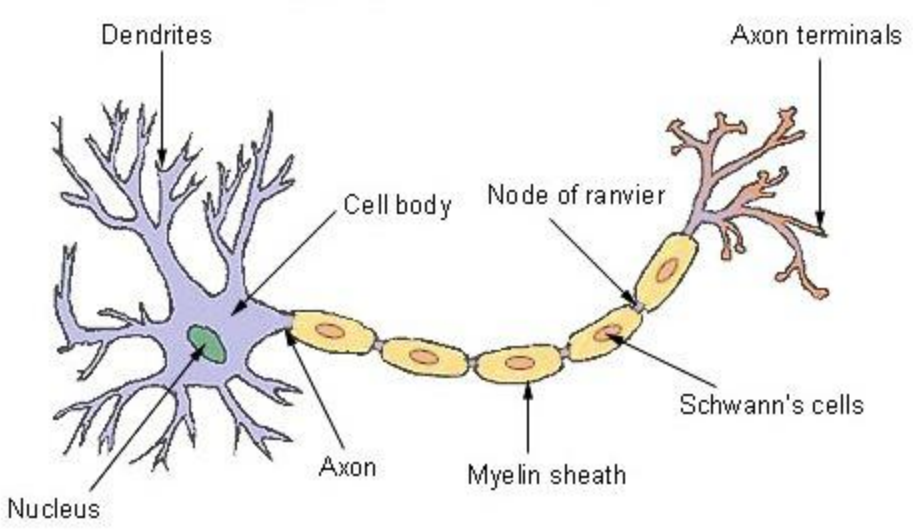

Figure 1.1 The structure of a typical neuron.

The cortical neuron consists of a cell body (or soma) with branching dendrites (signal receivers), and an axon (signal output). The axon is insulated by Schwann's cell-produced myelin. Unmyelinated points are the nodes of ranvier. After the myelinated region, the axon terminal releases chemical transmitters into the synapse.

(Figure originally published in [4])

Inside, the axon is filled with a viscous intracellular fluid called axoplasm, so the actual conductor of the action potential is the membrane of the axon [5]. The axon may be insulated by the supporting, Schwann's cells in the peripheral nervous system or oligodendrocytes in the central nervous system [6]. As it is described later, in 1.2.2, in uninsulated axons there is an impact of membrane leakage on the propagation of the signals. The main component in glial membranes is sphingomyelin (or ceramide phosphorylcholine), the complex lipid in which fatty acids are linked via amide bonds to a long-chain base or sphingoid [7]. Since the lipid serves as an excellent electrical insulator, it speeds the rate of the electrical impulse transmission along the axon, decreasing ion flow through the membrane about 5000-fold [2]. In the myelinated axon, what was empirically confirmed, the rate of an impulse propagation (in m) is six times the diameter of the axon (in µm). It is known as the "Hursh factor" [8]. Thus, the largest axons in the mammalian nervous system are approximately 20 µm in diameter, and their conduction rate is approximately 120 ms^{-1}, whereas the thin myelinated axons of about 1 µm in diameter have conduction rates of approximately 5 to 10 ms^{-1} [9]. Between myelin sheath cells along the axon there are small, uninsulated junctions, called the node of Ranvier. At these 2 to 3 micrometres long gaps, where there is no myelin cover, ions still can flow through the axon membrane [10]. There, the density

of voltage sensitive Na^+ channels is very high (10,000 μm^{-2}), in comparison to the internodal membrane where it is very low (20 μm^{-2}) [11]. Therefore, action potentials occur only at the nodes, while the electrical potential propagates from the both sides of the myelin; through the surrounding extracellular fluid as well as through the axoplasm, causing the impulse to jump and excite one node after another. This mechanism, called saltatory conduction, greatly increases the velocity of nerve signal transmission, as it affords excellent insulation, and reduces the metabolic energy required for re-establishing ion concentrations [2]. Additionally, specific membrane resistance (R_m) at the node is estimated to be only 50 Ωcm^2, what reduces the time constant and enables the nodal membrane to charge and discharge quickly [11].

1.1.1. Network signalling

All neurological processes are dependent on complex cell-cell interactions among single neurons as well as their networks. They can be categorised according to variety of features which are important determinants of the particular function. Along with the cardiomyocytes, skeletal myocytes and electrocytes, they are grouped as electrogenic cells; they share a property of electrical conductivity and morphology that can be equated with an electrical conductor.

Within the structural variation that depends on the niche and functionality that neurons cover, they can be categorised into three descriptive cell types [11]. Bipolar neurons have two extensions on opposite sides, an axon and a dendrite, and typically communicate with other cells in the nervous system through chemical signalling. They are exclusively involved in sensory transmission like retinal or olfactory neurons. In pseudo-unipolar sensory neurons only one neurite extends and branches from the cell body, so that both sides of the cell function as a single axon. Embryonically, they originate as bipolar neurons. Their specific structure is suitable for transducing sensory signals of physical stimulus (e.g. temperature, pain, light, sound). Multipolar neurons are the most common type and constitute the majority of neurons in the central nervous system. They have one axon and numerous dendrites in order to integrate a great deal of information from other neurons. [10, 11] (Figure 1.2).

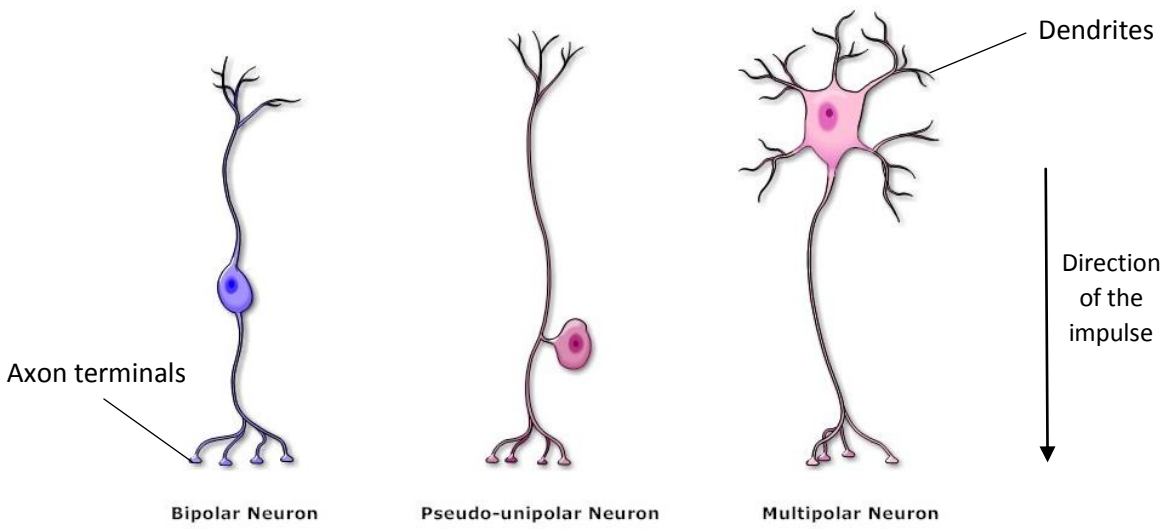

Figure 1.2 Three types of neuron morphology

Bipolar and pseudo-unipolar neurons are involved in sensory transmission directed to specific cells, while motor neurons constitute the majority of neurons in the brain. They have one long axon and many dendrites, what gives them possibility to make many contacts and receive plenty of information with multiple cells at once.

(Figure adapted from [12])

As the basic unit of neuronal information, there is an action potential. It is an event in which the membrane electrical activity is affected by the rapid rise and fall of the potential (1.3.2). The signal propagation plays the key role in the cell to cell communication.

1.2. Neural electric activity

The cell membrane and membrane potential

As the old adage “Good fences make good neighbours” makes clear, boundaries can be very influential. On the cell level, the identity and individuality that each cell possesses is conditioned by the plasma membrane, an essential boundary between the extracellular environment and the cytosol [5]. Although it defines the cell border and has an impact on cell stability and shape, the membrane is characterised as a dynamic, fluid structure with freely movable components within the membrane plane. Biomembranes, according to the order and fluidity, are classified as smetic liquid crystals; they

have a lower degree of order than crystalline solids, but a higher degree than liquids, due to the parallel alignment of elongated phospholipid molecules [13].

As a universal component that constitutes 50% of the membrane mass, there is a phospholipid bilayer. Amphipathic phospholipids have two main parts: a polar, hydrophilic head (phosphate group) and two hydrophobic non-polar hydrocarbon tails (usually fatty acids). The bilayer is formed in a way that the hydrophobic tails are sandwiched between the hydrophilic phosphate heads, with the heads facing the aqueous environment of the cytosol and extracellular fluid. For the membrane composition it was widely accepted that lipids and proteins were randomly distributed, according to the Singer-Nicolson fluid mosaic model [14]. However, from attempts to explain how lipids could selectively direct proteins to different surfaces [15] it is assumed that the membrane lipids are organised into microdomains or rafts [16], which serve as anchorage points for specific signalling molecules [13, 17].

Despite phospholipids being the most prevalent component in the membrane, the most important functional characteristics are conferred by the protein composition. The quantity of proteins present is highly variable - from 20% to 75% of the mass [2, 13], depending on the cell type and subcellular location. The proteins, based on their structure, associate with the membranes in different ways (Figure 1.3). There are several ways for proteins to interact with the membrane. Proteins that are localised and confined to either the cytosolic or exoplasmic side are peripheral proteins, and they are usually bound to the membrane indirectly, through electrostatic interactions and hydrogen bonding with the hydrophilic domain of integral proteins [18]. The other group of proteins, the amphitropic proteins, are attached to the membrane via covalent bonds to a lipid anchor by a mechanism involving post-translational modifications of these proteins [19], so the polypeptide chain does not enter the membrane itself. Features of the amphipathic proteins enable them to integrate into the hydrophobic moiety of the biomembranes. These transmembrane proteins consist of three domains and span through the phospholipid bilayer. The cytosolic and exoplasmic domains are hydrophilic and therefore interact with the aqueous solution, while hydrophobic domain is embedded in the lipid core of the membrane [13]. The way in which protein is associated with the lipid bilayer reflects the function of the protein. Indeed, the only proteins that can serve as transit conduits through the plasma membrane are transmembrane proteins.

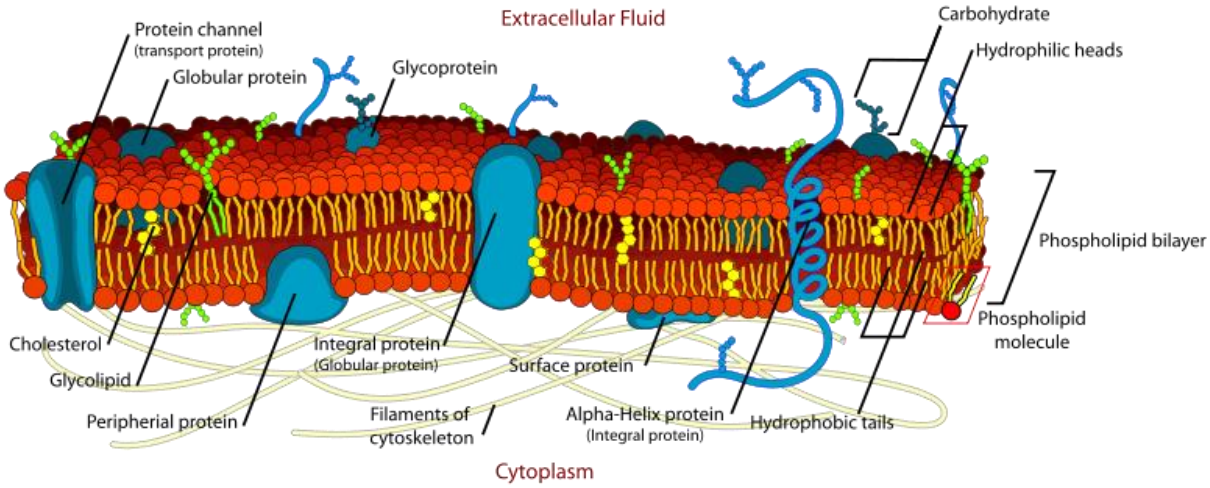

Figure 1.3 Scheme of the cell membrane and its components.

The cell membrane is a semipermeable lipid bilayer that consists of hydrophobic fatty acids (orange lines) sandwiched between the hydrophilic phosphate heads (red dots) faced towards the cytosolic and extracellular side. It has variety of incorporated or attached proteins (blue forms), glycolipids (green dots) and carbohydrates (dark blue forms).

(Figure originally published in [20])

There are two major classes of transmembrane proteins that move substances into or out of the cell: channels and carriers. Carriers undergo a series of conformational changes in order to actively perform the transfer across the membrane, while channels form a hydrophilic pore across the lipid bilayer through which specific solutes can freely pass to the other side of the membrane [2]. According to the transport efficiency, channels have an advantage over carriers; the rate of transport is several orders of magnitude greater than the fastest rate of transport mediated by carrier proteins [5]. Besides, their other advantage is in rapid flux down the electrochemical gradient across the lipid bilayer. Also, channels are non-saturating; the rate does not approach a maximum at high substrate concentration [18]. Unlike carriers, ion channels are passive; they do not require a source of energy for their functionality. Thereby, the force that drives the ion through the channel is an electro–chemical gradient; the combination of the ion concentration gradient and electrical transmembrane potential [21].

Ion–selective channels, proteins specific for inorganic ion transport, first have been recognised in neurons [22]. Nowadays, they are known to be present in all eukaryotic biomembranes. Together with ion pumps, like Na^+K^+ATPase, they regulate the plasma membrane's permeability to specific ions.

The resulting cytosolic ion concentrations are responsible for the membrane potential [18], what is described later in chapter 1.2.1.

One kind of ion channels is the ligand–gated channels. Allosteric transition in the protein that opens or closes the channel is dependent on extracellular or intracellular ligand binding. To this group belong most of the neurotransmitter receptors, like serotonin or glutamate receptors [23]. They provide the transport of the chemical signals between bipolar neurons, as mentioned in 1.1.1.

An alternative type of ion channel is the voltage gated channel. In voltage-gated ion channels, opening or closing the channel is conditioned by the change in transmembrane electrical potential (V_m). If it is assumed that the resting potential across the membrane is about -60mV, considering the thickness of the membrane of 6 nm, the voltage drop is very steep and the potential gradient of -60 mV works out to 105 Vcm^{-1} [13].

1.2.1. Ionic gradients

For neurons, because of their electrical properties, is of significant importance to properly distribute ions and manage their movement across the plasma membrane, between the extracellular and intracellular space. This precise internal ionic concentration of monovalent (K^+, Cl^- and Na^+) and bivalent (Ca^{2+}) ions is affected by the operation of ion channels [11] (Figure 1.4). Asymmetrical distributions of these ions across the plasma membrane (Table 1) give rise to the ion concentration gradients, that can drive the diffusional movement across the membrane through the selective ion channels [10]. The charge the ions carry gives them electrical effects as well, so their movement across the membrane results in a redistribution of electrical charge.

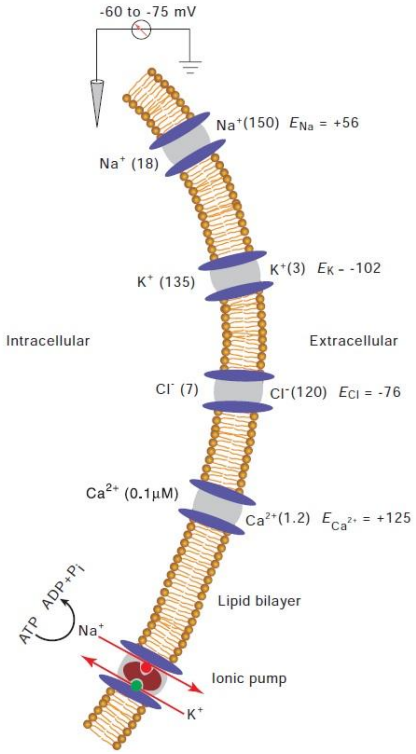

Figure 1.4 Differential distribution of ions across the plasma membrane of neurons.

Voltage–gated ion channels of K^+, Cl^-, Na^+ and Ca^{2+} are shown, as well as their concentration (in brackets) and equilibrium potentials (*E*).

(Figure originally published in [11])

Table 1. Major ionic components of intra and extracellular fluids and their equilibrium potential.

Despite their different role and compartmentalisation, the intracellular and extracellular fluid diverse in the composition as well. Except for the difference in sodium and potassium ion concentration that are important for keeping the balance of the negative membrane potential, the low intracellular calcium concentration compared to extracellular enables its role as the second messenger. Higher amount of charged macromolecules in intracellular fluid is critical for osmoregulation inside the cell. To emphasize the chemical power of the electrolyte in a fluid, the ion concentrations are given in miliequivalent per liter (10-3 mole divided by valence) [24]. The equilibrium potential for some ions are left out due to their little contribution to the resting membrane potential.

Table originally published in [24].

Ion	Intracellular concentration (mEq/L)	Extracellular concentration (mEq/L)	Equilibrium potential (mV)
Na^+	15	140	70
K^+	135	4	-94
Ca^{2+}	$2x10^{-4}$	4	132
Mg^{2+}	40	2	
Cl^-	4	120	-90
$HCO3^-$	10	24	
HPO_4^{2-}	20	4	
$SO4_2^-$	4	1	
$Proteins^-$, Amino $acids^-$, Urea, etc.	152	1	

1.2.2. Theoretical background

The condition in which the electrochemical gradient (also called the diffusion potential) of a species is at equilibrium across and through the membrane is described by the Nernst equation. The Nernst potential, however, is determined by the ratio of the concentrations of that specific ion on the two sides of the membrane [2, 21]. In a physiological application, it is used to calculate the potential of an ion of charge z across the membrane:

$$E = \frac{-RT}{zF} log_{10} \left[\frac{c_{in}}{c_{out}}\right] \qquad \textit{Equation 1}$$

where *E* is the membrane potential (V), *R* the ideal gas constant (J $K^{-1}mol^{-1}$), *T* thermodynamic temperature (K), *z* the ion valence, *F* Faraday's constant (C mol^{-1}), c_{in} the intracellular concentration of ions (moles l^{-1}) and finally, c_{out} the extracellular concentration of the particular ion (moles l^{-1}).

Expanding the Nernst equation to include the contribution of the most relevant ionic species across the membrane, one arrives at what is termed the Goldman–Hodgkin–Katz equation. It describes the ionic flux carried by ionic species across the cell membrane at the steady state potential, including the relative permeability of the membrane for each of those ions (K^+, Na^+, Cl^-):

$$V_m \frac{RT}{F} ln\left(\frac{p_K[K^+]_o + p_{Na}[Na^+]_o + p_{Cl}[Cl^-]_i}{p_K[K^+]_i + p_{Na}[Na^+]_i + p_{Cl}[Cl^-]_o}\right) \qquad \textit{Equation 2}$$

where, along already listed measurements and units ($E=\frac{-RT}{zF} log_{10} \frac{c_{in}}{c_{out}}$ Equation 1above), p_{ion} represents the membrane permeability for that specific ion (ms^{-1}).

It is assumed that the relative contribution of each ion is determined by its concentration difference across the membrane and the relative permeability of the membrane to the each type of ion. As described in 1.2, ions can pass from one side of the membrane to the other by specific transmembrane proteins; either freely gated through the channels down their electrochemical gradient or actively by carriers. Voltage-gated channels open and close in response to membrane potential. At the resting potential, voltage-gated ion channels are in deactivated state (closed) and no ions move through them. For the three ionic species with greatest impact on membrane potential, K^+, Na^+ and Cl^- at 20˚C the equation is:

$$V_m = \frac{58.2\ log_{10}\{(1\cdot 20 + 0.04\cdot 440 + 0.45\cdot 40)}{(1\cdot 400 + 0.04\cdot 50 + 0.45\cdot 560)\}} = -62\ mV \qquad \textit{Equation 3}$$

This result suggests that the membrane should have resting membrane potential at -62 mV [11].

Excitable membranes can be compared to capacitors due to their possibility to store energy in the form of electrochemical gradient that can be discharged to transmit electrical signals [24]. Described in the terms of electronics, the pores form a conductive branch in parallel with the capacitive lipid bilayer (Figure 1.5) [24].

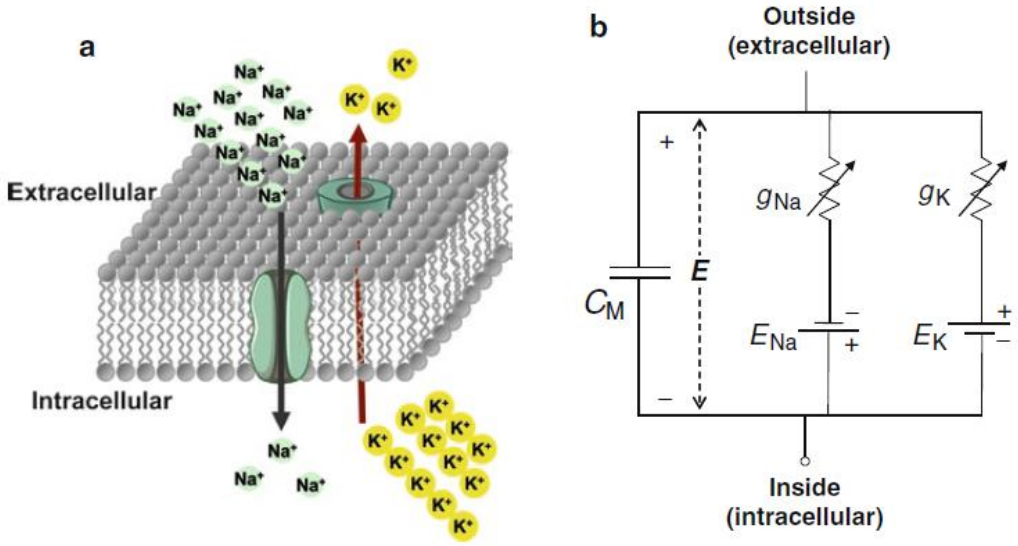

Figure 1.5 Schematic view of plasma membrane in 3D, with salient Na+ and K+ voltage-gated ion channels (a) and analogous electrical circuit (b).

The plasma membrane has properties similar to an electrical circuit with a capacitive branch (C_M), sodium and potassium selective ion channels with conductive branches (g_{Na} and g_K) as well as their equilibrium membrane potential that corresponds to an electromotive force (E_{Na} and E_K).

(Figure originally published in [24])

A membrane containing ion channels can also be represented as a resistor, whereby the resistance decreases with more channels that are open. To predict current flow during the channel opening, Ohm's law is used. According to it, the electromotive force or voltage (V) and current (I) are directly related to each other by resistance (R): [25]

$$I = \frac{V}{R} \qquad \textit{Equation 4}$$

To calculate the electric current and accompanying voltage along neurites, particularly dendrites that receive synaptic inputs, one uses the mathematical model named "classic cable theory". It is actually a set of assumptions and results related to the propagation and interaction of electrical signal in spatially expanded neurons. It has been developed over the last decade because the dendrites' distal synapses are out of reach of traditional electrophysiological studies using electrodes at the soma. It assumes that the extracellular space around the membrane acts as a perfect resistor, ignoring the unknown impact of its other electrical properties such as capacitive effect, diffusion etc. [26]. Essentially, the axons and

dendrites are assumed to be cylinders with capacitance C_m due to the electrostatic forces acting through the lipid bilayer and resistance r_m due to the axoplasm's resistance to movement of electrical charge, combined in parallel (Figure 1.6). Written in mathematical terms, the equation would look like this:

$$I_m = \frac{(V_m - V_{rest})}{r_m} \qquad \textit{Equation 5}$$

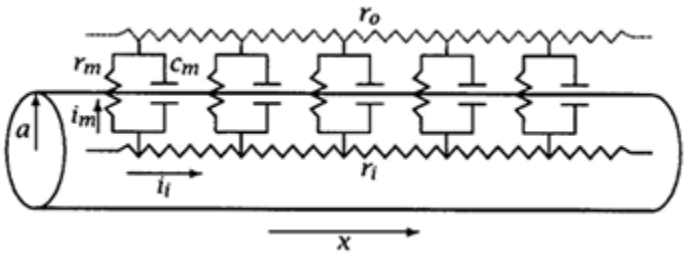

Figure 1.6 Cable theory's simplified view of a neuronal fiber as an electric circuit.

Uniform cylinder represents a segment of axon or dendrite. The upper side looks towards the extracellular fluid and in the cylinder is the cytoplasm. Compartments are spatially adjacent to each other and coupled through a linear resistance form. Signals decay over space and time in a mathematically understood fashion.

(Figure originally published in [27])

The cable properties of neurons determine the spread of action potentials along the axons (Figure 1.6). The premise for cable theory is that the dendrites have properties of a leaky electrical cable, such as low electrical resistivity of the axoplasm and high resistivity of the membrane. However, one of the key features of the membrane, which despite high resistivity cannot completely block the leakage of the current, is accounting for signal decay. These parameters are important in determination of the current flow because they direct the flow of the current across the membrane rather than down the axis of the dendrite. Additionally, the cable diameter has impact on the current flow as well; the signal spreads farther in a thick dendrite, resulting in more current flow towards the soma. During the signal transmission, the transmembrane voltage falls off exponentially with distance. Furthermore, the branches in the dendritic tree increase attenuation of the voltage signals. An important addition to the theory is to include the time component. Namely, the frequency of the signal affects its transmission. If there is a low-frequency of the depolarisation of excitatory postsynaptic membrane potential (EPSP), they are lost to membrane capacitance and there is less voltage change along the dendrite. As the

dendrites act as low-pass filters, they let more slowly changing signals pass, compared to rapidly changing one [28]. Thus, the accumulation of the low-frequency signals, as a passive event, enables sufficient membrane depolarisation to reach above the threshold and initiate an action potential (Figure 1.7).

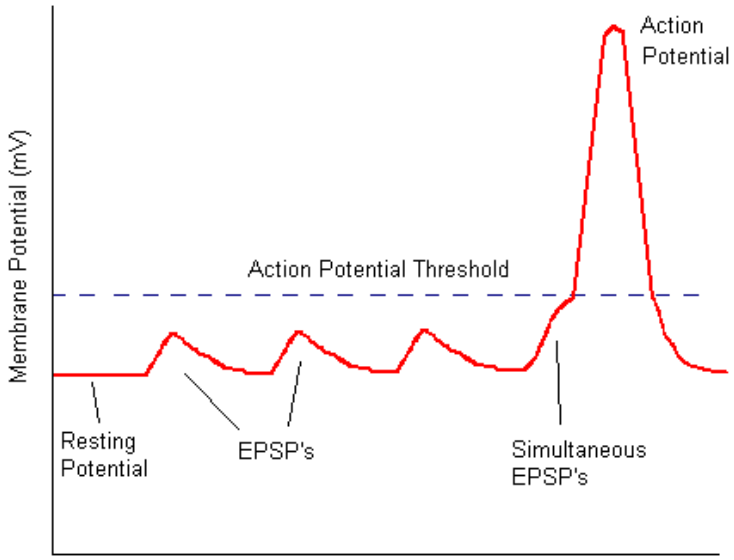

Figure 1.7 A model of the EPSP conductance

Once the EPSP response hits the threshold, the action potential will occur.

(Figure originally published in [29])

1.3. Voltage

1.3.1. Voltage sensors

In excitable cells, the most astonishing property of ion channels is their sensitivity to small changes in membrane potential. As a functional condition for the cell is underlying in dynamic equilibrium, the same can be perceived for ion concentration from both sides of the membrane. Due to the great difference in the ion concentration across the plasma membrane, the electric potentials differ as well. Their sudden change has an impact in achieving the signal generation and propagation. Thus, the ion channels need to be able to selectively block or allow ion flow.

Voltage sensitive proteins have linked a sensor domain (Figure 1.8) whose task it is to detect certain conditions like voltage or pH changes to their other functional domains [21]. The S4 sensor domain is responsible for detecting small gating current at the beginning and end of any small depolarisation. The exact biophysical mechanism is still under investigation, and there is still no consensus model, but a huge advance happened with elucidation of finer structural information at atomic level of the voltage-gated potassium channel in 2003, courtesy of the MacKinnon laboratory [30].

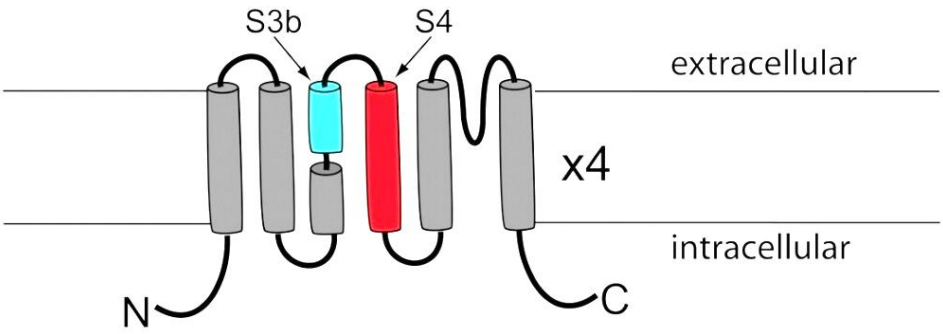

Figure 1.8 Model of a voltage-gate potassium channel subunit in the plasma membrane.

Six transmembrane segments, S1-S6 (cylinders), of which S3 is divided into two helices, S3a and S3b (blue) are positioned in between the plasma membrane (horizontal lines). The S4 segment (red) is situated among S3 and S5 segment.

(Figure adapted from [30])

In the primary sequence of S4, there are positively charged amino acids on every third place; it exhibits a homologous pattern of positive charge distribution of 83% [31]. Projected into secondary structure, an Arg-containing α-helical conformation is assumed. These crucial amino acids are arranged in the same planar direction [13]. In the lipid bilayer, they are stabilised with negatively charged amino acids originating from the other domains of the transmembrane ion channel. Arginine actually maintains the structure by electrostatic interactions in a manner that inside negative transmembrane potential exerts a pull on positively charged Arg side chains in S4. When the membrane is depolarised and negative potential is reduced, the inward pull is lessened for 5Å [32] (Figure 1.9). Thus, the N-terminus of S4 screws outwards for a 60° turn, to the extracellular side through a short hydrophobic gating pore. This results in displacement of 5Å [13, 18]. This conformational change leads to physical opening and closing of the ion channel.

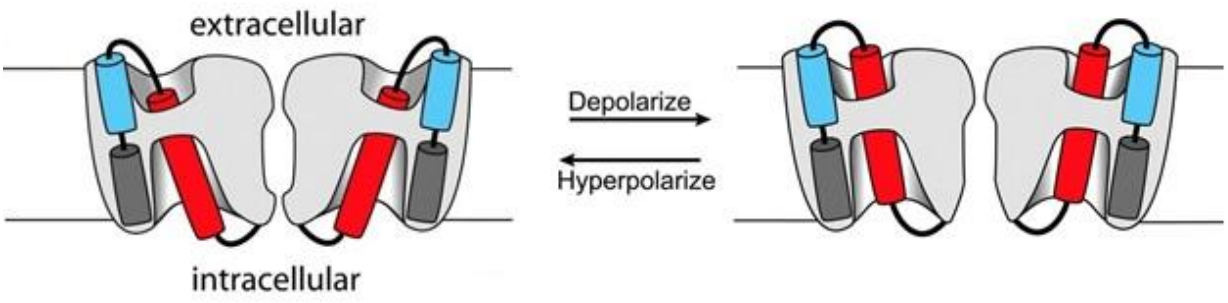

Figure 1.9 Conventional model of voltage sensor movement during depolarisation.

Four subunits are shown in order to expose the gating pore. Voltage changes move the N-terminal extracellular portion of the S4 segment (red) through a hydrophobic gating pore, opening or closing the permeation pathway.

(Figure adapted from [30])

1.3.2. Action potential

The discovery and understanding of electricity itself has helped a number of notable scientists to contemplate about the nature of nerve communication – the flow of an action potential. During the second century A.D. in ancient Greece, the cradle of science, the great physician Claudius Galen prospered that "humors" flowed from the brain to the muscle [11], what indicates that even then people were intrigued with informational pathways in human bodies. With improvement in experimental techniques, scientists, including Luigi Galvani, Emil Du Bois-Reymond, Hermann von Helmholtz and many others, examined this idea [11]. Hodgkin and Huxley however, gave the final proof – recording of the action potential, which signified the start of modern electrophysiology, in the early 1950s [13]. Their work not only forms the basis of the classical electrophysiology that has been in use for more than 50 years, but also gave us a theoretical framework for many properties that have since been verified [33]. Using an electrode placed inside a giant squid axon they were able to record the shape of the action potential and determine the nature of the ion flows, as well as measure transmembrane potential of about -60 mV under resting conditions [34]. The original photo from their experiments (Figure 1.10) shows when an impulse of action potential passes the measured part of the membrane, the internal electrode measures +35 mV compared to the external electrode because the membrane potential is reversed. Shortly after (1,5 ms), the membrane has returned beneath its resting potential,

and afterwards (1-2 ms) the normal resting potential is re-established [13]. For their work, they were awarded the Nobel Prize in Physiology or Medicine in 1963 [10].

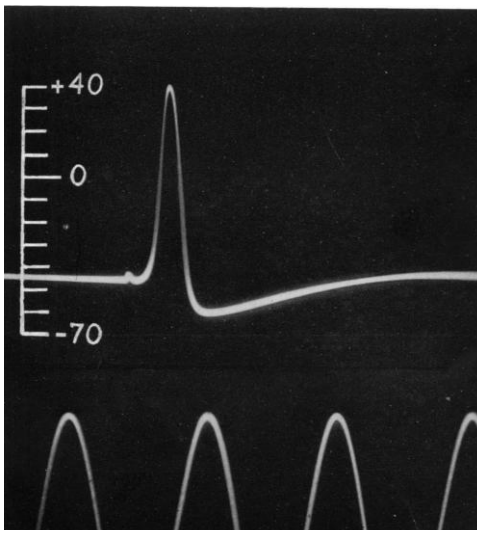

Figure 1.10 Action potential recording between inside and outside of a giant squid axon.

Time marker at the bottom indicates 500 cyc./s. The vertical scale on the top indicates the potential of the internal electrode in millivolts. As the zero potential, the seawater outside was being taken.

(Figure originally published in [35])

In the normal, resting stage, preceding the action potential, the membrane is polarised to around -60 mV [13]. A local change in membrane polarity or a local depolarisation which is insufficient to pass the threshold potential causes a subthreshold potential. When there is enough accumulation of depolarisation, a rapid rise in the membrane potential above the threshold, an action potential is initiated. The principle of generating an action potential is so called “all-or-none principle” since they occur fully or do not occur at all. Just as quickly as the potential is generated, it drops (repolarisation) and overshoots reaching the more negative potential values than when resting, called hyperpolarisation. Finally, it returns towards resting potential. Starting at the axon hillock with a sufficiently strong depolarisation, an action potential is generated reaching the peak where the second phase of potential drop (repolarisation) starts; reaching the more negative membrane potential then in the resting stage (hyperpolarisation) and returning towards resting potential (Figure 1.11) [2].

Due to the voltage-gated sensory properties of sodium channels described in previous chapter (1.3.1), they detect small depolarisations in transmembrane voltage. Triggering this sensor promotes their opening through a conformational change and the membrane suddenly becomes permeable to sodium ions, allowing them to diffuse inside the membrane [36]. Inflow of positively charged sodium ions raises the potential rapidly. If the depolarisation is below the threshold value (at about -45 mV), the outward potassium current overwhelms the inward sodium current and the membrane repolarises back to its normal resting potential. This state is called sub-threshold depolarisation. In contrast, if the threshold value is reached, the inward sodium current increases more than the outward potassium, which leads to higher V_m increase. That in turn causes more sodium channels to open and even higher V_m and as such, the action potential is termed an "all-or-nothing" response; once threshold is reached, the full action potential is always generated. With this, the initial phase called depolarisation, where there is sudden change in potential from -60 mV to +40mV, starts. This positive feedback continues until the sodium channels are fully open, sodium permeability is maximised and V_m is close to the sodium equilibrium voltage, E_{Na} [37]. Then, there is the peak of the action potential. Near the peak of the action potential, calcium channels begin to be activated [38]. Calcium currents are the largest during the falling phase, when channels have been opened. This reflects powerful and rapid coupling of calcium entry to the activation of large conductance calcium-activated-potassium channels, what will have large impact in the hyperpolarisation phase [38].

A return towards the resting membrane potential happens in the repolarisation stage. In a very short period of time (1 ms) after opening, the sodium channels switch to a conformation that no longer allows Na^+ to pass, because of their inherent properties, although the membrane is still depolarised [37]. The other set of voltage-gated ion channels that participate in repolarisation are potassium channels. The required time for reaching the threshold to open the channels is the time when Na^+ flows into the cell and increases the membrane potential. Afterwards, potassium channels open and increase the membrane permeability for K^+ ions. K^+ ions outflow from the neurons bring the membrane potential towards E_K. These changes cause a quick drop of V_m and thus, membrane repolarisation [37].

Unusually high membrane permeability for K^+ ions even after the repolarisation stage leads to the next stage, called hyperpolarisation. This is caused by slow inactivation of K^+ ion channels, as well as their further opening due to the Ca^{2+} influx during the action potential [34], as mentioned above. This can result in an undershoot of the resting membrane potential, generating after-hyperpolarisation [37]. Transiently hyperpolarised membrane recovers over about 10 ms [38]. During this relative refractory

period during which the neurons are unable to generate an action potential, ions are redistributed until the membrane potential reaches -70 mV. This is the mechanism of recuperation of ion channels and an initiation of the second action potential is inhibited. In the absolute refractory period, though, a second action potential cannot be initiated due to the Na^+ channels inactivity and lasts the entire duration of the action potential.

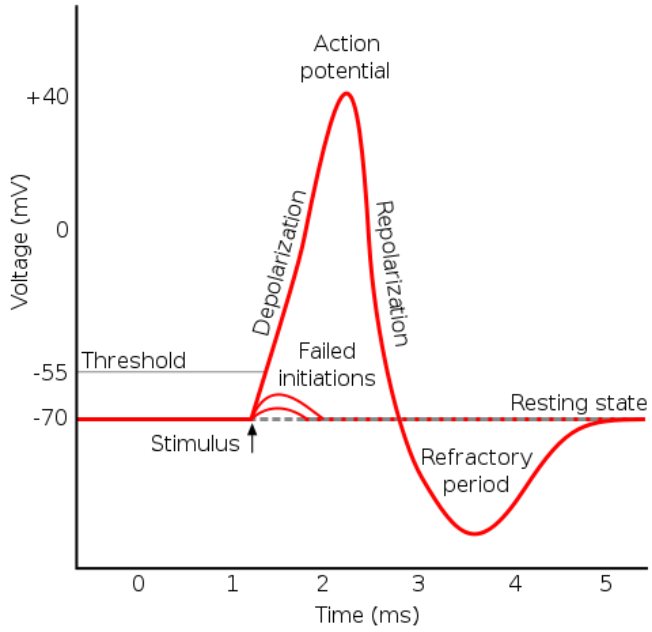

Figure 1.11 Schematic of a neuronal action potential.

If the stimulus reaches the threshold value (for example -55 mV), voltage gated sodium channels change conformation so the membrane becomes permeable to Na^+ ions. Inflow of Na^+ raises the potential to +40 mV (depolarisation). Repolarisation occurs when sodium channels rapidly close and potassium channels open. Their rapid outflow re-establishes the normal resting membrane potential (-70 mV). Slow inactivation of potassium channels causes hyperpolarisation. After a few milliseconds of relative refractory period, the membrane returns to resting potential.

(Figure originally published in [39])

Under physiological conditions, propagation of the action potential is unidirectional, ensured by the absolute refractory period mentioned above. The flow of current is spread out in both directions along the axon, but only an unfired part can respond with an action potential. The reason for this is inactivation of Na^+ channels in the part where action potential already happened and the local current circuit that is primarily outward flowing K+ ions that repolarise the membrane [10].

1.3.2.1. Propagation of the action potential

At the time when research of action potentials started to be the main point of electrophysiology experiments, giant invertebrate axons were used as a model of conducting fibre. Because of their morphology and large diameter, they were suitable for variety of electrode measurements. Vertebrate animals, however, evolved an alternative ways for speeding the impulse down the axon, as a need of larger body control and more complex behaviour, with conduction of impulses as rapid as possible. One of the mechanisms is increase in the number of conductive cells (neurons); with smaller diameters, there are more axons within a given space [11]. The other mechanism of increasing the rate of conduction is to make the rate of conduction faster. The ability to conduct with great rapidity whilst remaining small is achieved by electrical insulation of axons with myelin sheath, as a significant component for the propagation of impulses [13] (Figure 1.12).

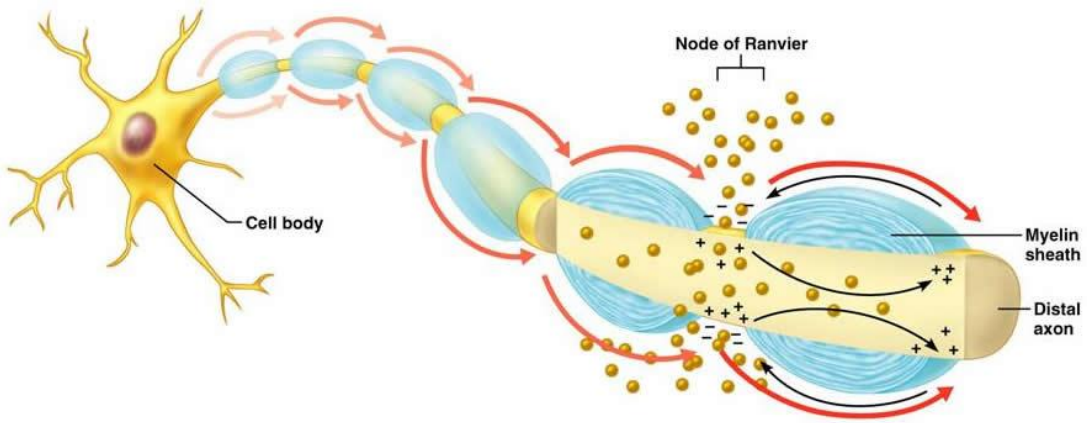

Figure 1.12 The saltatory conduction.

Propagation of the action potential (red arrows) goes along myelinated axons, from one node of Ranvier to the next one, increasing the conduction velocity. The high density of voltage – dependent Na^+ channels is in the area of the nodes of Ranvier, where the generated signal jumps from one node to another one.

(Figure originally published in [40])

The action potential propagation along the membrane of the unmyelinated axon (Figure 1.13) is enabled by the local current spreading through the internal resistance. The rate of propagation is determined by the kinetics of the action potential and cable properties [11]. The mechanism is that the sufficiently strong local circuit current flows across the resting membrane to depolarise it toward

threshold; the inward diffusing Na^+ ions that carry positive electrical charge also serve as a current source for further membrane depolarisation. Behind the active region, the outward current is carried by K^+, which repolarises the membrane [11].

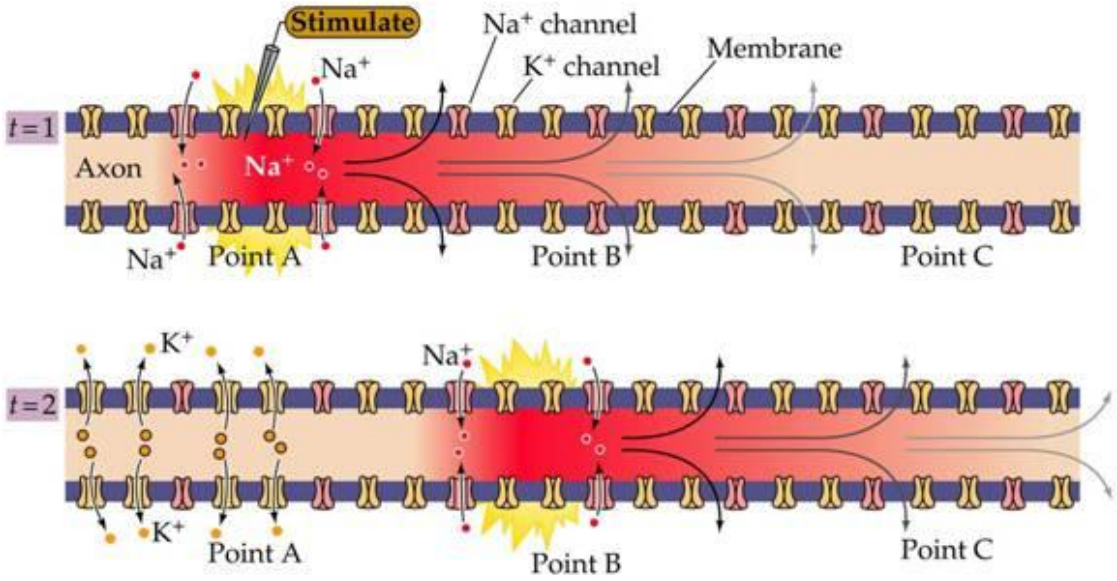

Figure 1.13 Propagation of action potential.

In the point A in t=1, sequence of events lead to the generation of action potential (Point A). Afterwards, it is propagated along the axon (Point B) by opening Na+ channels in the membrane and their influx enables enough current to push it towards the point C.

(Figure originally published in [41])

1.4. Voltage sensitive fluorescent proteins

1.4.1. History of VSFP development

Establishment of transient coherent electrical activity across the cortex, recruited from neuronal assemblies, forms the backbone of the whole palette of complex lifelong brain activities such as perception, learning and memory, sensory and motor reflexes loops, determined mental states etc. [42]. Unravelling the secrets of exact neuronal behaviour on the single cell level as well as its effect on the neuronal network, contributes to the indistinct puzzle of how the brain functions. Therefore, it is not surprising that trials examining neurophysiological recording have been represented for decades. Recording electrical activity from the brain was performed first as a whole organ study, with silver dish electrodes attached to the scalp. Measured electrical currents, or brain waves, recorded from the cerebral cortex by the electroencephalography method are used for evaluating abnormalities of the central nervous system [43]. Further, a range of different stimulation (electroconvulsive therapy), recording (magnetic resonance imaging (MRI)) and imaging (computed tomography, positron emission tomography) techniques were developed [44]. Most of these methods gather only structural information about the brain. In a case with hemodynamic methods (MRI), where blood flow is studied, lack of temporal and spatial resolution provide restricted data only. In fact, these listed methods, applicable *in vivo* on whole organ studies, rely on the same role of synchronised population activity, which correlate with behaviour and mental state.

In parallel, curiosity for neurophysiology research on a lower, cellular scale, has led to the development of plenty of *in vitro* methods. Due to the limitations in electrode number and size, poor spatial coverage**,** indistinguishable location of signal generation and invasiveness, there was a need for the expansion of the neurophysiologic recording toolbox. In order to do that, during the past 20 years optical imaging of neurons *in vitro*, as well as *in vivo* were developed. Among these methods, intrinsic optical approaches enabled a simpler execution and observation of the experiments. Besides, they have multiple advantages over the electric means: they do not require application of an exogenous agent for the stimulation, nor are they subject to neural interface issues and thus. They are also less harmful for the biological samples. The spatial resolution is provided by the optical limitations of the camera/microscope used for the measurements. These experiments were achieved with a less invasive method; calcium-sensitive and voltage-sensitive (or potentiometric) dyes.

The voltage-sensitive dyes are small organic lipophilic molecules that contain a pair of hydrocarbon chains acting as membrane anchors and a hydrophilic group that links the chromophore to the membrane. After delivery, dyes integrate into the lipophilic part of the plasma membrane. It provides spatial and temporal resolution sufficient to optically record changes in the membrane

potential by changes in fluorescence. The electrochemical mechanism lies in the induced charge redistribution in the dipole chromophore transferred from the cell membrane upon depolarisation [46]. Their size and ability to enter through all cell membranes, has the advantage that they are easy to use. However, that also means that lack of specific targeting makes them unsuitable for monitoring specific cell populations. Their functionality and stability in the membranes that they offered for *in vitro* experiments was not applicable for *in vivo* research on brain tissues. Procedures for the dye delivery involve invasive craniotomy and usage of organic solvents for increasing chemical stability. Besides that, issues that limit their usage are also cytotoxicity, high optical noise and with it, loss of valuable signal, as well as indistinguishable signals origin [46]. Further investigation in the domain of the enhancing the optical methods developed in parallel with the expansion of the molecular biology, such that this function could be implemented with proteins. Thus, the need for more accurate and specific measurements has led to development of genetic voltage sensors. They are analogous to voltage sensitive dyes but offer the possibility to target specific cell populations on a genetic basis. Based on molecular fusion of a GFP-related fluorescent reporter protein and a voltage sensor domain, a newly created protein family of genetically engineered fluorescent voltage reporters was generated.

1.4.1.1. Ciona intestinalis VSP

Entering the 21st century, bioinformatics tools were developed and improved, as well as the variety of experimental methods in molecular biology. Comparative genomics analyses, enabled by fast and reliable sequencing, unravel the evolutionary secrets. To understand the evolutionary relationships of the proteins, they should be classified to structural families to facilitate the comparison of their domains. The domains often form the independent functional units that are actually conserved parts of the protein's tertiary structure. As a main theme within the scope of our interest there is the existence of a family of voltage-sensing phosphatases that are represented in a variety of species. This protein family is made up of two protein domains: a voltage-sensing domain and a phosphatase domain. One of the first organisms in which human transmembrane phosphatase homologues were found is *Ciona intestinalis*, an ascidian from the *Chordata* phylum. Ancestral prototype genes for neuronal signalling and voltage gated cation channels in *Ciona* are represented in only a minimal set, while in vertebrates there is palette of diversity. Structural characteristics of members of the voltage-gated ion channel superfamily are, primarily, six transmembrane domains divided into two main functional domains: the sensor and the pore. The same structural pattern is discovered in *Ciona intestinalis* transmembrane

proteins (Figure 1.14) and thus this novel protein got a descriptive name – *C. intestinalis* voltage sensor containing phosphatase (Ci-VSP) [47]. Interestingly, although it belongs to the voltage dependent family of proteins, it is the only member that is not functioning as an ion channel; just as a phosphatase [48].

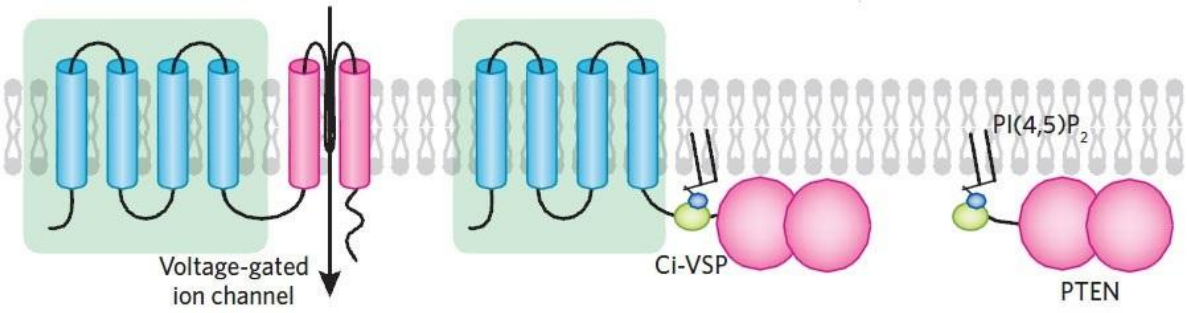

Figure 1.14 Structures of a voltage-gated ion channel and Ci-VSP.

Ci-VSP shares similarity with voltage-gated ion channels by possessing a voltage-sensing domain (green box), but it does not have a pore for the ion flux. Its cytoplasmic region has significant homology to PTEN phosphatase (pink circles).

(Figure adapted from [49])

Voltage sensing domain (S4) is located on the N terminus and the pore (S5, S6) on the C terminus. Phosphatase activity specificity of these proteins lays on the C terminus: it contains highly conserved active site motif C-$(x)_5$-R specific for the tyrosine phosphatase protein superfamily. This may imply their role as a combination of voltage sensors and phosphatases included in cell signalling and ion channels [18].

After discovering structural patterns, there was a question how, if at all, these two functional domains depend on each other. The fact that most of the membrane proteins involved in signalling have at least one phospholipid binding domain [18], suggested that the mechanism (Figure 1.15) by which domains are allosterically coupled is through the activation of the enzyme phosphatase. It is supposed that the change in the membrane potential is sensed by the Ci-VSP S4 transmembrane domain, causing its conformational change and further, activation of the phosphatase domain.

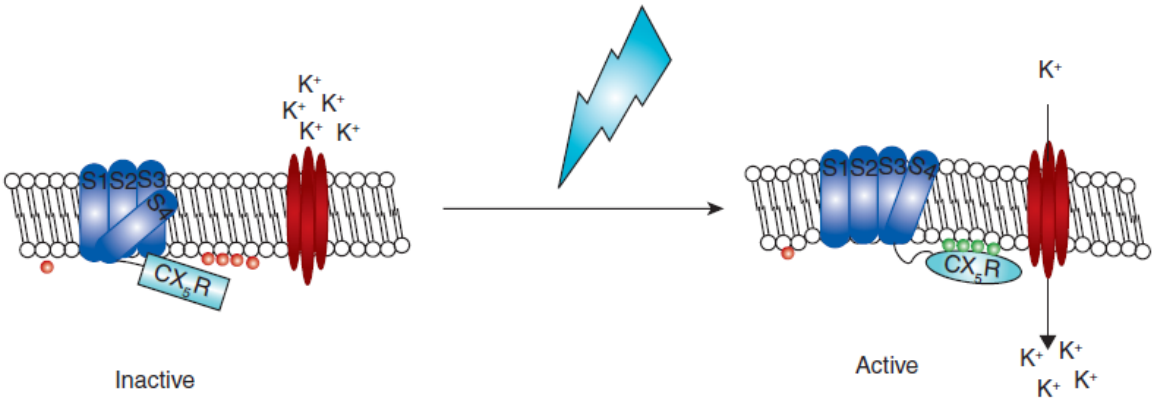

Figure 1.15 Schematic mechanism of Ci-VSP action.

In the resting state (left), VSP (dark blue) and the CX5R phosphatase linker (light blue) are both inactive. A change in potential (right) shifts S4, activating the phosphatase, probably by moving it closer to substrate bound PIP3. Activation of CX_5R locally increases the concentration of PIP2 and released phosphate opens nearby K^+ channels.

(Figure adapted from [47])

The new genetic voltage sensors are named voltage-sensitive fluorescent proteins (VSFP). They function in a way that the conformational change of the voltage sensor in response to membrane potential changes the fluorescence of the reporter protein. This new, non-invasive optogenetic tool is valuable for recording electrophysiological signals in electrogenic cells and provides reliable detection of single action potentials in individual neurons, as well as in neuronal networks simultaneously [42, 50-53]. Before their brief description, since the voltage-sensitive part is already described, it is necessary to introduce the part about the fluorescent proteins.

The green fluorescent protein (GFP) is the famous chemiluminiscent protein from *Aequorea Victoria* jellyfish, which initial discovery was rewarded by Nobel Prize in Chemistry 2008. Its emission peak is in the green portion of the visible spectrum, at 509 nm. Due to its wide usage as a reporter of expression, many new variants have been designed by introducing the mutations. This way, a broad spectrum of emission colours was produced (Figure 1.16). A few of those specific variants, as a fluorescent part of VSFP, are denoted here. As a monomeric variant of the yellow fluorescent protein (YFP), there is a Citrine that has been demonstrated to be more resistant to photobleaching than other YFP derivatives. Besides this, another one to single out as the far-red spectrum variant is mKate. From the derivatives spectrum of GFP, an enhanced ratiometric super ecliptic pHluorin will be described (1.4.2) as a part of VSFP.

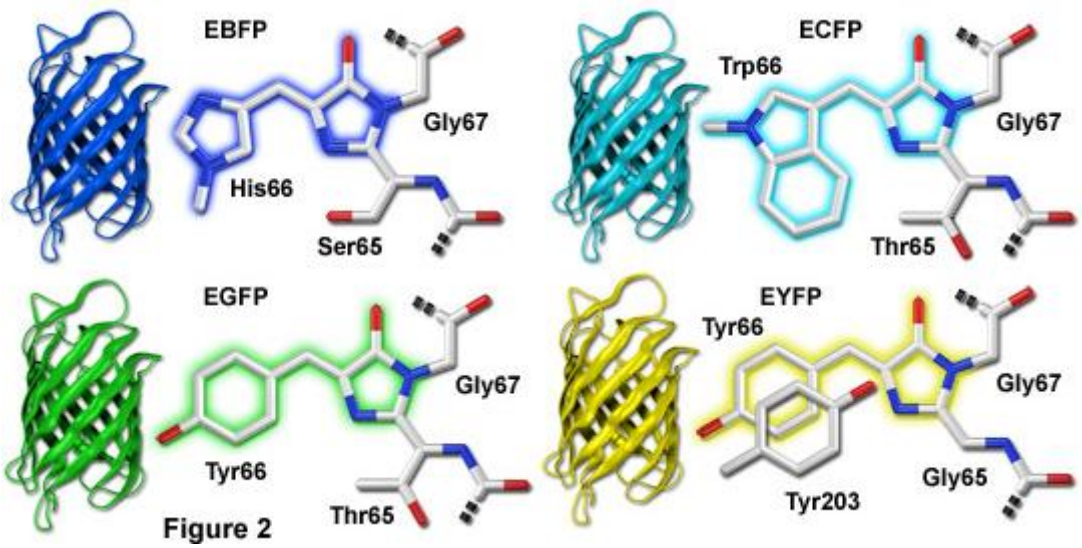

Figure 1.16 Chromophore structural motifs of GFP variants

In order to shift the emission spectrum and to improve folding, the variants of GFP have been designed by site-directed mutagenesis.

(Figure originally published in [54])

1.4.2. ArcLight A242

Great advantages in further development and improvement of VSFPs were brought by results of the experiment done on Ci-VSP. Interestingly, by cDNA transfer by injection into *Xenopus* oocytes [47], it has been experimentally proven that Ci-VSP transmembrane domains (S1-S4) can perform as a voltage sensor with or without the C-terminus phosphatase domain. This defined a small independent subunit that could be fused to other functional domains in order to achieve enhanced properties of existing VSFPs.

During 2013, by using the benefits of genetic engineering, the desirable characteristics of Ci-VSP's voltage-sensing domain were coupled with a novel mutant fluorescent protein, super ecliptic pHluorin A227D, into a novel monochromatic voltage indicator called ArcLight (Figure 1.17). This fluorescent protein is a derivative of wild type aqGFP that carries several mutations; the most important, a critical point mutation on the 680th position in the DNA, where the nucleotide Cytosine was replaced with Adenosine. This change caused substitution in amino acid sequence between Alanine (A)

and Aspartic acid (D) on the 227th position. In addition, with respect to the parental aqGFP, pH/fluorescence intensity of super ecliptic pHluorin A227D is basic-shifted. Luckily, the critical mutation does not alter the level of protein expression at the cellular membrane. [50]. The other mutations simplify the excitation spectra to a single peak at 490 nm wavelength, provide production of more stable fluorescent protein and increase the response magnitude [50]. The emission spectra reaches the highest value at 509 nm [55].

Compared to the previous variants of VSFPs, the improved variant of ArcLight, indicated as A242, displays larger changes (ca 5x) in fluorescence intensity in response to voltage changes. Thus, in response to +100mV depolarisation, fluorescent intensity decreases by up to +35%. One of the explanations for the fluorescence response of ArcLight-A242 may be a result of the A227D structural modification on the β-barrel of the super ecliptic pHluorin, which loosening allows fluorophore quenching. Concomitantly, the super ecliptic pHluorin may associate/disassociate with the plasma membrane upon a voltage change. The position of the voltage-sensing S4 domain during the resting state may allow dimerization of the two neighbouring super ecliptic pHluorins. Upon depolarisation, the movement of the S4 domain would disrupt dimerization and produce monomers, which then show reduced fluorescence. Also, movements that depend on the depolarisation may reversibly alter association of the super ecliptic pHluorin with the plasma membrane [56]. Nevertheless, the response kinetics still leaves a place for significant improvement. The slow component of the synaptic response is in a range up to 10 ms, while the fastest response of ArcLight is achieved within 50 ms [57].

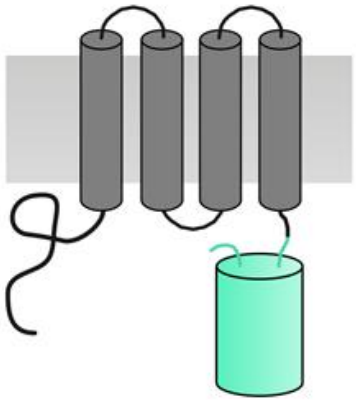

Figure 1.17 Scheme of ArcLight-A242 VSFP

ArcLight A242 VSFP contains *Ciona intestinalis* voltage – sensing domain (S1–S4 grey cylinders) crossing the plasma membrane. On the N-terminus, there is fused fluorescent protein probe named super ecliptic pHluorin A227D.

(Figure adapted from [42])

1.4.3. Butterfly 1.2

Since the VSFP have the potential for further functional customisation and optimisation, recently, a new probe named Butterfly 1.2, was introduced by the T. Knöpfel laboratory. [58]. It is created in a way that the voltage sensor domain of Ci-VSP is sandwiched between a mCitrine/mKate2 Förster resonance energy transfer (FRET) pair (Figure 1.18). The S4 transmembrane segment of the Ci-VSP is linked to the mCitrine donor, and the S1 domain to the mKate2 acceptor. The monomeric yellow fluorescent protein is the more intense variant of YFP. It reaches its maximum excitation at 514 nm, and emission at 529 nm [55]. Consequently, the emission from mCitrine donor directly excites the mKate2 acceptor, which achieves maximum emission at 633 nm [59]. This data imply that the novel probe exhibits a decrease in mCitrine (donor) and increase in mKate2 (acceptor) fluorescence emission as voltage–dependent FRET upon membrane depolarisation. The mCitrine/mKate2 FRET pair was chosen because it offers a larger Förster radius (5.8 vs 5.4 nm) [42] than previously used pairs, which means that the distance at which energy transfer is 50% efficient is larger [42]. Besides that, the red-shifted mKate2 spectrum has an advantage for avoiding green–blue tissue autofluorescence overlap.

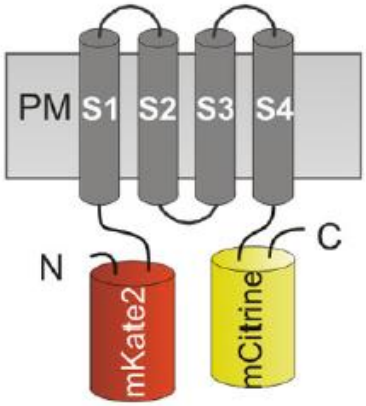

Figure 1.18 Scheme of Butterfly 1.2 VSFP

Similar to ArcLight, Butterfly 1.2 contains *Ciona intestinalis* voltage – sensing domain (S1–S4 grey cylinders). However, it is fused betwwen a FRET donor mCitrine (yellow barrel) on the C-terminus and acceptor mKate2 (red barrel) on the N-terminus.

(Figure adapted from [42])

With enhanced sensitivity features, it became the first genetically enhanced voltage indicator (GEVI) sufficient to report spontaneous neuronal activity in addition to initiated signal propagation [58].

The primary idea was to report subthreshold voltage fluctuations in targeted neurons, but besides that, it also enables optical recordings at high spatial resolution. It activates at more negative potentials than the previous VSFP variants, so the FRET response covers -140 to +60 mV of the voltage range [42]. According to the literature, it achieves maximal voltage sensitivity of 22% of ratiometric fluorescence per 100 mV and a response time of a fast component for single cell synaptic responses of 2 – 8 ms, and 10 – 90 ms for the slow component. In addition to all other features, it shows superior targeting to the plasma membrane and hence reduced optical noise (high signal–to–noise ratio), making it one of the best genetic tools for recording neuronal response [42].

1.5. Adeno – associated viral vectors

Adeno-associated virus (AAV) is one of the smallest single-stranded animal viruses with a non-enveloped capsid (22 nm). It belongs to the *Parvoviridae* family, which are Group II viruses according to the Baltimore classification [60]. Due to its inability to replicate and assemble viral particles in the absence of helpervirus (*Adenovirus* or *Herpes simplex virus*) it is often referred to as *Dependovirus* genus [61]. Nowadays, they are greatly used as a tool for gene transfer *in vivo*, as well as *in vitro*, due to their advantages over other vectors. They are ideal vectors for cell transduction in the CNS because of their non-pathogenicity, ability to infect non-dividing cells, significantly longer expression compared to other transduction vectors, little to no immunogenicity and lack of cytotoxicity [62].

1.5.1. The structure

AAV has a linear single-stranded DNA (ssDNA) genome, either positive or negative sensed, of approximately 4,7 kb enclosed with characteristic multipalindromic sequences termed inverted terminal repeats, ITR [60]. These 145 bp long palindromic repeats can fold on themselves via Watson-Crick base pairing into a hairpin shape [63]. They are positioned at each end of the viral genome and have multiple roles: they are required for efficient multiplication of the genome, for its integration into the cell, as well as rescue from it, and contribute to self-priming that allows primase-independent synthesis of the second DNA strand [64].

Two viral genes in the open reading frames (ORFs) that AAVs carry are *rep* and *cap*, encoding packaging and structural proteins. The four overlapping *rep* genes encode for regulatory proteins Rep78,

Rep68, Rep52 and Rep40, which are required in genome replication. All of them possess helicase activity, bind ATP and regulate the transcription from promoters [63]. The capsid proteins VP1, VP2 and VP3 are the products of *cap* gene expression [63]. Exactly 60 protein subunits interact together to form a capsid of an icosahedral symmetry in a ratio of 1:1:10.

1.5.2. Serotypes and native tropisms

Despite their common properties including genome size and organisation, numerous AAV serotypes have been identified with variable tropism. Naturally occurring AAV serotypes (1-9) primarily differ in surface properties of the capsid, which determinates tissue specificity. The overall level of amino-acid identity in their capsid protein is nearly 45% [65], but the serotype variability is not evenly distributed in the arrangement of individual proteins in the capsid shell. This variability in the serotype, which affects the difference in expression levels and duration of expression, is considered to be caused by variable domains that are displayed on the surface [65]. Thereby, they use different receptors and entry pathways to introduce their genome into cells.

Due to the variety of serotypes, AAVs have different transduction efficiency in different cell types. In the mouse brain, AAV1 and 5 are capable of transducing both neuronal and glial cells, while AAV2, 7, 8 and 9 appear to transduce neurons specifically [62]. However, concretely for the cortex region, AAV6 is among the highest rank of serotypes due to its ability to drive transgene expression [61]. Besides tropism, the kinetics of expression varies greatly between serotypes. AAV7 and 9 have the fastest onset of expression and AAV3 and 4 the slowest [65]. According to the experimental system, the region of the brain (for *in vivo* studies) or cell type (for *in vitro* studies), an appropriate serotype of AAVs has to be chosen to provide sustainable expression.

1.5.3. Life cycle

Infection with AAV is initiated when viral capsid proteins bind to cell proteins that serve as its receptors on the host cell plasma membrane [5]. AAV2 attachment to the cell membrane is currently the only serotype with a fully understood mechanism of AAV virion entry [63]. Broad tropism that AAV2 shows can partially be explained by usage of heparan sulphate proteoglycans as docking sites [66]. After entry into the cell, trafficking of AAV particles towards the nucleus involves receptor-mediated

endocytosis via the formation of clathrin-coated vesicles. Instead of being transferred from endosomes to lysosomes, as in the normal endocytic pathway, the virus escapes from the endosome. The viral capsid fuses with endosome membrane and releases the internalised virions into the cytosol [5, 63]. Due to their small size, they can access the nucleus through the nuclear pore complex [63]. In the nucleus, viruses can enter a latent state in the lysogenic cycle or an active state in the lytic cycle. The lytic cycle is established when there are helper viruses as well, like adenovirus or herpes simplex virus, while in lysogenic cycle this is not the case. Then, latency is ensured by preferential integration of the virus genome into a region of roughly 2 kb on the long arm of human chromosome 19 [67]. After the AAV gene expression is activated, AAV-Rap mediated excision of the virus DNA from the host cell chromosome is followed by replication and packaging. Cell lysis is induced and helper viruses and the newly assembled virions are released (Figure 1.19).

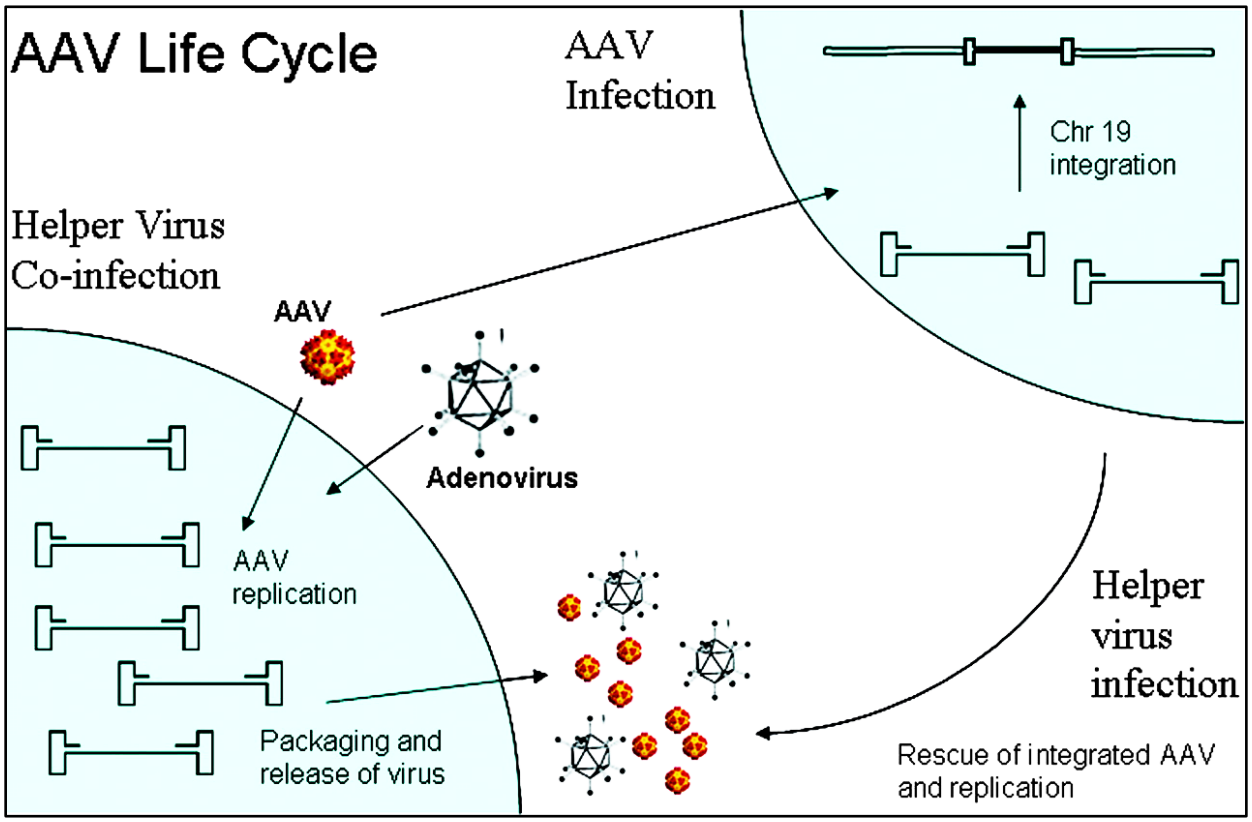

Figure 1.19 AAV life cycle.

Initiation of AAV infection in parallel with helper virus presence starts with capsid binding to the host cell membrane receptors. Afterwards, the genome is replicated and expressed, and new viruses packed and released. In the absence of helper viruses, AAV can establish latency by integrating into chromosome 19. Upon adenoviral superinfection, the AAV viral genome can further replicate.

(Figure originally published in [68])

1.5.4. Recombinant AAVs

The defective replication and non-pathogenic nature of wild-type AAV triggered the rapid development of recombinant AAVs (rAAV) as gene delivery vectors derived from AAV. They are single stranded vectors able to deliver genes to both dividing and non-dividing cells. In these vectors, the rep and cap genes are replaced with a gene-expression cassette flanked by ITRs (*cis*-plasmid), whereas the replication proteins and those required for replication are supplied by helper viruses in *trans* [60]. rAAV particles are generated by transfecting producer cells with *cis*-plasmid and a separate construct expressing in *trans* the viral *rep* and *cap* genes.

As in wild-type, rAAVs' limitation is small packaging size. Without loss of infectivity, only 4,7 kb [69] can be inserted into ss genomic AAV DNA (Figure 1.20). Because the rate–limiting step involves *de novo* synthesis of a second strand on the single-stranded genomic AAV DNA [70], the expression onset is delayed. The uncoiling of double helix DNA, thus, may be circumvented by the use of self-complementary (scAAV) vectors (Figure 1.20). Due to a mutation in one of the ITRs, the sense and antisense chains cannot dissociate. Therefore, although the size of the cassette is reduced by half (to 2,4 kb), onset of expression is improved, as well as increased expression levels [69].

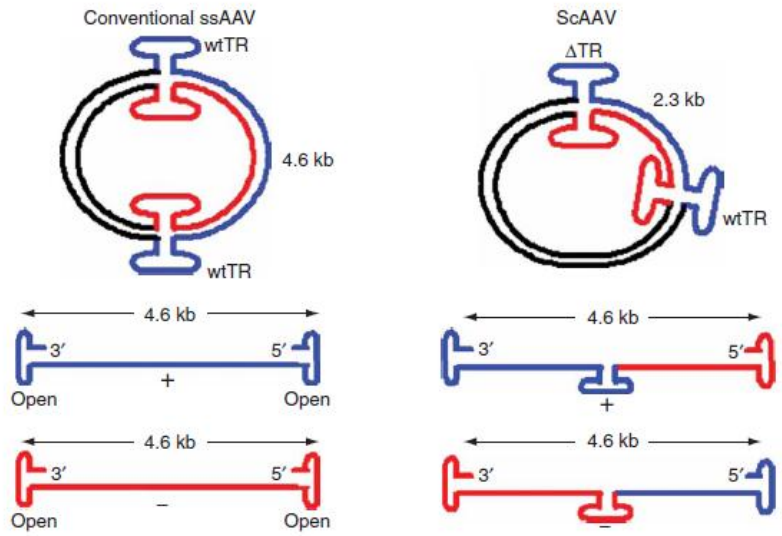

Figure 1.20 Comparison between conventional ssAAV and scAAV vectors

In the wild type, ssAAV vector, the coding and complementary sequences are on separate strands. In scAAV vectors, both sequences of the cassette are present on each strand of the genome. The blue and red line represent coding and complementary sequence of the transgene cassette, and black respresents the bacterial genomic backbone.

(Figure originally published in [71])

There are several ways to encapsulate rAAV plasmids. Their genome can be packaged with the capsid derived from wild-type; most commonly AAV2 because the mechanism of infection through heparan sulphate proteoglycan receptors is known [63]. Besides that, it can be pseudo typed with capsids from other serotypes or with genetically altered capsids, which increases the number of possible serotypes [69].

1.6. Aim of the study

The "gold standard" for investigating neuronal signalling is electrophysiology, the discipline founded on electrode usage in *in vivo* (living animals), as well as in *in vitro* (cell-culture) samples. The direct recording of the electrical activity and therefore, high signal-to-noise ratio is the main strength of the method. However, for the electrical access to the nervous system there is a necessity of physical contact with the investigated sample. Since it is a robust, cell-damaging method, it has been challenged by a new generation of optical probes. These probes are being developed in parallel with the new forms of microscopy, allowing measurements and control of neuronal signals with spatial resolution and genetic specificity. This way, there is no need for direct physical contact with the sample since the light travels through it and hereof, does not interfere with neuronal function.

The specific aims of the study:

- Design of the novel probes at DNA level by manipulating with their plasmid sequences
    - The final constructs consisted of hSyn; neuron-specific promoter before the coding sequence for the VSFP, flanked by two ITR, incorporated into plasmids which support rAAV packaging
- Recombinant AAV production
- Transduction of the rat cortical neurons by rAAVs and determination of its efficiency by fluorescent cells counting
- Determination of the optimal titer concentration and therefore optimisation of the transduction protocol
- Electrophysiology experiments on fluorescent neurons to validate VSFP functionality

2. MATERIALS AND METHODS

2.1. Cell culture

For the purpose of optogenetic experiments, two kinds of cultured cells were used as a model system. As the main cell type, we used primary neuronal cells that were directly prepared from a rat embryonic brain tissue. Besides those, the Human Embryonic Kidney (HEK293) cell lines served as an easily maintained culture for the fast control experiments. *E.coli* bacteria culture was obtained for recombinant DNA manipulation in order to produce plasmids. Prior to production of construct containing AAVs, we aimed to insert the foreign DNA containing the genes for voltage sensitive fluorescent proteins into cells using a chemical transfection reagent and an electroporation method (2.3).

2.1.1. Embryonic rat cortical neurons

Primary cortical neurons were obtained from pregnant Wistar rats at gestation day 18 under sterile conditions by laboratory technicians. All animals were sacrificed according to Landesumweltamt für Natur Umwelt und Verbraucherschutz Nordrhein-Westfalen §4 & 6 TierschG and §2 TierSchVerV on the protection of animals used for scientific purposes. Rat embryo brains have been dissected and stored in 1.5 ml Hank's Balanced Salt Solution ($HBSS^-$, without Ca^{2+} and Mg^{2+}, containing 0.035% sodium bicarbonate, 1 mM pyruvate, 10 mM 4-(2-hydroxyethyl)-1-piperazineethanesulfonic acid (HEPES buffer; Sigma-Aldrich) and 20 mM glucose 7.4 pH; Sigma-Aldrich) on ice. Isolated cortices without dura have been transferred to 7 ml $HBSS^-$ in a 15 ml Falcon tube on ice. Afterwards the cells were mechanically dissociated with a silanised, fire polished glass pipette, two volumes of HBSS+ (with Ca2+ and Mg2+), 0.035% sodium bicarbonate, 1 mM pyruvate, 10 mM 4-(2-hydroxyethyl)-1-piperazineethanesulfonic acid (HEPES buffer; Sigma-Aldrich) and 20 mM glucose 7.4 pH have been added. The cells were allowed to settle down for 3 min on ice. The top half of the preparation has been transferred to a clean tube and centrifuged at 200 g for 3 min. HBSS has been aspirated and the pellet resuspended in 1 ml supplemented Neurobasal® Medium 1x (NB) (Table 2). For providing live dead staining, the marker for dead cells, trypan blue (the standard volume of 25 µl) was diluted 1:2 in NB media. After adding 1 volume of cell suspension, the final mixture was 1:2:1 for trypan:NB:cell suspension. Live, non-coloured

cells were counted in a cytometer (Neubauer chamber) and diluted to the appropriate plating concentrations in NB. For the purposes of our experiments, the cells were plated onto sterilised 15 mm in diameter glass coverslips in 12-well plates. The coverslips have been coated with the mixture of poly-D-lysine (PDL) : Extracellular matrix (ECM) : Gey's Balanced Salt Solution (GBSS) at 1:1:100 and left for 1 h at room temperature (RT). Additionally, they have been washed with 0,5 ml GBSS. After distribution to substrates, the cells, in the final concentration of 50k or 75k have been left for 10 min at RT and then transferred to a 37˚C, 5% CO_2, humidified incubator. After 1-4 hours, NB was aspirated completely and replaced with fresh supplemented NB. Half of the media was replaced with fresh, warm NB media twice per week.

Table 2. Neurobasal medium (NB) contents

Substance	Contribution	Company
NB medium	98.65% / 5 ml	Gibco® by Life Technologies, USA
B-27 supplement	1% / 50 µl	Gibco® by Life Technologies, USA
L-Glutamine	0.25% / 12,5 µl	Gibco® by Life Technologies, UK
Gentamicin	0.1% / 5 µl	Sigma-Aldrich, Germany

2.1.2. HEK293 cell line

Human Embryonic Kidney 293 (HEK293) cells are a well-established, cell line derived from human embryonic kidney cells grown in tissue culture. They serve as a mammalian expression tool for recombinant proteins due to their capability of carrying out the post-translational folding processes to generate functional proteins. Their wide usage in electrophysiological studies has been based on their quick and easy reproduction cycles (approximately once per day), good survival after transfection, high efficiency of transfection and functional protein expression, as well as their morphology and cell size appropriate for patch-clamp experiments.

The listed attributes of the HEK293 cell line facilitate the selection of an expression system for validation of the new protein construct. The cells were maintained in Dulbecco's Modified Eagle Media (DMEM) + Glutamax (Gibco® by Life Technologies) supplemented with 10% fetal bovine serum (FBS) and penicillin/streptomycin, in T-25 tissue culture flasks, incubated at 37˚C with 5% CO2 in a humidified incubator. The confluent culture was washed with 1 ml pre-warmed trypsin EDTA (0.0025%

concentration) and then aspirated. Adherent cells were detached from the flask by adding a new portion of 1 ml pre-warmed trypsin for an incubation time of 5 min at 37˚C. Afterwards, trypsin inactivation was done by adding 5 ml of freshly prepared media to the cell-trypsin mixture. The complete flask contents were transferred to a tube and spun for 5 min at 1200 rpm in a centrifuge. The liquid supernatant was completely aspirated, and the cell pellet was resuspended with 1 ml of pre-warmed media by pipetting up and down. $8x10^4$ cells were plated in a new T-25 flask in a final volume of 5 ml. Onto poly-L-lysine (PLL) coated glass coverslips 400 cells were plated. These cells were transfected with the new protein constructs (2.3.1). The cells were investigated by patch-clamp experiments 4 days post transfection (DPT4).

2.1.3. *Escherichia coli* bacteria culture

E. coli cells, as the most common model organism used for experiments in molecular biology, were used for a variety of DNA manipulations. The chemically competent One Shot® TOP10F´ strain (Invitrogen™ by Life Technologies™), with the addition of an F' episome, provide high-efficiency cloning and plasmid propagation.

For the purpose of plasmid amplification, the following transformation procedure was performed. For each transformation reaction, one vial of One Shot® TOP10F´ was placed on ice. To transform, 1 µg of plasmid DNA was added directly to the competent cells and mixed by tapping gently. The mixture was incubated on ice for 30 min, followed by 30 s incubation in the 42˚C water bath. Then, the vials were placed on ice. 250 µl of rich, pre-warmed Super Optimal broth with Catabolite repression (SOC) medium was added in each vial. The vials were placed at 37˚C for 1 hour at 225 rpm in a shaker-incubator (Eppendorf Thermomixer® comfort). From each transformation vial, a volume of 10 µl to 50 µl was spread on labelled Luria Broth (LB) agar plates containing Ampicillin antibiotic (Sigma-Aldrich) for selection of positively transformed cells, or directly into liquid LB medium containing Ampicillin. The plates were incubated at 37˚C overnight. Afterwards, the plasmid extraction was done depending upon the inoculated volume of liquid LB medium with Mini, Midi or Maxi prep plasmid extraction kits by Qiagen.

2.2. Molecular cloning – construction of the plasmids

In order to create enhanced DNA constructs of the GEVIs, the VSFPs were cloned behind the strong constitutive *human cytomegalovirus (HCMV)* or neuron specific human synapsin-1 (hsyn1) promoters. Consequently, varieties of strategies were used. This chapter describes them briefly.

All DNA constructs were produced in One Shot® TOP10F´ *E.coli* strain (Invitrogen™), transforming them following the manufacturer's protocol. The positive clones were verified first by test-reaction with restriction enzymes. The cut DNA fragments have been separated by their size by the process of gel electrophoresis. The 1% gels were made of agarose (Sigma-Aldrich®) dissolved in 1x Tris/Acetate/EDTA (TAE) buffer. Before polymerisation, after the diluted agarose was poured into the chamber, a fluorescent nucleic acid stain (GelRed™, Biotium) was added in ratio 1:10000. The electrophoresis was performed at standard voltage conditions (8 V/cm). DNA fragments were visualised with an ultraviolet (UV) transilluminator. In the downstream procedures, the desired DNA fragments at proper position on the gel have been cut, diluted, and purified by GenElute™ Gel Extraction Kit (Sigma-Aldrich®), according to the manufacturer's protocol. The isolated plasmid DNA was resuspended in MilliQ water to a final concentration of 0.5 – 1.4 µg/µl and stored at -20˚C. Subsequently, they were verified by sequencing (Eurofins MWG Operon, Ebersberg, Germany).

2.2.1. psc_hSyn1_ArcLight

The psc_hSyn1_ArcLight plasmid was created by insertion of the coding sequence of ArcLight from the plasmid ArcLight-A242 (plasmid 36857, Addgene) into psc_hSyn1 plasmid (a gift from the Baumann Lab, Forschungszentrum Jülich GmbH). ArcLight was cut out of ArcLight-A242 using the restriction endonucleases HindIII/EcoRI (Thermo Scientific) in R buffer (Thermo Scientific). The same procedure was applied for the psc_hSyn1 plasmid, with exception of using SacI/EcoRI restriction enzymes in BamHI buffer (Thermo Scientific). The reactions were performed for 1h at 37˚C at 300 rpm in a microtube shaking incubator (Eppendorf Thermomixer® comfort). Fragments were separated by agarose gel electrophoresis, cut, and extracted by GenElute™ Gel Extraction Kit (Sigma-Aldrich®).

Afterwards, purified ArcLight fragment was added to an extra sequence coding for introduced restriction sites, SacI on the 5' end and EcoRI on the 3' end by polymerase chain reaction (PCR) (Table 3) using KOD Hot Start Polymerase. In order to create an optimal Kozak consensus sequence in 5'-forward

primer, an extra codon GAG was inserted immediately after the start codon (ATG). Primers used for this amplification reaction were:

(fwd) 5'-AAAAGAGCTCCCACCATGGAGGGATTCGACGGTTC-3' SacI Kozak Start codon

(rev) 5'-TTTTGAATTCTCATTTGTATAGTTCATCCATG-3' EcoRI

Table 3. PCR reaction contents and procedure

PRC reaction contents				
5 µl	10 Buffer	**PCR reaction procedure**		
5 µl	dNTPs (final 0,2 mM)	94˚C	3 min	
2 µl	$MgSO_4$ (final 1 mM)	94˚C	1 min	
50 ng	Template (ArcLight)	54˚C	45 s	30x
5 µl	5' primer	72˚C	1 min	
5 µl	3' primer	72˚C	5 min	
1 µl	KOD Hot Start Polymerase			
26 µl	H_2O to a final volume of 50 µl			

Immediately after the PCR reaction, the insert (ArcLight) was subjected to gel electrophoresis, cut out from the agarose gel and extracted via Gel-extraction (Gel and PCR Clean-up, Macherey Nagel). Then, it was cut with EcoRI/SacI restriction enzymes. After restriction, the fragment was purified via PCR Clean-up (Gel and PCR Clean-up, Macherey Nagel). After having purified DNA of both, the insert (ArcLight) and the plasmid backbone (psc_hSyn1) with cohesive sticky ends; SacI and EcoRI, they were ligated (Figure 2.1). Ligation reaction was performed using the Rapid DNA Dephos & Ligation Kit (Roche) with a ratio of insert/vector of 0.47.

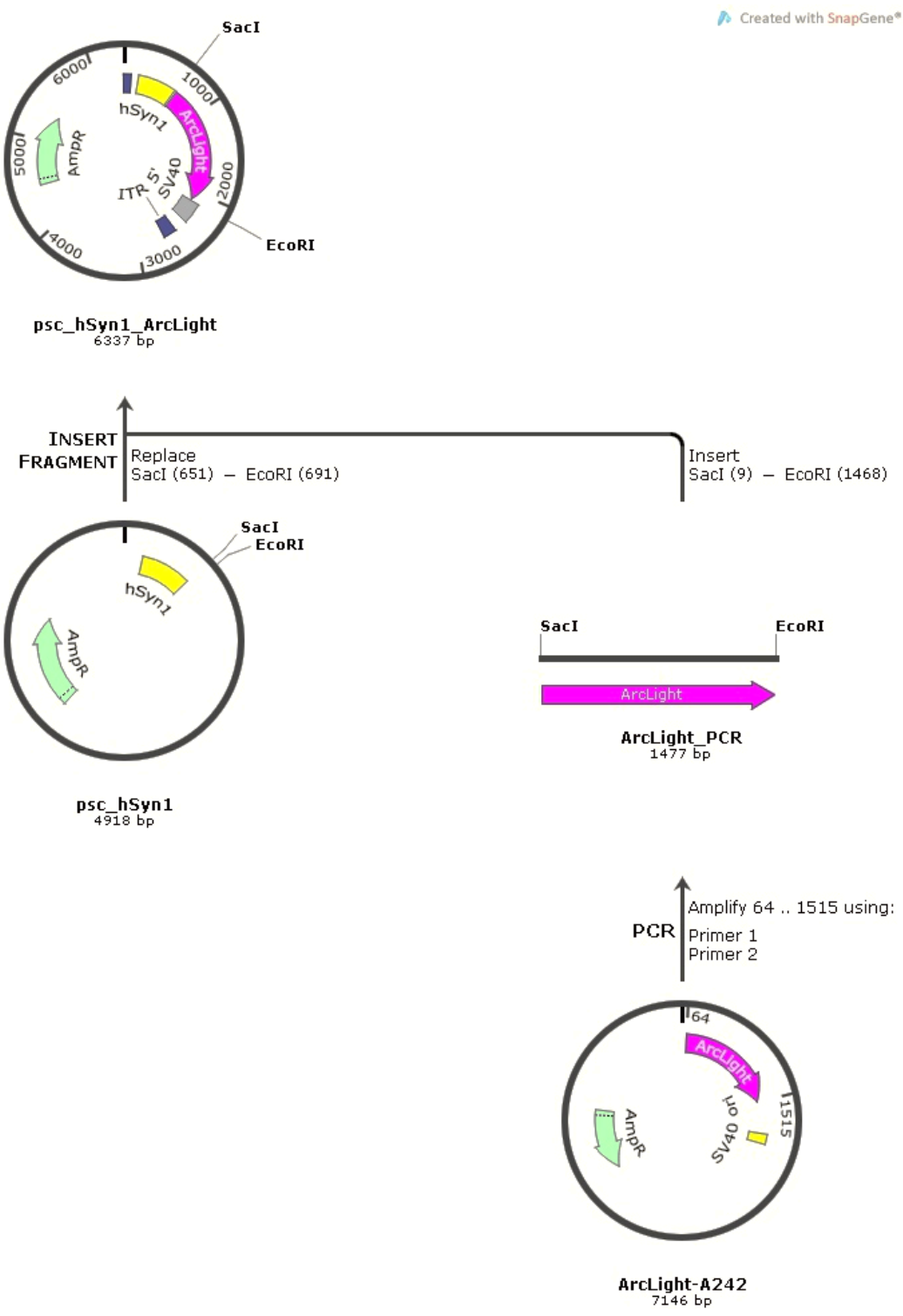

Figure 2.1. Molecular cloning scheme of psc_hSyn1_ArcLight plasmid

Psc_hSyn_ArcLight plasmid was produced in a way that psc_hSyn plasmid was opened with SacI/EcoRI restriction enzymes. From the ArcLight-A242 plasmid, the ArcLight coding sequence was first multiplied by PCR with designed primers that introduced new restriction sites: SacI and EcoRI. Afterwards, this sequence, cut by SacI/EcoRI was ligated into open psc_hSyn plasmid.

2.2.2. pSub_hSyn1_Butterfly

In order to create the pSub_hSyn1_Butterfly plasmid, the coding region of the Butterfly VSFP from the pCAG_Butterfly plasmid (a gift from the Knöpfel Lab) was inserted into pSub_hSyn1_eGFP plasmid backbone (given by ICS4). Butterfly was cut out of the pCAG_Butterfly plasmid by BamHI/XbaI restriction enzymes (Thermo Scientific). The backbone, in turn, was cut only with BamHI (Thermo Scientific), aiming to excise the *eGFP* coding sequence. The reactions were performed for 1h at 37˚C at 300 rpm in microtube shaking incubator. Fragments were separated by agarose gel electrophoresis, cut and extracted by GenElute™ Gel Extraction Kit (Sigma-Aldrich®).

Due to their overhanging end-incompatibility, a blunt-end cloning strategy was performed Figure 2.2). In the first reaction, sticky ends on separate fragments were filled with compatible nucleotides in separate reactions for each fragment by T4 DNA polymerase (Fermentas Inc.) for 10 min at 37˚C. The vector was dephosphorylated in the same reaction when both blunt-ended fragments were ligated by the kit Rapid DNA Dephos & Ligation Kit from Roche for 10 min at 17˚C (Figure 2.3).

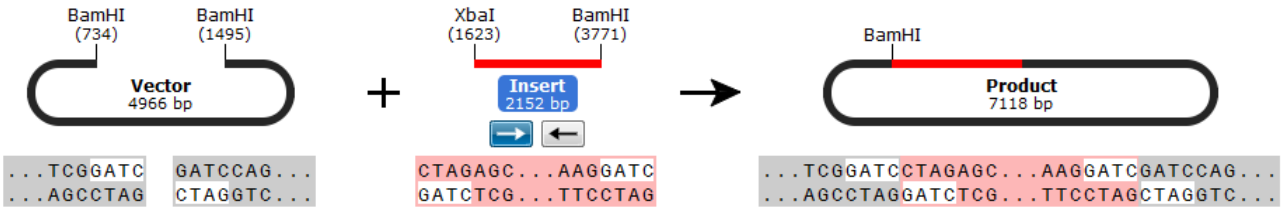

Figure 2.2 Molecular cloning scheme (1) of pSubc_hSyn1_Butterfly plasmid: blunt end ligation

Psc_hSyn_Butterfly plasmid was produced in a way that pSub_hSyn_EGFP plasmid was cut by BamHI restriction enzyme, which resulted in EGFP excision. Butterfly sequence was cut by BamHI/XbaI from pCAG_Butterfly plasmid. Since the overhanging ends were not cohesive, they had been filled with nucleotides aiming to blunt end production. Finally, the backbone and the insert fragment were ligated in the new plasmid.

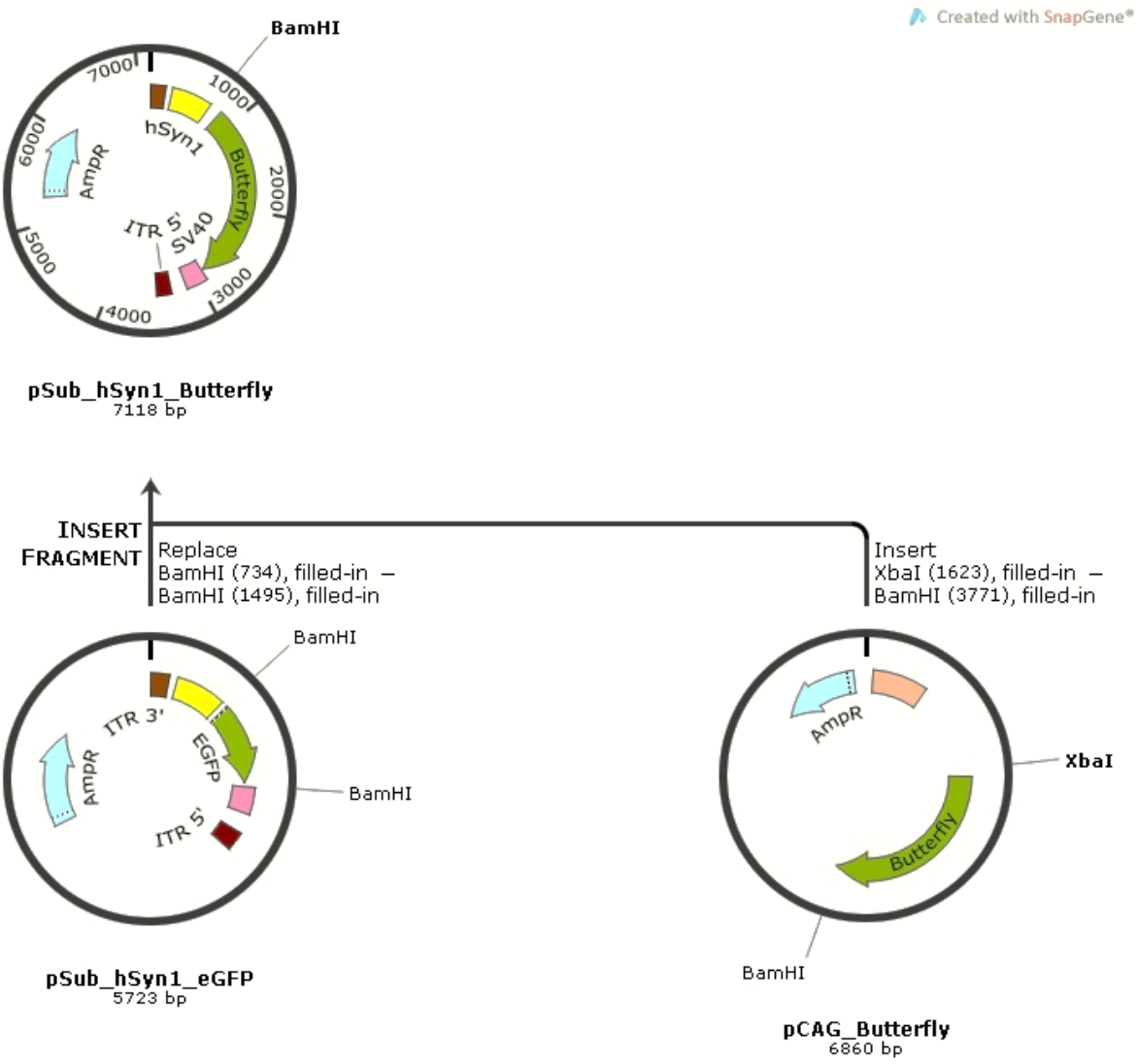

Figure 2.3 Molecular cloning scheme (2) of pSubc_hSyn1_Butterfly plasmid: general overview

Psc_hSyn_Butterfly plasmid was produced in a way that pSub_hSyn_EGFP plasmid was cut by BamHI restriction enzyme, which resulted in EGFP excision. Butterfly sequence was cut by BamHI/XbaI from pCAG_Butterfly plasmid. Since the overhanging ends were not cohesive, they had been filled with nucleotides aiming to blunt end production. Finally, the backbone and the insert fragment were ligated in the new plasmid.

2.3. Recombinant DNA insertion

The vectors that were made, consisting of an insert and the plasmid backbone, were inserted into the target cells (2.1) by three different insertion methods. Recombinant DNA, taken by the recipient cells, has the purpose to transfer genetic information and afterwards, to express the insert. Hence, the genetically modified cells will be given new characteristics that can be used for further experiments.

At first, the characterisation of VSFP was provided by inserting the recombinant DNA into the cells by chemical transfection and electroporation. For these insertion methods sufficient is, besides reagents and device, only pure DNA, so they are simple and fast to maintain. While the DNA construct was verified for proper protein production, despite low transfection rate of these methods, the VSP were afterwards characterised on the cells transduced by rAAVs. According to the previous methods described, it has certain advantages. Since it does not show cytotoxicity, the transduced cells show better viability, among the high translation rate.

2.3.1. Chemical transfection

For transfection of the cortical neurons and HEK293 cells, nonliposomal FuGENE® HD Transfection Reagent (Promega) was used. The transfection parameters, as recommended in the protocol by the supplier, were optimised for each cell type. The complete protocol is described here.

For the preparation of transfection aliquots for a 12 well plate (see below), 0.75 µl of FuGENE® Transfection Reagent per well was mixed with NB medium for neurons and HEK293 cells (up to 50 µl) in the eppi, reducing the contact with plastic (the sides of the tube). The FuGENE® Transfection Reagent/NB medium mixture was vortexed for 1 s and afterwards, incubated for 5 min at RT. The maximal recommended rate FuGENE:DNA 3:2 was used; 0.5 µg of DNA per well added to the previously prepared mixture. The FuGENE® Transfection Reagent/DNA mixture was vortexed for 1 s and incubated for 15 min at RT. The total volume of prepared mixture per well was 50 µl.

The adherent cortical neurons were plated on the coated coverslips in the final concentration of 50k one week before, and 0.5% of the confluent HEK293 cells on the day of transfection. Before the procedure of transfection, ¾ of the cell media was removed and stored for later use. Thereafter, 50 µl of FuGENE® Transfection Reagent/DNA mixture was added drop wise to each well in the plate. The plates were swirled to ensure equal distribution and placed into the incubator at 37˚C and 5% CO_2 for 1 hour.

Afterwards, the mixture was removed completely in order to increase cell survival and viability rate and to decrease the damage caused by the nonspecific transport of molecules into the cells. Wells were refilled with ½ of the old, stored media and ½ of the freshly made media.

2.3.2. Electroporation

Electroporation is another method used for recombinant DNA introduction into mammalian cells. The permeability of the plasma membrane is caused by an externally applied electrical field. Thus, the following procedure was used.

The supplemented transfection solution (TS) was prepared according to the manufacturer's recommendations (Lonza Amaxa™ Rat Neuron Nucleofector). A cuvette was preloaded with 10 µg of recombinant DNA. The cell suspension of 10^6 cells was prepared. They were spun down for 2 min at 200 g. Afterwards, the supernatant was removed and the pellet resuspended in 100 µl TS. The cells were quickly transferred to the transfection cuvette. The cuvette was placed in the electroporator (Lonza Amaxa™ Nucleofector) and program G-013 "Neurons – Chicken DRG" was applied. For neuronal recovery, 1 ml of supplemented RPMI (see Table 4) was added to the cuvette. The complete mixture (cells & RPMI) was transferred to a falcon tube using the Pasteur pipette provided in the kit. Counted cells were plated 50k per substrate onto the coated coverslips in a 12-well plate. The media was replaced by NB medium after 1 hour of adhesion.

Table 4. Supplemented RPMI contents

Substance	Contribution	Company
RPMI medium	98,75%	Lonza Amaxa™, Cologne, Germany
L-Glutamine	0,25%	Gibco® by Life Technologies, UK
FBS	1%	Sigma-Aldrich, Germany

2.3.3. AAV transduction

Recombinant AAVs, produced by the Baumann Lab, Forschungszentrum Jülich GmbH, were used as a transduction vector for inserting recombinant DNA into the cortical neurons. The viral stocks, in a final concentration of 5.07 x 10^7 for rAAV_psc_hSyn1_ArcLight and 2.14 x10^9 for rAAV_pSub_hSyn1_Butterfly, were stored at -80˚C in the freezer and thawed before usage. The cells were plated onto sterilised and coated glass coverslips in 12-well plates, as described in 2.1.1. At the DIV7, they were transduced with 2k of virus particles per cell (vp/cell); the calculated volume of rAAVs was added to the cell media, so it achieved the desired multiplicity of infection (MOI). Afterwards, the usual care for neuronal cells was maintained, what included replacing half of the NB media twice per week. As the negative control, iodexanol, in which rAAVs were purified, was added to the cell medium.

Table 5. List of used reagents and their suppliers

Reagents	Suppliers
NB medium	Gibco® by Life Technologies, USA
B-27 supplement	Gibco® by Life Technologies, USA
L-Glutamine	Gibco® by Life Technologies, UK
Gentamycin	Sigma-Aldrich, Germany
GBSS	Sigma-Aldrich, Germany
RPMI medium	Lonza Amaxa™, Cologne, Germany
Penn/Strep	Gibco® by Life Technologies
FBS	Sigma-Aldrich, Germany
ECM gel	Sigma-Aldrich, Israel
HBSS	Sigma-Aldrich, Germany
PDL	Sigma-Aldrich, Germany
PLL	Sigma-Aldrich, Germany
SOC	Invitrogen™ by Life Technologies
Ampicillin	Sigma-Aldrich, Germany
DMEM	Gibco® by Life Technologies, UK
Trypsine 0,05%	Gibco® by Life Technologies, UK
LB	Sigma-Aldrich, Germany

2.4. The electrophysiology measuring setup: Voltage-clamp fluorometry technique

In the electrophysiology measurements, with the aim of correlating the changes in membrane potential and fluorescence intensity in live transgenic cortical neurons, the voltage-clamp fluorometry was used. This biophysical technique combines simultaneous patch-clamp as an electrical recording and optical recordings of fluorescence. The following section describes each part separately.

2.4.1. Optics

The core of the system is a Zeiss Axio Scope.A1 upright microscope with HXP 120V mercury arc lamp and Carl Zeiss 12V 100W Power Supply halogen lamp as a standard and fluorescent light sources. The microscope is linked to the Andor Zyla sCMOS camera with water-cooling that keeps the camera temperature at 0˚C for low noise. Objective lenses Achroplan (Zeiss) W 20x/0.5 and W 10x/0.3 (magnification/NA) were used. With the tube lenses of 1,6x and 4x, additional magnification and re-inversion of the images was obtained.

The primary filtering element is the set of three filters housed in a fluorescence filter cube (Figure 2.4). For imaging of ArcLight and Calcein, a Zeiss filter set 09 HE was used. It was consisted of bandpass excitation filter 450-490 nm, a dichroic beam splitter at 510 nm and a longpass emission filter of 515 nm. Butterfly, in turn, was imaged with a Zeiss filter set 15 HE; a bandpass excitation filter 520/44 nm, a beam splitter at 580 nm and a longpass emission filter of 593 nm (Table 6).

Table 6. The list of filters and accompanying wavelengths

Channel	**ZEISS filter**	**Excitation filter**	**Beam splitter**	**Emission filter**
DIC	Epi DIC	n.a.	n.a.	n.a.
Green	09 HE	BP 450-490	BS 510	LP 515
Red	15 HE	BP 520/44	BS 580	LP 593

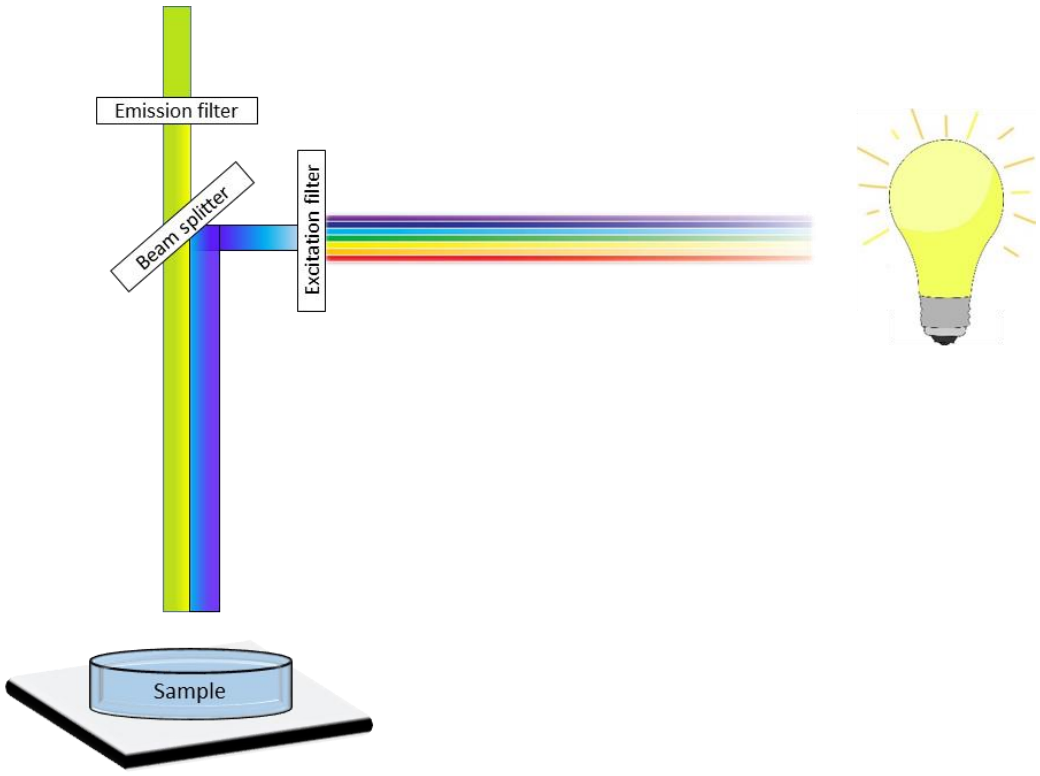

Figure 2.4 Schematic depiction of the illumination path in VCF setup

As a light source, there is halogen or mercury lamp. Light from the illumination source is directed to the excitation filter, which attenuates longer wavelengths and transmits shorter wavelengths over the active range. The dichroic beam splitter reflects it through the objective towards the sample, which is then excited by the specific wavelength. Consequently, the emitted fluorescence is transmitted through the beam splitter towards the emission filter, while the excitation light is blocked. Light passed through the emission filter is measured with the camera.

The optical recordings were performed at a resolution of 512x512 pixels and 2x2 binning in a global shutter mode. For image capture and analysis, the Andor Solis software platform version 4.23.30002.0 was used. It provides the user full control over the camera, including pixel readout rate, exposure time, triggering options etc. To chart quantities in real time, the software's region of interest (ROI) feature, was used manually select the area of the patched cell.

2.4.2. Electronics

For electrical stimulations and recordings of the signals, EPC10/3 (HEKA Elektronik, Germany) patch clamp amplifier was used. It is operated by the TIDA software (HEKA Elektronik, Germany). Technically, it has a special feature of series-resistance compensation functions for the pipette offset (C_{fast} and C_{slow}) and the extremely wide brandwith of 100-15000 Hz [72].

Mechanically, the whole setup was placed on the vibration isolation table inside the grounded Farady cage, for reducing the ambient electrical noise picked up by the electrodes. The recording micropipettes were glass capillaries, coated and heat-polished (Sutter Instrument Co.). They were pulled in a pipette puller (Shutter instrument Co.) and showed the resistance of 5-7 MΩ. When filled with intracellular patch (IP) solution (Table 7), they were attached to the probe containing the silver/silver-chloride measuring electrode. The probe, which is mounted on a micromanipulator (Luigs & Neumann SM-I), enabled movement of these components in three axis (x, y and z). For the microscope movement in z direction, a micromanipulator was also used (Luigs & Neumann SM-8).

Table 7. Extracellular and intracellular patch solution contents

Intracellular patch solution (V = 100 ml, 260 mOsmol/kg, pH 7,3)			
Substance	Mr [g/mol]	Final concentration [mM]	Initial weight [g]
NaCl	58,44	2	0,01178
KCl	74,56	120	0,891
MgCl2	203,3	4	0,081
Hepes	238,31	5	0,119
EGTA	380,4	0,2	0,008
Na-ATP	551	4	0,22044
Extracellular patch solution (V = 1l, 248 mOsmol/kg, pH 7,3)			
NaCl	58,44	120	7,013
KCl	74,56	3	0,224
$MgCl_2$	203,3	1	0,203
Hepes	238,31	10	2,383
$CaCl_2$	110,99	2	0,222

The cells were electro physiologically examined in the described setup at the earliest DIV14, i.e. DPT7. The first step in the sample preparation entailed checking the osmolarity of the cell media in the cryoscopic osmometer (Gonotec Osmomat® 030). In order to prevent osmotic stress for the cells, extracellular patch (EP) solution with theoretical osmolarity of 248 mOsmol/kg (Table 7), was adjusted to the NB media level by adding certain amount of D-(+)-Glucose (Sigma-Aldrich). This calculation was done by the following formula:

$$m(glc)[g] = V_{EP}[l] \cdot \left\{ (osmolarity_{NB} - osmolarity_{EP}) \left[\frac{Osmol}{kg}\right] \right\} \cdot Mr(glc) \left[\frac{g}{mol}\right] \qquad \textit{Equation 6}$$

where m(glc) represents the mass of the glucose (glc), V volume and Mr(glc) molecular mass of glucose.

Afterwards, the glass coverslips with the cells were glued to the 35 mm petri dish with vacuum grease. The dish was filled with adjusted, warm EP solution. The micropipettes were filled with IP solution. The experiments were performed at RT in the dark, due to the bleaching sensitivity of VSFPs. After the fluorescent cell was clamped in the whole-cell voltage-clamp (VC) mode, the resting potential was set at -70 mV. C_{FAST} and C_{SLOW} compensation was set before opening the cell. Afterwards, compensation of R was done as well. The standardised VC check protocol was used to check the responsiveness of the cell to the electrical stimulation (7.3.1). Afterwards, the electrical recording, by TIDA 5.25 software, was triggered directly by the starting signal of optical recording in the Andor Solis software for the Andor Zyla camera, through the transistor-transistor-logic (TTL) signal.

For simultaneous voltage recordings and current stimulations, two channels in HEKA EPC10 amplifier were used. The stimulation protocol (Figure 2.5; code in 7.3.2), where the membrane potential was stepped from resting potential to the holding potential by 10 mV increment and then stepped back to the resting potential, was designed according to the applied exposure time in ms. It included the initial recording at the resting potential in duration of 10x exposure time, followed by a loop that was repeated 26 times. Each loop differed from the previous by 10 mV increases in voltage, in duration of 6x exposure time. Finally, the last step included 10x exposure time long recording at the holding potential. The designed protocol included a 50 ms pause after every of 26 loops.

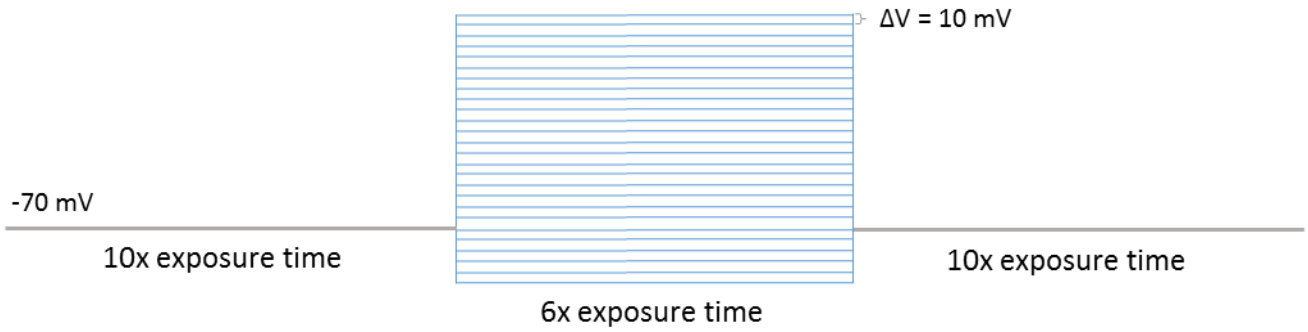

Figure 2.5 Visualisation of the stimulation protocol

By starting the optical measurements on Andor Solis software, it triggered the electrical stimulation and recording through the TTL signal. The first recording phase is at the resting potential in duration of 10x exposure time. The loop, repeated 26 times, in each cycle increased holding potential for 10 mV, compared to the previous loop. Each loop ended with recording at the holding potential in duration of 10x exposure time.

As an alternative approach, the cells were chemically stimulated by adding potassium chloride (KCl) drop wise instead of electrical stimulation. 0.15 M KCl was added manually in 5 portions of 100 µl, in a time span of 5 s per each. Addition of KCl transiently increases local concentrations of K^+ ions and therefore, induces depolarisation of the cell membrane. In turn, this is expected to cause the change in fluorescence intensity. In this case, only optical recordings were obtained.

2.4.3. Data analysis

The cell stimulation efficiency was observed by the change in fluorescence intensity and afterwards analysed using Andor Solis's hand-mediated ROI feature and Origin. The background was first subtracted from the raw data of the ROI. The resulting curve of the fluorescence intensity over time was smoothened by Savitzky-Golay method applied in Origin. Afterwards, the curve has been fitted to linear plot to eliminate bleaching effect. F_0 was determined as the mean value of all data points prior and after the signal occurrence. With this variable we have been able to determine $\Delta F/ F_0$ parameter as a measure for maximal change in fluorescence due to the basal fluorescence applying the following equation:

$$\frac{\Delta F}{F_0} = \frac{F_{max} - F_0}{F_0}$$ *Equation 7*

Considering this parameter we have been able to calculate another; signal-to-noise ratio (SNR). The ΔF/ F_0 value was divided by standard deviation (SD) of F_0:

$$SNR = \frac{\frac{\Delta F}{F_0}}{SD(F_0)}$$ *Equation 8*

2.5. Live cell imaging setup

For the observation of the transduced cells (2.3.3) expressing VSFP in real-time, the ZEISS live cell imaging setup was used. The setup includes an inverted microscope and the camera. The cells on the transparent substrates, glass coverslips, were placed in the 35 mm petri dish and filled with warm EP solution. Recordings of the cortical neurons expressing ArcLight A-242 VSFP were performed in the FITC/AF488 channel. This channel uses filter set 38 HE GFP with the excitation filter BP 450-490, emission filter BP 500-550, and beam splitter BS495. The light source was set to 100% intensity and the exposure time was 20 ms. The used magnification was 40x, with the air objective LD Plan-Neofluar with the numerical aperture 0.65. The collected data were saved as ZEISS .czi files and analysed in Zen software using a manually set regions of interest (ROI).

3. RESULTS

3.1. Molecular overview of the constructs

As a result of the molecular cloning, the desired recombinant DNA molecules were assembled, aiming for the recombinant protein production. Both of the constructs, ArcLight-A242 and Butterfly 1.2 are coding for VSFP. In order to improve and enhance their properties for the experimental system we use (primary cortical neurons), they have each been incorporated into a plasmid behind the neuron-specific hSyn1 promoter.

From the starting idea of making functional VSFP constructs till their performance, we have been struggling with a variety of issues. The two original plasmids, ArcLight-A242 and pCAG_Butterfly, have needed a promoter addition/exchange in order to adjust them for our purpose. As a first step, there was an addition of the HCMV promoter in front of the both VSFP coding sequences and their incorporation into sc plasmid. HCMV is a strong promoter used to drive the transgene expression in mammalian cells. Since it is not type-specific, it can equally promote the expression in any kind of cells; gradually, however, becoming silenced. The new plasmids, psc_HCMV_ArcLight and psc_HCMV_Butterfly, were constructed in a short time and in relatively easy few steps of standard restriction enzyme digestion (HindIII/EcoRI for ArcLight and BamHI/EcoRI for Butterfly) and cohesive-end ligation. Afterwards, they have both been validated in order to produce functional fluorescent proteins by chemical transfection of HEK293 cells. Since it was so, the rAAV production with these two constructs seemed a reasonable step for achieving less harmful and more specific insertion of recombinant DNA, and higher expression rates of the proteins. Hereby, we become acquainted with the issue of the limited size of the construct suitable to be used for rAAV production. We have been warned by the collaborators in charge for rAAV production that the observed limitation in the insert size is smaller than published values (~2 kb). Our vector (sc), in which we have incorporated recombinant DNA, can accept only 2.4 kb (as mentioned in 1.5.4). Since the size of the HCMV promoter is ~570 kb, and Butterfly is 2053 kb, it was clear that we have been compelled to search for alternative solutions to achieve the viral production. In such a way, the conceived alternative involved a new design of the construct. Due to the unsuitability of the self-complimentary vector according to the size of our recombinant DNA insert, we have decided to exchange it for an ss vector (described in 1.5.4). Into its single-strained genome, 4.7 kb of the recombinant DNA can be inserted. Since the expression takes longer than for sc vector due to the

second strand synthesis, the strong promotor (such as HCMV) that drives the transgene expression would be desired. However, there is the second issue that remained – lack of expression specificity. To address that, we have chosen the hSyn1 promoter instead of HCMV. In addition to its smaller size, ~450 kb, which gives us more space for the transgene, it has certain advantages in specificity. This promoter restricts transgene expression exclusively to neurons, which means that one could be able to distinguish different cell subpopulations (e.g. neurons and glial cells) by fluorescence and thus, specifically patch only neurons expressing VSFPs. This way, we enabled rAAV production by overcoming certain packaging limitations as well as the cell-specific recombinant DNA expression.

3.1.1. psc_hSyn_ArcLight construct

The idea of a new ArcLight construct (Figure 3.1) was to incorporate it into a sc vecor. The sc vector structurally contains double stranded DNA, bypassing the requirement for the second strand synthesis. Due to that, the size of the potential recombinant cannot exceed 2.4 kb in between ITRs; hereby, our ArcLight construct fits perfectly (1.4 kb). In the plasmid, it is positioned behind the hSyn1 promoter that drives neuron-specific expression. Downstream of the ArcLight VSFP sequence, there is a region of *Simian virus 40* PolyA (SV40) that enables the nuclear import of a plasmid by adding a PolyA tail to the mRNA. Among other functions, it terminates the transcription activity. Due to the rAAV production, the construct has to be flanked by two 145 nucleotide-long ITRs on 5’ and 3’ end. Since the ITRs are the “hot spot” of the genome instability, they have to be checked by the restriction enzyme digestion. As a selection marker for the positive-clone selection during the cloning procedure, inside the plasmid, there should also be an Ampicillin resistance gene.

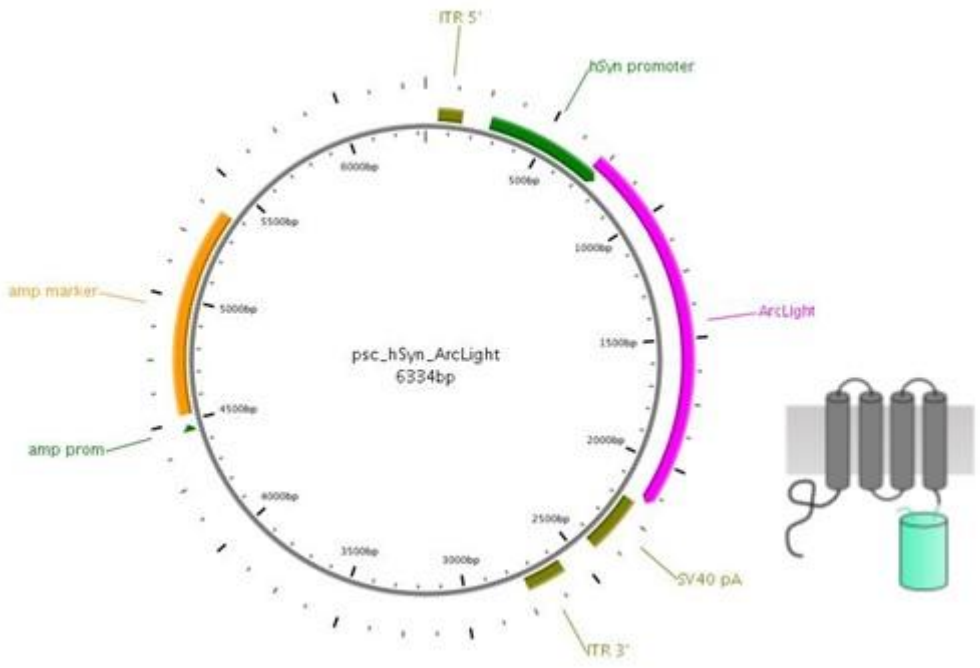

Figure 3.1 Map of the psc_hSyn_ArcLight plasmid

A plasmid map shows two ITR sites on each end of the construct; the hSyn promoter followed by ArcLight-A242 VSFP sequence and SV40 PolyA site. The plasmid also contains an Ampicillin resistance site as the selection marker. Expressed and inserted into membrane, ArcLight-A242 VSFP is schematically shown on the right.

The ArcLight-A242 VSFP construct was made by adding backbone-compatible restriction sites (SacI on 5' end and EcoRI on 3' end) to the purified ArcLight fragment (cut from ArcLight-A242 plasmid by the restriction endonucleases HindIII/EcoRI) by PCR, as described in 2.2.1. Since the size of the ArcLight fragment is 1464 bp (Figure 3.2), it is considered small enough to be packed into the sc AAV vector. Altogether, including the hSyn1 promoter, the insert reaches ~1900 kb. For this purpose, a sc_hSyn1 plasmid (a gift from the Baumann lab, Forschungszentrum Jülich GmbH) was used. Ligating those two components with the sticky-ends (SacI and EcoRI), the final product was made: pcs_hSyn1_ArcLight. A verification of the ITRs existence and positions in the plasmid was done by the restriction enzyme digestion using SmaI/SacI and AhdI/EcoRI and analysed by gel-electrophoresis (Figure 3.3).

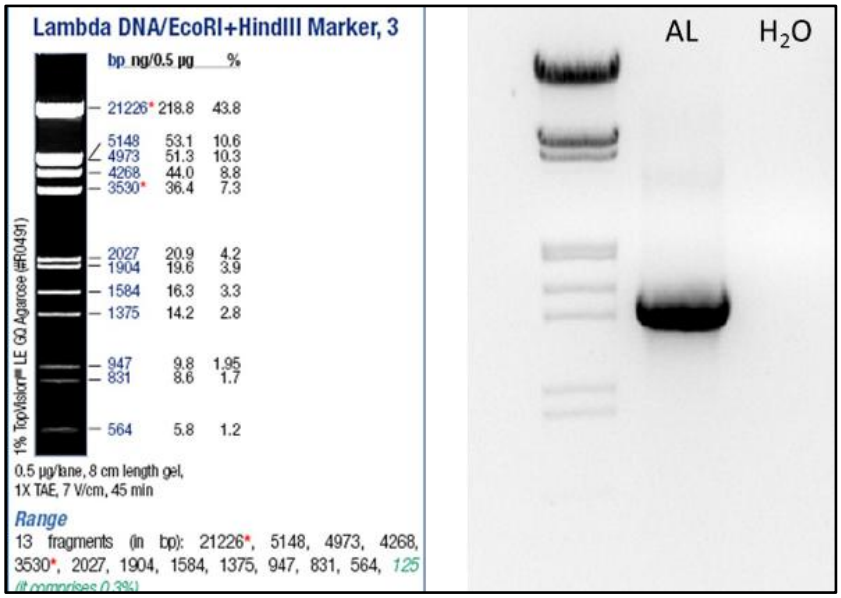

Figure 3.2 ArcLight-A242 fragment evaluation by restriction enzyme digestion and gel-electrophoresis

After cutting the ArcLight fragment out of the ArcLight-A242 plasmid (36857, Addgene), it has been multiplied by PCR in order to add a new restriction site (SacI) that would be compatible with the psc_hSyn1 backbone. Afterwards, the final check of the fragment size (1464 bp) was done using restriction enzyme digestion (SacI/EcoRI) and gel-electrophoresis. This way, the proper fragment could be visualised on the gel, separated from the reaction mixture, extracted and used for further cloning procedures.

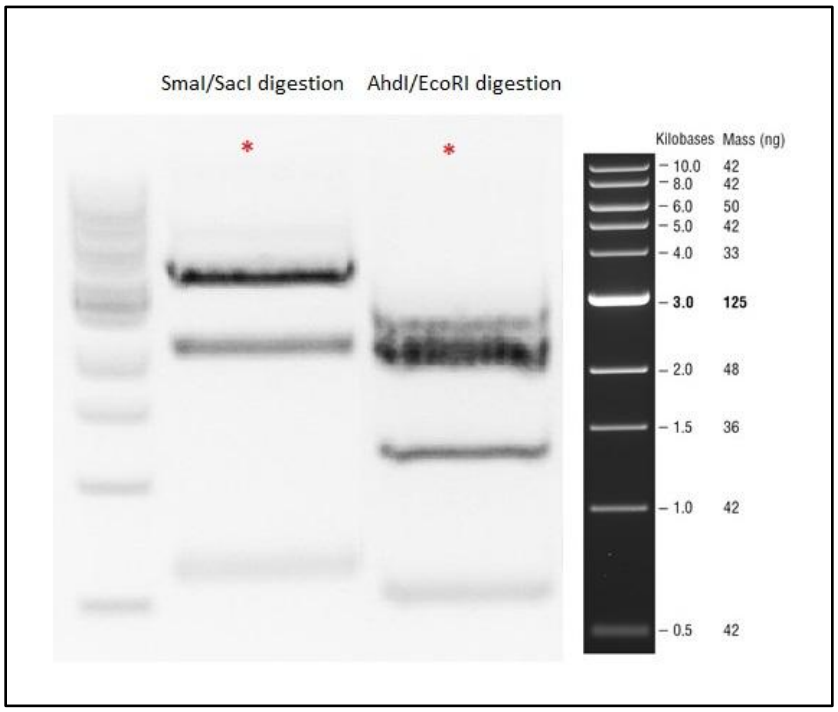

Figure 3.3 ITR evaluation by restriction enzyme digestion and gel-electrophoresis for psc_hSyn1_ArcLight

The photo of the gel represents pSub_hSyn_ArcLight clone enzyme restriction in order to prove the presence of ITR on each end of the construct. In the second well there was the SmaI/SacI enzymatic digestion, and in the third AhdI/EcoRI. Cut fragments visible on the gel serve as a proof that ITRs on both ends of the construct are present in the plasmid, since we have gotten the fragments of expected size. (* indicates the well)

3.1.2. pSub_hSyn_Butterfly construct

After the blunt-end cloning procedure described in 2.2.2, the final product was the pSub_hSyn_Butterfly construct (Figure 3.4). The advantages of pSub plasmid as the AAV vector have influenced our selection of the plasmid. It can accept the foreign DNA that is bigger than 2.4 kb. Because our Butterfly transgene (~2.1 kb) is reaching the limit in size predicted for sc vector incorporation (up to 2.4 kb), pSub was the more appropriate choice. pSub, as a ss AAV vector is transcriptionally inactive. It requires the conversion of of ssDNA to double-stranded (ds) template. This synthesis can be either *de novo* or the annealing of the plus and minus strands from two separate viral particles coinfecting the same cell. This process is a rate-limiting step that contributes to the slow onset of transgene expression after vector delivery; taking at least twice as long as expression from a ds vector (e.g. sc).

Apart from already mentioned hSyn promoter followed by VSFP coding sequence, the other elements required for the successful expression found their place in the plasmid as well. A region of *Simian virus 40* PolyA (SV40) enables the nuclear import of a plasmid by adding PolyA tail to mRNA. Besides, it terminates the transcription activity, so it is positioned behind Butterfly coding sequence. Regarding the rAAV production, the transgene is flanked by two 145 bp ITRs on each end; in front of the promoter and behind SV40. With the purpose of facilitated selection of the bacterial cells that received plasmids, there was a sequence coding for the Ampicillin antibiotic resistance. This way, bacterial cells during the cloning experiments could easily be positively selected by adding Ampicillin in the growth medium.

The original construct of Butterfly 1.2 VSFP, pCAG_Butterfly 1.2, was a gift from the Knöpfel Lab (Imperial College London). In this plasmid, the VSFP coding sequence, consisting of mKate2, VSD and mCitrine domains, was positioned behind a CAG promoter. The VSFP coding domain from this construct was transferred to get a plasmid with more specificity. The neuron-specific targeting was done on two levels. On the one hand, there is an incorporation of the neuron-specific hSyn promoter into the pSub plasmid, on the other hand, the serotype-specific packaging in rAAV6. This serotype confers a higher neuronal transduction rate than other naturally occurring AAV serotypes. ITRs, prior to the rAAV production, were checked by enzyme digestion (AhdI, SmaI and HindIII) and gel-electrophoresis (Figure 3.5).

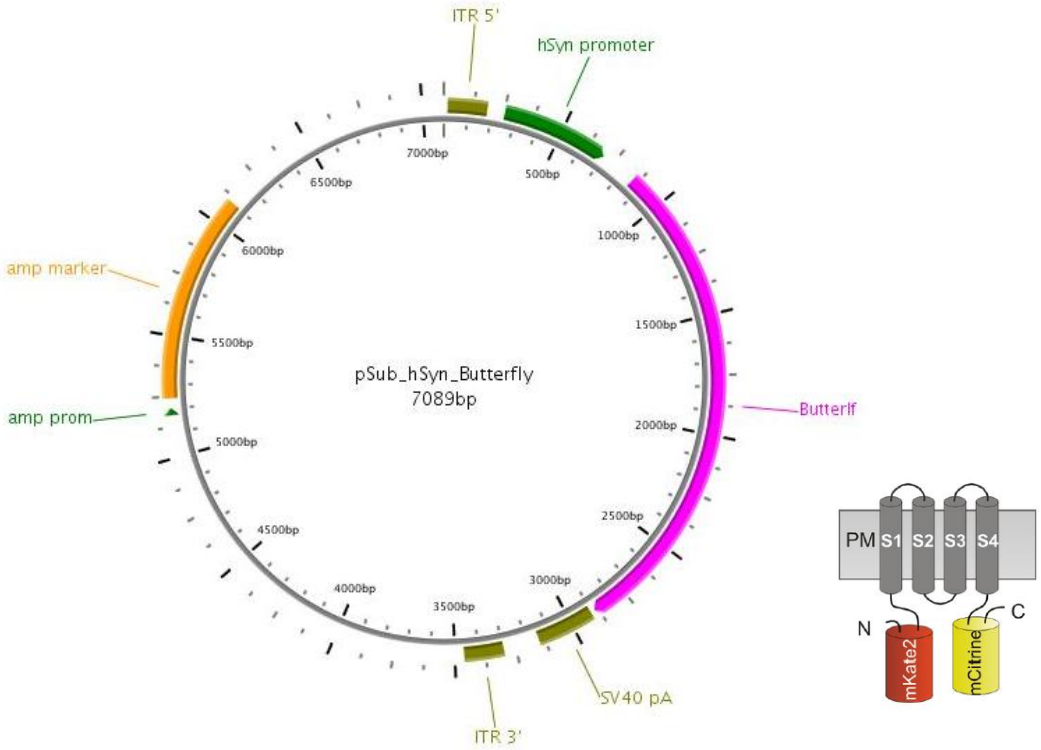

Figure 3.4 Map of the pSub_hSyn_Butterfly plasmid

A plasmid map shows two ITR sites on each end of the Butterfly construct, hSyn1 promoter followed by Butterfly VSDP sequence, SV40 PolyA site and an Ampicillin resistance site as the selection marker. Expressed and inserted into membrane, Butterfly VSFP is schematically shown on the right.

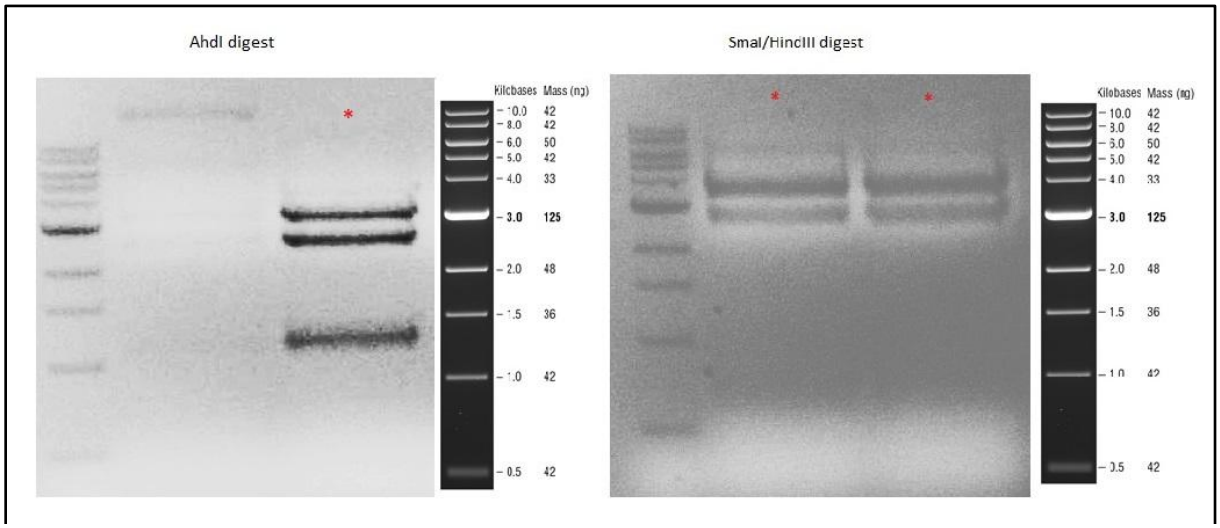

Figure 3.5 ITR evaluation by restriction enzyme digestion and gel-electrophoresis for pSub_hSyn1_Butterfly

The photo of the gel represents pSub_hSyn_Butterfly clone enzyme restriction in order to prove the presence of ITRs on each end of the construct. On the left, there is AhdI, and on the right, SmaI/HindIII enzyme digest. All bands are as big as expected, which means that ITRs are on the positions where they should be. (* indicates the well)

3.2. Transfection/transduction rates and viability

For successful performance of the electrophysiological experiments, it is necessary to obtain healthy, genetically modified cells in the culture. Since the further experimental procedure involves cell by cell examination, it is necessary to have at least few cells per substrate expressing at sufficient levels. The two methods to achieve the goal were used (transfection and transduction), so their comparison is mentioned here. In order to determine efficiency of the individual methods for inserting recombinant DNA into the cells and their survival rate, they have been quantitatively evaluated. The parameter that was experimentally observed was expression of the fluorescent proteins, an indicator for successful transfection/transduction. The total number of the fluorescent cells was divided by the number of all potentially viable cells for each construct and insertion method.

3.2.1. FuGene transfection

As a quick method for genetic modification of the cells (both, HEK293 and cortical neurons), FuGene chemical transfection was used for the first evaluation of the protein expression. Despite the good preparation of the primary neuronal cultures and their transfection at DIV7, when they are supposed to be robust enough to survive the chemical agent, only a few cells per well behaved as expected. The percentage of the neuronal cells that fulfil the prerequisites as healthy, fluorescent cells ready to be electrophysiologically measured is 38.38% (n = 99).

With regards to the HEK293 culture, the cell health was improved compared to the same treatment on the neuronal cells. These results are in accordance with the life cycle of the cells; since they divide every day, only those who survive the treatment can have an impact on the perpetuation of transfection. The transfected cells, due to the damage caused by chemical agents, divide slower than untransfected. Thus, the transfection efficiency is artificially depressed over time and the culture cannot be kept for a longer period of time. However, the high cellular metabolic rate of quickly dividing HEK cells enables stronger fluorescence compared to the neuronal cells (Figure 3.6).

ArcLight could be detected in cells expressing from the newly made psc_HCMV_ArcLight plasmid in both HEK293 cells and neurons. Overall, FuGene chemical transfection performed on HEK cells had an expression factor of 16.9% (n = 71). The results on the neuronal cells were 38.38% as an expression factor.

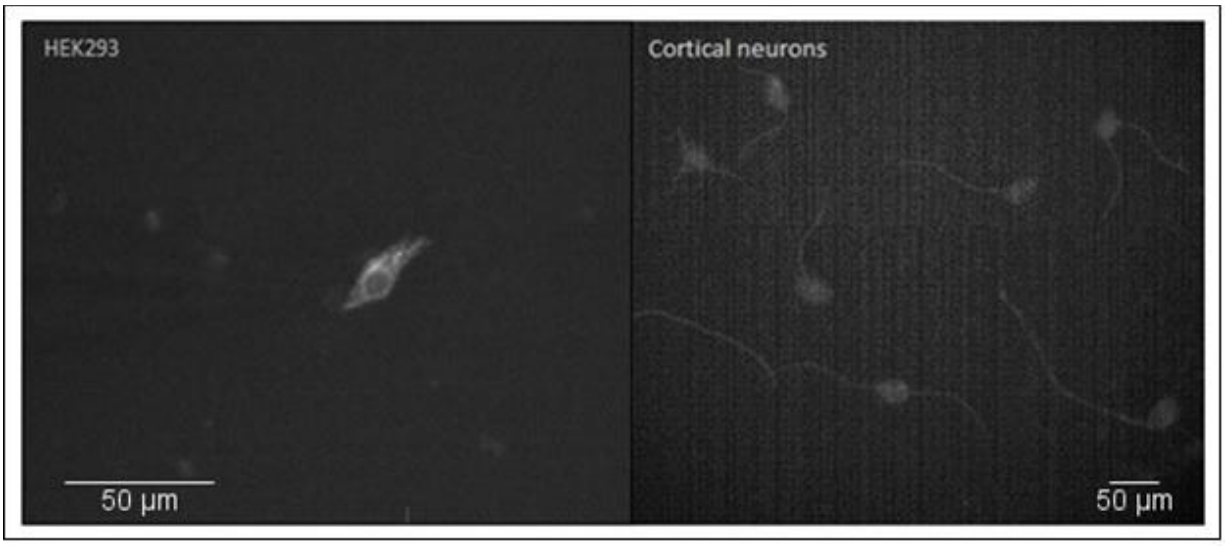

Figure 3.6 Transduced HEK293 and cortical neurons

The HEK293 cells and cortical neurons were FuGene transfected with psc_HCMV_ArcLight construct (HEK293 at DIV1, cortical neurons at DIV7). The photos of HEK293 transfected cells were taken at DPT3 and at DPT7 for the neurons, at the highest illumination intensity and 100 ms exposure time. Transfected HEK293 cells, due to the fast metabolism rate, show much higher expression rate and due to it, fluorescence intensity, than transfected cortical neurons.

3.2.2. AAV transduction

Introducing the rAAV transduction serves as the specifically directed method for recombinant DNA insertion to cortical neurons, due to the AAV6 natural serotype that favours neuronal cells. Thus, it was expected to notably improve the cell viability, soundness and expression rate. The process of rAAV packaging of the novel constructs (psc_hSyn1_ArcLight and pSub_hSyn1_Butterfly) into serotype 6 was done at Baumann lab, Forschungszentrum Jülich GmbH. The procedure of virus packaging in HEK293 cells included co-transfected cells with an expression vector, a helper vector and a rep-cap vector. After the virus was produced in the cells, the particles were isolated in 40% iodexanol.

The best relation between the cell survival and expression rate was achieved by using between 1.5k and 2.5k virus particles per cell (vp/cell). This was empirically proven by testing various ratios of vp/cell, where with vp increase the volume of iodexanol is also increased. Since the iodexanol shows cytotoxicity, it is necessary to balance the ratio of vp that will transduce the specific number of cells, considering the volume of added iodexanol. The cells were transduced at DIV7, while sufficiently measurable fluorescence intensity was achieved at DPT7 or more. Since the viruses contain constructs

with the neuron-specific hSyn1 promoter, the transduction rates were quantified on the neuronal cells for every construct.

3.2.2.1. psc_hSyn1_ArcLight

For the ArcLight construct, due to its self-complementary vector, the first expression onset could be observed already at DPT4. However, for the electrophysiology measurements, the cells were cultured until the DPT7 or more. Compared to the FuGene transfection rates, the expression factor for AAV transduction of this construct was higher (Figure 3.7) along while cells stayed healthy and able to form networks. Quantitatively, 84.31% of all transduced cells showed observable fluorescence. From our experience, we expect that about 10 – 20% of our cultured cells are glia. Since the ArcLight construct is driven by hSyn1 promoter, which is neuron-specific, we assume that all fluorescent cells are neurons. This result implies on the high transduction efficiency directed only towards the neuronal cells, omitting the supporting glial cells.

As already mentioned, AAV transduction has other advantages besides it is gentler for the cells than other DNA insertion methods. One of them, that was shown to be important for our experiments, is serotype tropism. On the Figure 3.7 one can see comparison between FuGene transfected and AAV6 transduced cells with the same construct: psc_hSyn1_ArcLight. Besides the efficiency rate and overall condition of the cells, there is a difference in the cell type where fluorescence can be observed. Although driven by neuron-specific hSyn1 promoter, from the photos of FuGene transfected cells it seems that the expression is not limited only to this cell type. According to the shape of the cell and its flatness, we can assume that the cell marked with purple arrow belongs to glia.

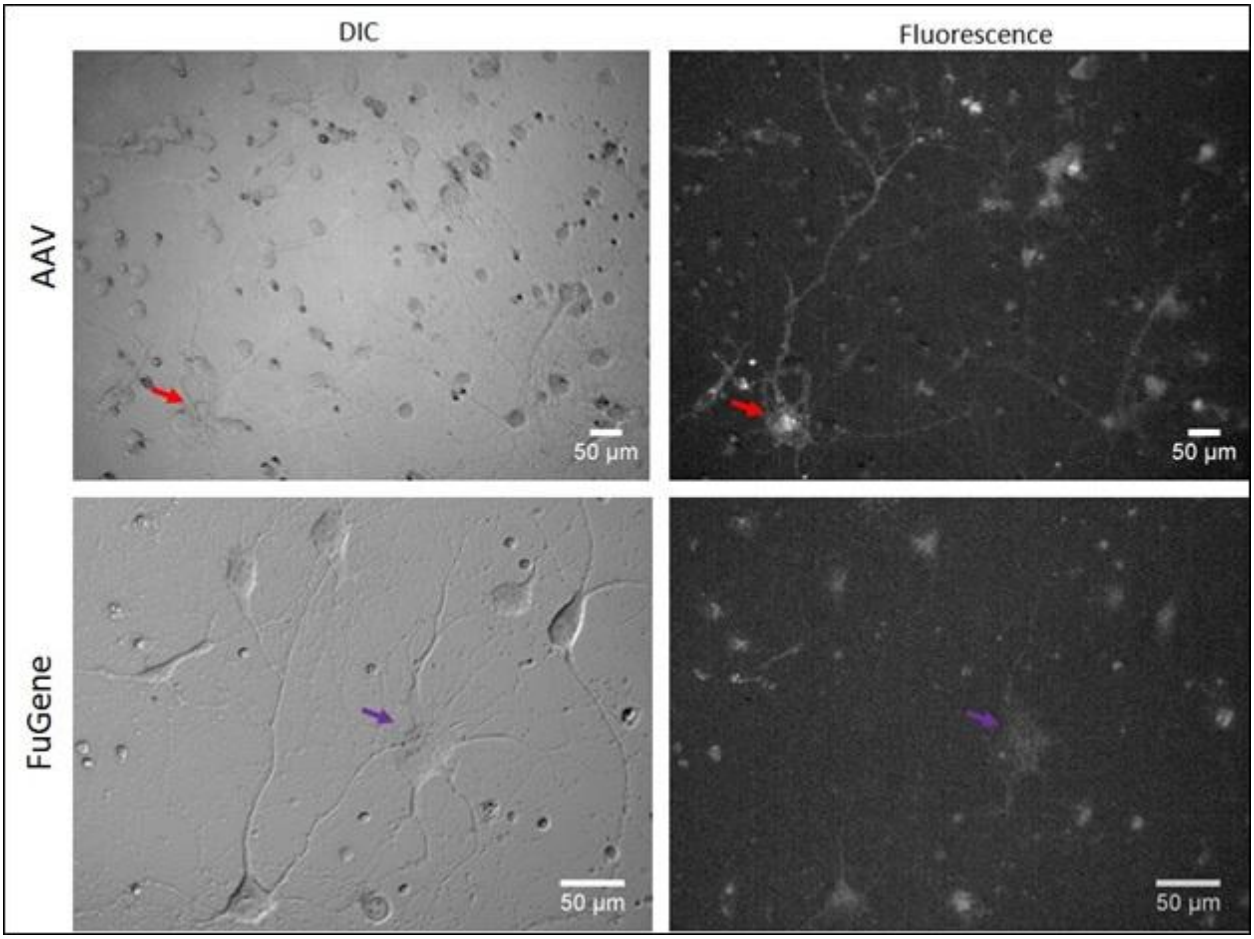

Figure 3.7 Comparison between FuGene transfected and AAV transduced cortical neurons with ArcLight construct

The cortical neurons, transduced with AAVs (4k vp/cell) on the upper photos and FuGene transfected on the lower photos, at DPT7-14. On the left, there are DIC photos and on the right fluorescence. Both fluorescence photos were taken at 100 ms exposure time with maximal intensity of the lamp. As expected, AAV transduced cells that were fluorescent were neurons (red arrow), while with the transfected cells this was not the case. On the fluorescent photo of FuGene transfected cells, there is visible weak fluorescence probably in glia, not only in neurons (purple arrow).

Previous work in the institute supports efficiently different serotypes transduce cortical neurons. In the work of Lange, primary culture was transduced with a GFP construct behind the HCMV promoter (that is not restrictive to certain cell type) within naturally occurring serotypes of AAVs. The cells were immunostained and counted separately according to the cell type. Among all live fluorescent cells (n=242), the transduction efficiency rate was 97.1% for the neurons. The glial cell transduction was only 2.9%. Thus, it was shown how AAV serotype 6 has favourable cell specific targeting. [73]

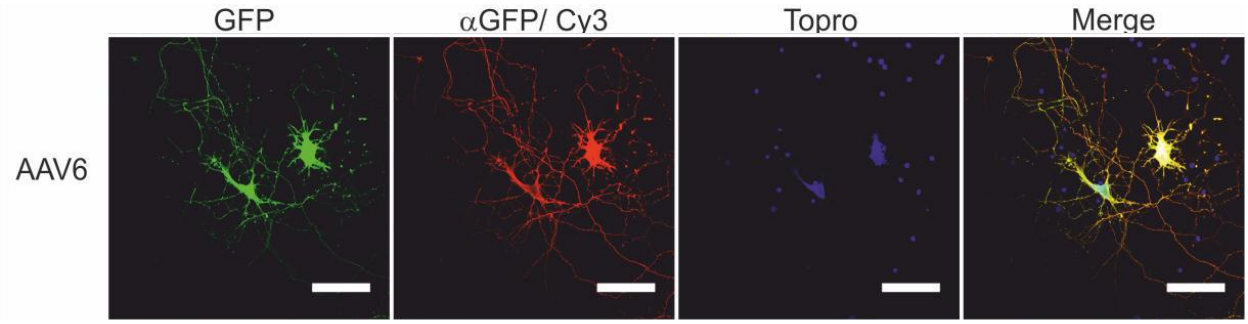

Figure 3.8 In vitro transduction of embryonic cortical neurons with rAAV6 serotype

The cortical neurons were transduced with GFP construct driven by HCMV promoter by rAAV6 at DIV7. First photo shows GFP expression in the cells. On the second there are the same cells but immunostained with αGFP antibody, while the third contains DNA stain Topro. The last photo shows all those photos merged; both of the fluorescent cells are neurons.

(Figure adapted from [73])

3.2.2.2. pSub_hSyn1_Butterfly

Since the construct that is expressed in our Butterfly VSFP construct is actually a FRET pair, its expression can be observed at two different wavelength. As a first option, there is mCitrine as a donor, which is excitable at 514 nm. Its emission maximum is at 529 nm, which is in the green range. The other option is observation of the acceptor fluorescence, which is mKate. Its excitation is at 588 nm, and emission maximum at 633 nm. Considering this, the quantification of the expressing cells, transduced with AAV6_pSub_hSyn1_Butterfly (2k vp/cell), was made using the both filter ranges. Results of the expressing cells among the all possibly transduced cells were 70.7% for the mCitrine, and 52.8% for the mKate fluorescence. Based on the properties of Butterfly 1.2 and camera properties, this difference in fluorescence for each fluorophore is expected. Since it is a FRET pair, the energy transfer from donor to acceptor may occur only when the distance between them is small enough. This happens when there is a conformational change, due to the membrane depolarisation. Thus, the fluorescence decrease in mCitrine (donor) is expected when the membrane is depolarised, i.e. during the action potential. For the acceptor, mKate, the fluorescence is expected to increase at the same conditions. To achieve the sufficient energy transfer towards the acceptor, the donor has to be fully excited in order to emit its maximal energy. Regarding the camera properties, wavelengths in red spectrum are more difficult to detect than those green/yellow. More specifically, due to the higher background in the red channel, the

contrast is worse. Combining those parameters, it is explainable why there are more fluorescent cells observing mCitrine rather than mKate.

As mentioned earlier (1.5.4), the expression onset of a single-stranded vector takes more than twice as long as for the self-complementary vector. Since the Butterfly construct was cloned into such a vector (pSub_hSyn1), it is expected that the desired expression will be achieved by employing a longer time period of expression. To check this assertion, photos of the different expressing cells were taken at time points, spanning from 3 to 17 DPT. On each healthy, fluorescent cell, the ROI was hand-marked as an area of the plasma membrane, avoiding overexposed nuclei. The exposure time was set to 100 ms at maximum light intensity. The fluorescence intensity was quantified as the maximal value of the photon counts for each ROI, subtracted from the background. Afterwards, the statistical analysis has been made (Figure 3.9). For the cells measured in red channel at DPT3 (n=7, SE=0.71), the maximum value of a.u. was 1.5. The cells measured at DPT10 (n=3, SE=0.33) have shown the a.u. value 2.33, and in those measured at DPT17 (n=3, SE=1) it was almost three times as from the first measurement, or 4.3 a.u. Measuring mCitrine in the green channel, the correlation of incensement in the counts over time is found to be similar. Thus, for the measurements taken at DPT3 (n=7, SE=1.26) the maximum a.u. value was 4, at DPT10 (n=3, SE=3.92) 6.33 and finally, at DPT17 it was 16 (n=3, SE=5.61). Besides the increment trend of counts over time in both fluorophores, it is also shown that the fluorescence intensity is higher in mCitrine than mKate, as described above. It is shown that the fluorescence intensity is correlating with DPT due to the slow onset of expression.

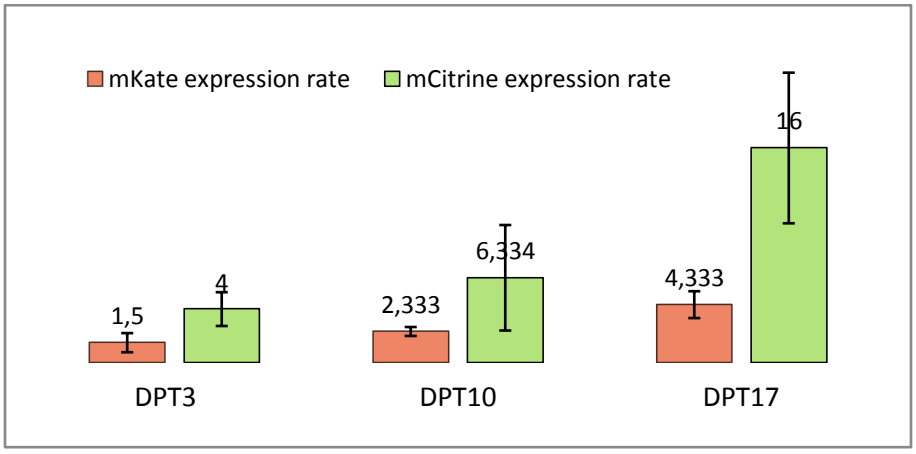

Figure 3.9 mCitrine/mKate expression rates

Cortical neurons, transfected with pSub_hSyn_Butterfly, were measured by their fluorescence intensity on both channels of the FRET pair. The applied exposure time was 100 ms at maximum light intensity. For the measurements taken at DPT3 n=7 and for those taken at DPT10 and DPT17 n=3. The numbers above refer to the average mean count value measured for each hand-marked ROI in the plasma membrane at given DPT.

3.3. Electrophysiological results

Performing electrophysiological experiments on the genetically modified neurons with both constructs aimed to correlate electrical and optical signals. AAV transduced neurons, due to their healthiness, were stimulated by patch-clamp in whole-cell mode. In addition, transfected neurons were stimulated by locally applying KCl solution.

3.3.1. Voltage - clamp fluorometry

In AAV transduced cortical neurons, the patched cells in whole-clamp mode were first checked for their responsiveness to electric stimulation by the standard V-C protocol (described and attached in 7.3.1). Afterwards, the voltage-clamp stimulation protocol in 26 steps (described and attached in 7.3.1) was triggered by the start of the optical recording to allow for *post hoc* analysis (2.4.2). The first action potentials were formed around the 9^{th} step, which was a depolarisation of 30 mV from the holding potential of -70 mV. The typical action potential peak lasted for ~10 ms, sometimes even multiple action potentials occurred during the one voltage step. For the optical measurements the exposure time of 100 ms was used with the maximum light intensity. The optical and electrical recording results are shown for both, ArcLight-A242 (Figure 3.10) and Butterfly 1.2 VSFP (Figure 3.11). Black traces indicate applied voltage during the stimulation protocol, and red indicate iteratively measured current in the electrical recordings. Both variables were coordinated with sequentially extracted time (in s) from the TIDA file. Four out of 26 representative pulses are shown. The raw data from ROI optical recordings were first subtracted from the background. The adjusted curve of the fluorescence intensity over time was smoothened by Savitzky-Golay method applied in Origin. Afterwards, the curve has been fitted to linear plot and correlated with electrical variables over time.

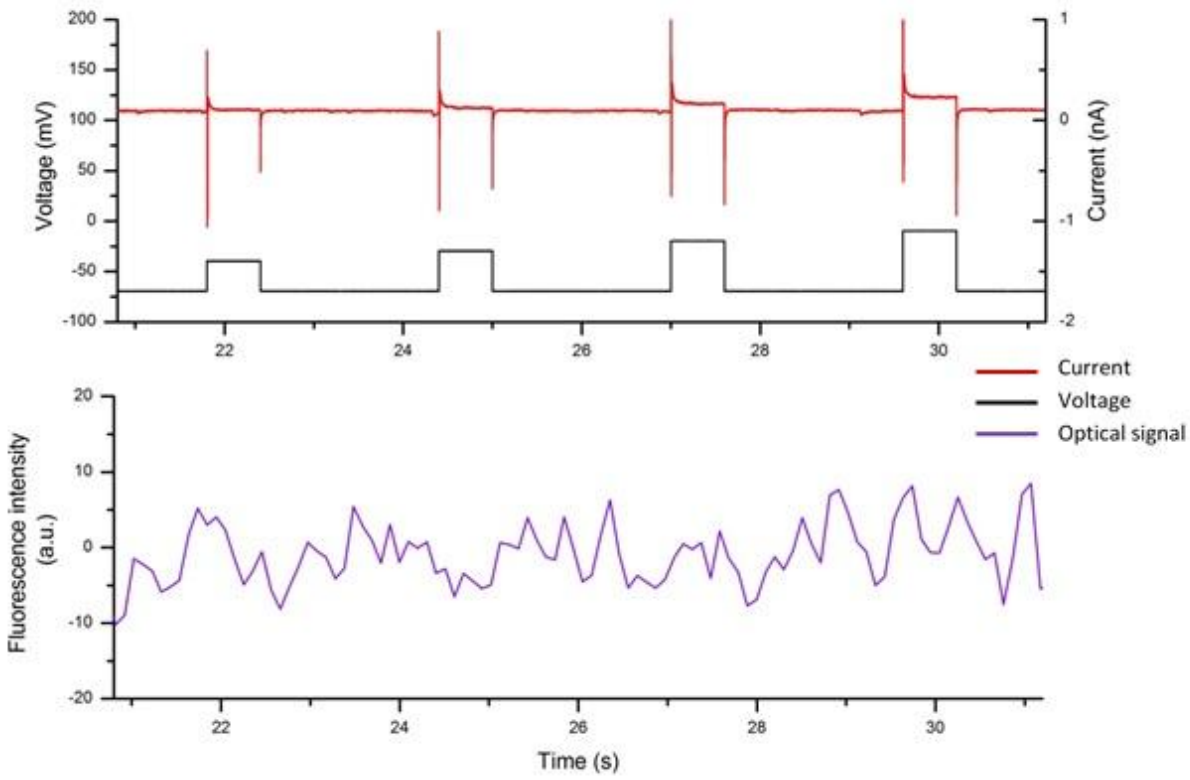

Figure 3.10 Correlated electrical and optical signals for ArcLight-A242 VSFP

The cortical neurons, transduced with rAAV6 psc_hSyn1_ArcLight, were at DPT7/DIV14 stimulated by V-clamp and in parallel, optically recorded. On the upper graph there are traces of the electrical responses of the cell (red) and applied voltage (black) from the patch-clamp pipette, while the lower graph shows the time-correlated processed optical trace (violet).

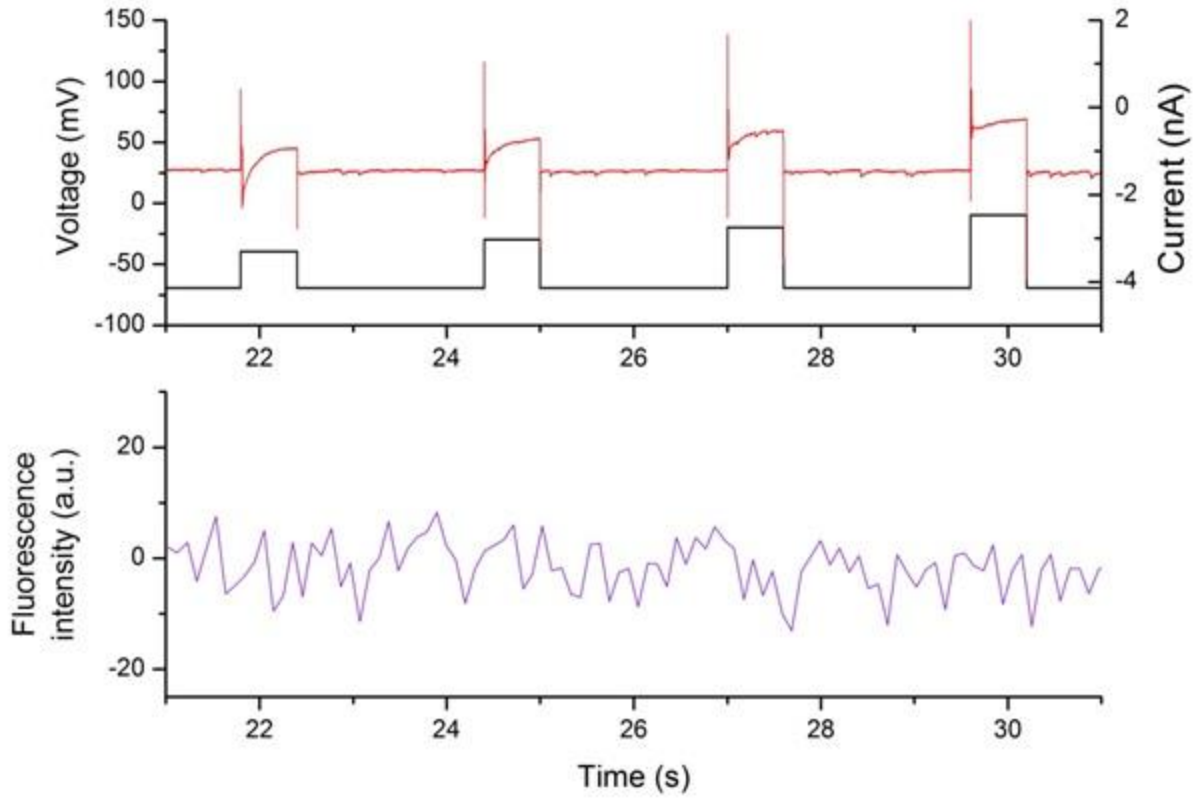

Figure 3.11 Correlated electrical and optical signals for Butterfly 1.2 VSFP

The cortical neurons, transduced with rAAV6 pSub_hSyn1_Buterfly, were at DPT7/DIV14 stimulated by V-clamp and in parallel, optically recorded. On the upper graph there are traces of the electrical responses of the cell (red) and applied voltage (black), while the lower graph shows time-correlated processed optical trace (violet).

In order to correlate electrical and optical responses of the cells, simultaneous electrical stimulations and optical recordings were performed. In 26 voltage steps applied to transduced cells with one or the other construct, we have been able to achieve membrane depolarisation and to induce few action potentials. Despite that, according to the readout from the graphs (Figure 3.11) there is no correlation between the electrical and optical signals (discussed in 4.2). The signal we expect would be the fluorescence decrease for both proteins at given wavelengths (green filter set for both fuorophores), correlating with the time when the action potentials actually occurred. Visualised in the processed graphs, like those above, that would be a downward peak. In our recordings, the optical traces reveal just noise and bleaching. From the raw data (**Pogreška! Izvor reference nije pronađen.**), as discussed below (4.2), the bleaching rate is 9% per 70 s measurement at 100% intensity and 100 ms exposure time. The optical noise, in turn, is high and caused by the fluctuations around. It becomes larger when

the number of detected photon counts is low, therefore causing the drop of SNR. The signal in raw data terms, if it would be recorded, should be at least 2 SNR to be significant. Therefore, in voltage-clamp fluorometry measurements for both proteins we have not successfully recorded significant decrease of fluorescence that one can expect while stimulating action potentials.

3.3.2. Local KCl stimulation

As an alternative method for validating the protein functionality *in vitro*, the cells expressing ArcLight A-242 and Butterfly were exposed to increased local concentrations of KCl solution. The cortical neurons (from Figure 3.12) were chemically transfected by FuGene with pCAG_Butterfly construct. This construct (a gift from the Knöpfel Lab) was used as a starting point for design of the further Butterfly variants (2.2.2). The expression was driven by strong CAG promoter, HCMV-enhanced beta-actin promoter. On the second example, the cortical neurons were also transfected by FuGene, but with psc_HCMV_ArcLight construct (Figure 3.13). Here, the expression was driven by the strong HCMV promoter.

The applied 0.15M KCl was added manually in the vicinity of the recorded cell (DIV15/DPT6 for pCAG_Butterfly and DIV15/DPT5 for psc_HCMV_ArcLight) in a 4 ml plate, in order to transiently increase the local K^+ concentration. Thus, the membrane depolarisation was induced. This way, we have been able to induce the fluorescence change in the cell membranes which we attribute to chemically stimulated action potentials.

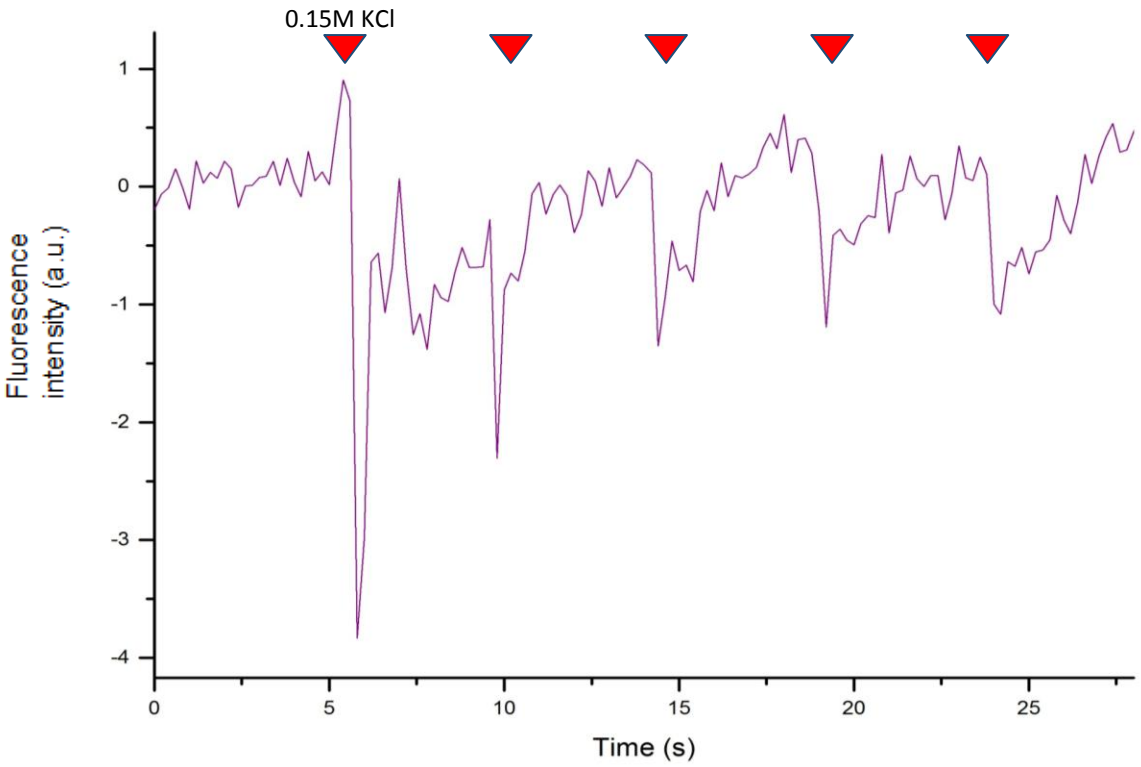

Figure 3.12 The fluorescence change of Butterfly VSFP induced by local KCl application

The cortical neurons were transfected with pCAG_Butterfly construct and optically recorded at DIV15/DPT6. Adding 0.15M KCl solution locally to the cell in 5 portions of 100 µl every 5 s, the fluorescence decrease has been observed (using the green emission filter for mCitrine fluorescence observation and 200 ms exposure time). This implies stimulation of action potentials which cause the decrease of fluorescence by 22.6 ± 4.37%.

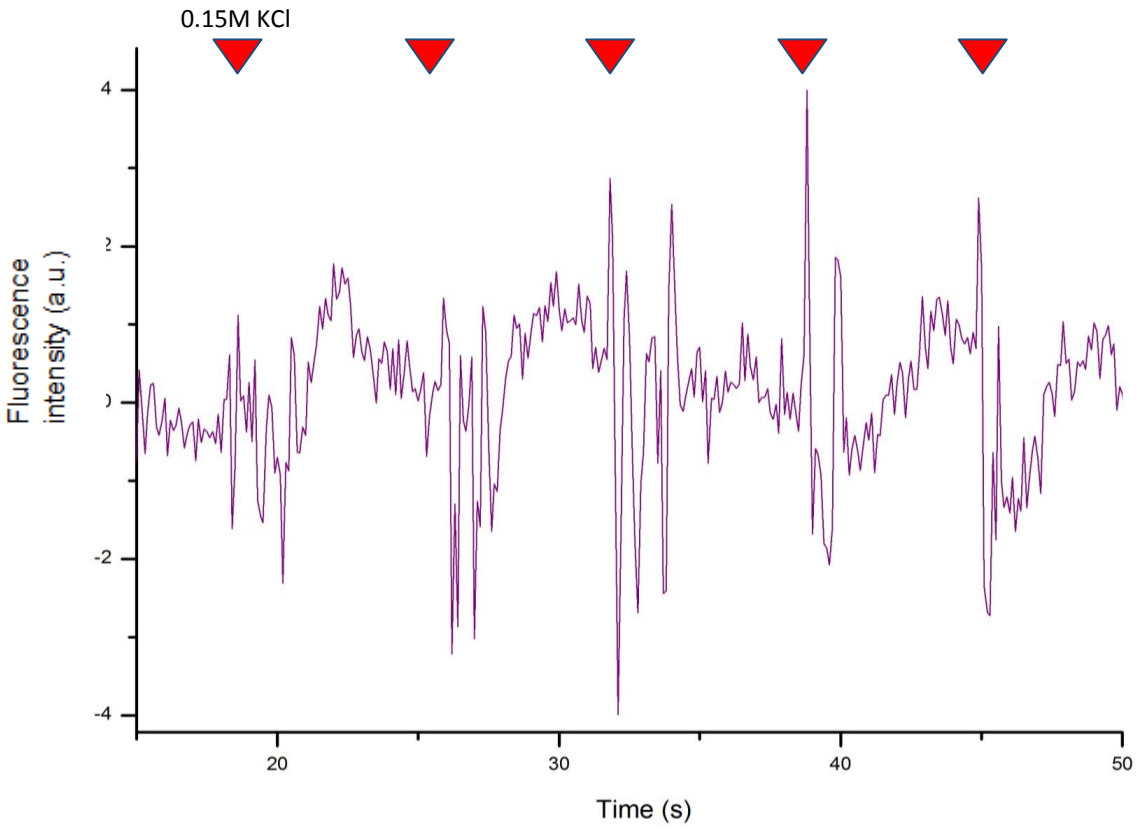

Figure 3.13 The fluorescence change of ArcLight-A242 VSFP induced by local KCl application

The cortical neurons were transfected with psc_HCMV_ArcLight construct and optically recorded at DIV15/DPT5. Adding 0.15M KCl solution locally to the cell in 5 portions of 100 µl every 5 s, the fluorescence decrease has been observed at 200 ms exposure time. This implies the stimulation of action potentials followed by the decrease of fluorescence by 11.27 ± 1.51%.

Observing both of the proteins upon membrane depolarisation in the green filter channel, it is noticeable that their fluorescence intensity changes in the expected direction. The decrease in fluorescence intensity in both VSFP expressing cortical neurons (Figure 3.12, Figure 3.13), correlates with the time when 0.15M KCl solution was locally applied towards the measured cell. Since the solution was injected manually, the time span between adding each portion is not exactly 5 s. In the case of ArcLight A-242, in total 200 data points from raw data prior and after the peaks (0 - 5 s and 30 - 67 s) were used to calculate F_0. The maximum value, $F_{max,}$ is the highest value of the peak. Those values were used to calculate $\Delta F/F_0$. For this measurement, $\Delta F/F_0$ is 22.6 ± 4.37% (n = 5). The signal-to-noise ratio (SNR) was 4.43.

KCl addition to Butterfly 1.2 expressing cells should cause a local change of the membrane potential, i.e. reduction of the negative potential. Thus, the Butterfly 1.2 domains undergo conformational change what further leads to emission of the fluorescent light from both of the FRET pairs. Depending on the observed wavelength, the output differs. In this case, mCitrine (donor) fluorescence intensity change was observed, so a decrease of fluorescence is expected. In total 303 data points from raw data prior and after the peaks (0 – 18 s and 55 – 67 s) were used to calculate F_0. $\Delta F/F_0$ value in this measurement is 11.27 ± 1.51%. SNR was 1.72.

3.4. Imaging in real time

In order to observe the transduced cells expressing VSFP in real-time, the ZEISS live cell imaging setup was used. The cortical neurons were transduced with psc_hSyn1_ArcLight AAV6 at the DIV7. At DPT10, the cells were continuously recorded in the green channel with the filter set of 450 - 490 nm excitation band, 500 - 550 nm emission band and beam splitter of 495 nm (2.5) every 100 ms exposure. The cells could be easily distinguished according to their fluorescence (Figure 3.14), while the illumination source was set to 100% intensity. The experiment was set in a way that there is continuous recording of fluorescence in duration of 60 s. During this time, there is probability (due to the age of the cells) that they will spontaneously fire and possibly propagate action potentials. This way, we should be able to observe the change in fluorescence intensity at the time of spontaneous potential firing, but there is no stimulation of the same at certain time.

Since the background fluorescence interferes with our cells of interest so they seem dim, it was necessary to increase the exposure time. With 100 ms of it the cells appeared clearer, intensity of their fluorescence was higher and thus, they were easier to distinguish from the background. These settings enabled us optical recordings at the speed of 100 ms frame-rate, or 10 frames per second. Lowering the exposure time trading-off the contrast between fluorescent cells and the background, we succeeded to get down to 20 ms. With this settings, the recording speed is higher, but the cells expressing VSFP need to appear very bright in order to avoid the background interferences. To determine optimal appropriate exposure time, it is, besides the empirical settings, necessary to include information about the kinetics of observed proteins. It is recommended to use at least as ½ of their expected response time. In our case, that totals 25 ms (for 50 ms kinetics) for measuring ArcLight A-242.

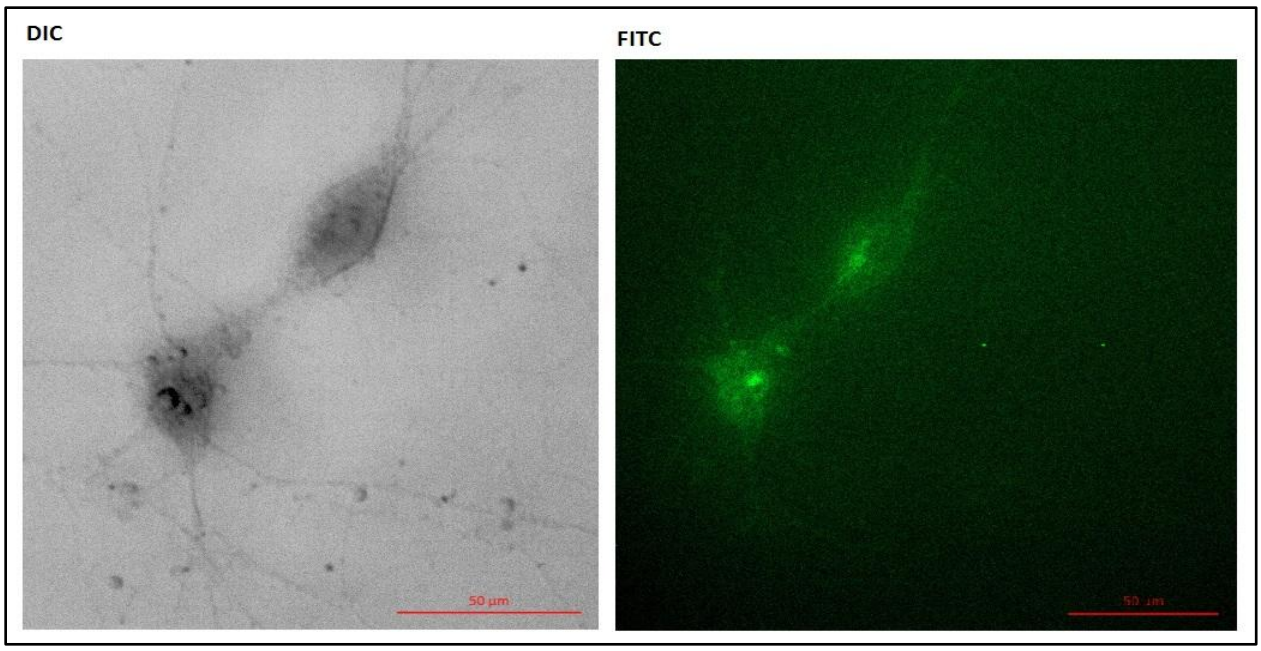

Figure 3.14 psc_hSyn1_ArcLight transduced cortical neurons

Cortical neurons were transduced with 2k vp/cell psc_hSyn1_ArcLight AAV6 at 7 DIV. On the left, there is a photo of the neurons taken with differential interference contrast. On the right, the same neurons are fluorescing at green channel at 100 ms exposure with 100% illumination source intensity.

On both of the cells shown, the ROI was marked as a fluorescent area in the plasma membrane. The upper cell was marked as R1, and the lower as R2. Using camera-associated program Zen for analysis of the signals produced during the recording time (60 s), we have been able to determine the decrease in the fluorescence for R1 in duration of 0.21 s (Figure 3.15). The post-processing of the raw data included linearization of the intensity fluorescence curve in order to eliminate bleaching effect. The amount of change in fluorescence ($\Delta F/F_0$) of the signal is -3.54%, where minus indicates decrease according to the baseline, and SNR is 1.4. The signal occurred at the very end of the recording, at 57.799 s. In parallel, in the coupled neuronal cell there was no significant change in the fluorescence.

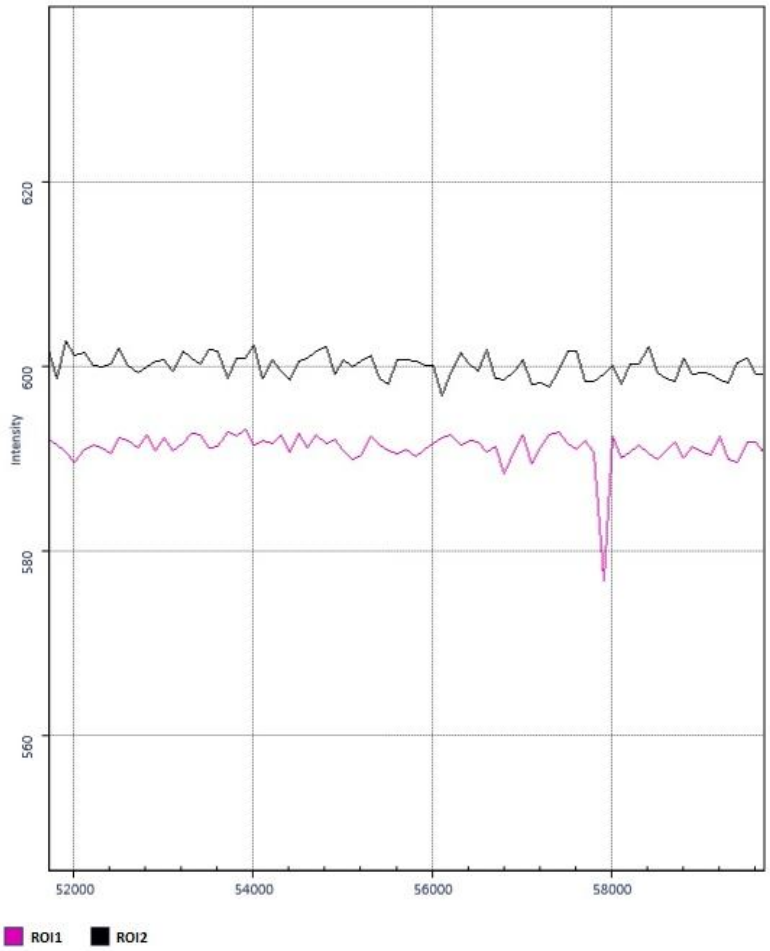

Figure 3.15 Fluorescence chart of the two transduced neurons expressing ArcLight-A242 VSFP

The traces show mean intensity values over time for ROI. Black trace corresponds to the ROI2 (neuron 2), and the purple to the ROI1 (neuron1). From 57.799 s to 58.009 s the fluorescent value of ROI1 is lower than baseline.

4. DISCUSSION

In this work we wanted to introduce new genetic tools for non-invasive monitoring of neuronal electrical activity and verify them. We used two types of VSFP: ArcLight-A242 and Butterfly 1.2. The starting point of our work was re-design of the constructs at DNA level, aiming to improve their expression features. Upon now, researches in the domain of voltage-sensors optogenetics have only been focused on examination and enhancing functional properties of the proteins by electrophysiology measurements [45, 50, 52, and 53]. Hereby, we decided to take additional approaches, improving and specifying the expression in the retrograde manner; manipulating the promoter at first.

In the current scientific research, since the constructs of the ArcLight-A242 and Butterfly 1.2 were designed [42, 57], they have been used as original plasmids ever after. As for the ArcLight-A242 and Butterfly plasmids, this means VSFP sequence has been positioned after HCMV or CAG promoter. The HCMV promoter is strong, constitutive promoter intended for mammalian cell expression [74]. The other one, CAG is actually a strong synthetic promoter made by enhancing chicken-β-actin promoter with HCMV enhancer element [75]. Both of the promoters are not cell type specific; they are used to drive high levels of gene expression in mammalian vectors. Endeavouring to achieve expression specificity, i.e. only in neuronal cells, we decided to change used promoters with neuron-specific hSyn. The additional approach of expression control included assembling of rAAV particles containing our constructs for neuron-specific viral targeting. The viral serotype 6 has shown native tropism towards neuronal cells [73]. To do so, the new plasmids were briefly designed and composed according to the needs for afterwards rAAV production.

The psc_hSyn_ArcLight plasmid was produced cutting and multiplying ArcLight fragment by PCR, adding EcoRI/SacI restriction sites on its ends to specify further ligation reaction. Produced in such a way, ArcLight fragment was a perfect cohesive fit for the backbone plasmid psc_hSyn1 that already contained rAAV necessary compounds like ITRs, SV40 etc., by SacI/EcoRI cohesive end ligation.

The Butterfly fragement was inserted into pSub plasmid, due to the remark from the collaborators that it exceeds the experimental limit in size for sc vector incorporation. Because the Butterfly fragment and Sub plasmid do not have the common restriction sites, a blunt-end ligation had to be accomplished. Although generally very inefficient, we have successfully selected the new construct pSub_hSyn1_Butterfly in right orientation.

4.1. Transfection/transduction rates and viability

To achieve quick and easy verification of plasmid expression, the HEK293 cells and neurons have been chemically transfected. Even if it is not lipid-maintained, the harmfulness to the cell membranes was apparent. Compared to the fragile neurons, the robust HEK293 cells have survived the transfection treatment better, although with the lower transfection rate (16.9% for HEK293 and 38.38% for neurons). This is not surprising, considering their everyday division and production of new, young and healthy cells. During the long experimental trials of producing the appropriate constructs aiming for rAAV production, however, the only remaining method of DNA insertion for the neurons was chemical transfection. Since it is very damaging for the cells, they could not be successfully patched or subjected to any electrophysiological experimental procedures in this condition. The flabby membranes could not be sealed to the pipette tip during the patch-clamp so the gigaseal actually could not occur.

Although the expression of ArcLight or its derivatives in the transfected neurons in the recent research did not appear to affect the protein properties [50], it has already been attempted to use either lentivirus or AAV to express constructs *in vivo* instead of transfection. Hereby, after the successful rAAV6 production, we transduced neurons. Since for the patch-clamp experiment is needed only one healthy, fluorescent cell, there is no data in the literature suggesting the efficiency of the insertion methods to compare with. The sufficient expression of ArcLight-A242 was observed from DPT7 (84%). As far as the Butterfly expression (70.7% for mCitrine and 52.8% for mKate), due to the slow onset of expression from the pSub vector, it was expected to achieve it later than for ArcLight. Accordingly, the expression rate increased over time. Although it was known before that the drawback of pSub vector-mediated gene transfer is the slow onset of expression, due to the rate-limiting step of ss to ds DNA conversion [76], this result resolved a time-scale of expression duration. The firmness of the membrane was improved and the neurons, have been successfully patched. This way, sealing the cell membrane to the patch pipette tip did not have negative influence to measured parameters, so the further electrophysiological measurements were carried out.

4.2. Electrophysiology results

On the healthy, fluorescent cells transduced by rAAV, we could perform the patch-clamp experiments in the whole-cell V-C mode. The shape of an action potential was in accordance with the

typical shape of action potentials found in the literature [77]. Sometimes, it has happened that the patch was lost during the recording, what could be seen from the shape of the current trace. It might be that the cell did not endure the procedure if the recording was taking too long, or there was a case where the patch pipette experienced drifts. Despite the technical difficulties before and during the experiment, we have successfully recorded the fluorescence of the cell while stimulating it electrically.

In our results (Figure 3.10, Figure 3.11) despite the action potential triggering, there is no detected change in fluorescence. Since the background noise was constantly at the high level, the contrast between the fluorescent cells and their surroundings was not adequate. This could be concluded considering the raw data, where the total number of photon counts was almost homogenous over the whole visual field. Depending on the observed protein, excitation and illumination source intensity, the difference between the ROI and the background was only 1%, respectively, 4%.

In all our recordings, there was no case of the noticeable signal appearance. One of the possible reasons is the trade-off between the recording settings for Andor Zyla sCMOS camera and the sensitivity of the measurements we would have liked to achieve. Considering the low contrast between the fluorescent cell and the background, it is necessary to set the illumination source to 100% intensity and increase the exposure time. Doing so, the bleaching effect is intensified (the photon count value during the 70 s measurement drops approximately 9%). A similar bleaching value of 8% we have gotten analysing the raw ROI data from the Live imager setup. This results, still, are in accordance with the literature [50], where the bleach rates were from 4.83% to 6.38% but measured only during the first two seconds of recordings. Considering the optical noise as a second by-product, we have calculated that it effects our measurements in time-frame rate more than bleaching. Thus, it takes the role as a dominant effector for our recordings in patch-clamp setup (2.4). In the live imager (2.5) the level of optical noise is significantly lower. This is explainable by the fact that the patch-clamp setup is an open one, while the live imager is completely closed in a shaded dark cupboard. This way, all the surrounding illumination from the lab may not influence the live imager recordings.

The other approach one may think about is another side-effect of those settings; the kinetics of our proteins cannot be shown (i.e. the ability for accurately defining an action potential is dropping off). Besides, the recording rate automatically slows down. The highest we have been able to achieve for 100 ms exposure time and ~70 s of recording length was just 9.7 frame rates per second. According to the kinetics of the VSFP we use and exposure time which is sufficient for their excitation, it is obvious that even if the optical signal exists, it may not be recorded due to the low frame rate.

4.3. Imaging in real time

Using the Zeiss live imager inverted microscope, the live monitoring of the fluorescent cells was done. The developer of ArcLight-A242 [50] provided reference values for the tested performance parameters. While they used transfected HEK293 and hippocampal neurons, we used transduced cortical rat neurons. The importance to examine characteristics of ArcLight under the new experimental conditions is highlighted by the fact that ArcLight-A242 shows great differences in signal properties across biological systems [50] and hardware of the used setup. The recording in duration of 60 s successfully detected an action potential in the ROI1 (Figure 3.15). The decrease of fluorescence ($\Delta F/F_0$) during the membrane depolarisation is -3.54%. It is lower than the literature values which is -35% [50], this may imply that there was depolarisation of the membrane, but not the full action potential change in potential.

Considering SNR, it is 1.4. This value is also below standard values that indicate significance of the signal (which is 2). Since it seems that the two fluorescent neuronal cells are forming a small network, one could expect the signal propagation from one to another. In this case, we should be able to notice the fluorescence decrease in ROI2 as well. Unfortunately, this is not the case. Fluorescence intensity of ROI2, during the whole recording period remains without any changes. It is supposed that the signal during propagation decreased and it was insufficient to cause the changes in VSFP. Besides, one can think about failed transmission as another possible explanation. If the signal in ROI1 would be significant, we could expect to see its propagation and the same outcome of the membrane depolarisation on ROI2 as a decrease in fluorescence.

In comparison to other imaging method such as calcium signalling, there are few differences we can discuss. Considering Ca^{2+} multiple pathways and roles in the cell signalling, gene transcription, muscle contraction and cell proliferation, it is not surprising that it is highly regulated [78]. During the action potential, Ca^{2+} enters the cell, what is by default time - consuming. Therefore, this method provides indirect measure of neuronal activity, limited to certain parts of the neuronal cell. Since VSFP are already there, incorporated into the cell membrane, it is not surprising that by them resolving an action potential is much faster and therefore more reliable (as we have shown, in ms time scale according to even s range in calcium imaging). These parameters, of course, depend on the applied exposure time and the frame rate of recording. Besides, their powerful advantage is resolving subtreshold action potentials, while calcium imaging can resolve only spiking activities.

5. CONCLUSION

Despite all the recent achievements in the neuroscience, the questions that have motivated scientists about the information processing in individual neurons still remain unanswered. Studying neuronal behaviour *in vitro* facilitates the availability of a single neuron investigation, but requires non-invasiveness with high spatial and temporal resolution. Expansion of the neurophysiologic recording toolbox with the optogenetic stimulation has enabled such recordings.

- The included work shows the usage of genetically encoded voltage-sensitive fluorescent proteins as a non-invasive optogenetic tool for recording electrophysiological signals in electrogenic cells.
- The cortical neurons have been transduced with the new constructs, hSyn_ArcLight and hSyn_Butterfly by recombinant adeno-associated viral vectors.
- These novel constructs, specifically expressed in the neuronal cells, have been evaluated by electrophysiological experiments with electrical stimulations recorded optically.
- It has been shown that ArcLight A-242 is a valuable tool for recording and detection of single action potentials.
- Although not successful so far (due to the available equipment), Butterfly should be an even more reliable tool for the detection of even sub-threshold potential changes.

Going forward, it might be assumed that the optogenetic toolbox, enriched by those two components, is a step closer to non-invasive, optical monitoring of neural electrical activity.

6. BIBLIOGRAPHY

1. Golding, B., Evolution: when was life's first branch point? Curr Biol, 1996. **6**: p. 679-82.
2. Guyton, A.C. and J.E. Hall, Textbook of Medical Physiology. 11th ed. 2006: Elsevier Saunders.
3. Byrne, J., An electronic textbook for the neurosciences. 2013: The University of Texas Medical School at Houston.
4. Jarosz, Q., Neuron. 2009: http://en.wikipedia.org.
5. Alberts, B., Johnson, A. and J. Lewis, Molecular Biology of the Cell. Vol. 5th edition. 2007, New York: Garland Science.
6. Nagel, S.M. and G.L. K., Introductory Biological Psychology Tutorials. 2008: Saginaw Valley State University, Athabasca University.
7. Christie, W.W. An Introduction to Sphingolipids and Membrane Rafts. 2013; Available from: http://lipidlibrary.aocs.org/Lipids/introsph/index.htm.
8. Hursh, J.B., Conduction Velocity and Diameter of Nerve Fibers. Vol. 127. 1939. 131-139.
9. Byrne, J.H. and J.L. Roberts, From Molecules to Network - An Introduction to Cellular and Molecular Neuroscience. Vol. 2nd Edition. 2009, London, UK: Elsevier Inc. .
10. Blaustein, M.P., J.P.Y. Kao, and D.R. Matteson, Cellular Physiology and Neurophysiology. Vol. 2nd Edition. 2012, Philadelphia: Elsevier, Mosby
11. Squire, L., Berg, D., Bloom, F., du Lac, S., Ghosh, A. and N. Spitzer, Fundamental Neuroscience. Vol. 3rd Edition. 2008: Academic Press.
12. Images, L.C., Types of Neurons Illustration showing three types of neurons. 1989-2001, Lippincott Williams & Wilkins: Baltimore, MD.
13. Smith, C.U.M., Elements of Molecular Neurobiology. Vol. 3rd Edition. 2002, Department of Vision Sciences, Aston University, Birmingham, UK: John Willey & Sons, LTD.
14. Singer, S.J. and G.L. Nicolson, The fluid mosaic model of the structure of cell membranes. Science, 1972. 175: p. 720-31.
15. Edidin, M., Membrane cholesterol, protein phosphorylation, and lipid rafts. Sci STKE, 2001: p. pe1.
16. Wisniewska, A., J. Draus, and W.K. Subczynski, Is a fluid-mosaic model of biological membranes fully relevant? Studies on lipid organization in model and biological membranes. Cell Mol Biol Lett, 2003. 8: p. 147-59.
17. Sonnino, S. and A. Prinetti, Membrane domains and the "lipid raft" concept. Curr Med Chem, 2013. 20: p. 4-21.
18. Nelson, D.L., A.L. Lehninger, and M.M. Cox, Lehninger principles of biochemistry. 2008, New York: W.H. Freeman.
19. Burn, P., Amphitropic proteins: a new class of membrane proteins. Trends Biochem Sci, 1988. 13: p. 79-83.
20. Ruiz, M., A detailed diagram of the cell membrane. 2007: http://en.wikipedia.org.
21. Cohen, J. and F. Khalili-Araghi, Case Study: Structure of Ion Channels. 2012, NIH Center for Macromolecular Modeling & Bioinformatics: Universitiy of Illinois at Urbana-Champaign.
22. Lai, H.C. and L.Y. Jan, The distribution and targeting of neuronal voltage-gated ion channels. Nat Rev Neurosci, 2006. 7: p. 548-62.
23. Lodish, H., et al., Molecular Cel Biology. Vol. 5th Edition. 2004, New York: WHFreeman.
24. Sigg, D.C., et al., Basic Cardiac Electrophysiology: Excitable Membranes, in Cardiac Electrophysiology Methods and Models. 2010, Springer.
25. Boron, F.B. and E.L. Boulpaep, Electrical Model of a Cell Membrane, in Medical Physiology. 2008, Elsevier Health Sciences.

26. Bedard, C. and A. Destexhe, Generalized cable theory for neurons in complex and heterogeneous media. Phys Rev E Stat Nonlin Soft Matter Phys, 2013. 88: p. 022709.
27. Jaeger, D., Realistic Single Cell Modeling – from Experiment to Simulation. Brains, Minds and Media, 2005.
28. Boron, W.F., Boulpaep, E. L., Signal Conduction in Dendrites, in Medical Physiology. 2008, Elsevier Health Sciences.
29. Beals, M., Gross, L., Harrell, S. Synapse transmission. 1999.
30. Horn, R., How ion channels sense membrane potential. Proc Natl Acad Sci U S A, 2005. 102: p. 4929-30.
31. Tiriveedhi, V., Miller, M., Butko, P. and M. Li, Autonomous transmembrane segment S4 of the voltage sensor domain partitions into the lipid membrane. Biochim Biophys Acta, 2012. 1818: p. 1698-705.
32. Li, Q., Wanderling, S., Paduch, M., Medovoy, D., Singharoy, A., McGreevy, R., Villaba'Galea, C., E Hulse, R., Roux, B., Schulten, K., Kossiakoff, A. and E. Perozzo, Structural mechanism of voltage-dependent gating in an isolated voltage-sensing domain. Nat Struct Mol Biol, 2014. 21: p. 244-52.
33. Bezanilla, F., The action potential: from voltage-gated conductances to molecular structures. Biol Res, 2006. 39: p. 425-35.
34. Barnett, M.W. and P.M. Larkman, The action potential. Practical neurology, 2007. **7**(3): p. 192-7.
35. Hodgkin, A.L. and A.F. Huxley, Resting and action potentials in single nerve fibres. J Physiol, 1945. 104: p. 176-95.
36. Mantegazza, M. and W.A. Catterall, Voltage-Gated Na+ Channels: Structure, Function, and Pathophysiology, in Jasper's Basic Mechanisms of the Epilepsies, J.L. Noebels, et al., Editors. 2012: Bethesda (MD).
37. Bullock, T.H., R. Orkand, and A. Grinnell, Introduction to Nervous System. 1977, San Francisco: W. H. Freeman & Co. .
38. Bean, B.P., The action potential in mammalian central neurons. Nat Rev Neurosci, 2007. 8: p. 451-65.
39. Schematic of an action potential. 2007, http://en.wikipedia.org.
40. Saltatory conduction. http://bio1152.nicerweb.com/Locked/media/ch48/myelin.html.
41. Propagation of action potential. http://www.rci.rutgers.edu/~uzwiak/AnatPhys/APFallLect18.html.
42. Akemann, W., Mutoh, H., Perron, A., Park, Y., Iwamoto, Y. and T. Knöpfel., Imaging neural circuit dynamics with a voltage-sensitive fluorescent protein. J Neurophysiol, 2012. 108: p. 2323-37.
43. Babiloni, C., Pizzella, V., del Gratta, C., Ferretti, A. and G. Romani, Fundamentals of electroencefalography, magnetoencefalography, and functional magnetic resonance imaging. Int Rev Neurobiol, 2009. 86: p. 67-80.
44. Wintermark, M., Sesay, M., Barbier, E., Borbely, K., Dillon, J., Glenn, T., Grandin, C., Soustiel, J., Nariai, T., Zaharchuk, G., Caille, J., Dousset, V. and H. Yonas, Comparative overview of brain perfusion imaging techniques. Stroke, 2005. 36: p. e83-99.
45. Perron, A., Mutoh, H. and T. Knöpfel, Second and third generation voltage-sensitive fluorescent proteins for monitoring membrane potential. Front Mol Neurosci, 2009. 2: p. 5.
46. Canepari, M. and D. Zecevic, Design and Use of Organic Voltage Sensitive Dyes, in Membrane Potential Imaging in the Nervous System. 2011. p. 13-23.
47. Murata, Y., Iwasaki, H., Sasaki, M., Inaba, K. and Y. Okamura, Phosphoinositide phosphatase activity coupled to an intrinsic voltage sensor. Nature, 2005. 435: p. 1239-43.
48. Kohout, S.C., Bell, S., Liu, L., Xu, Q., Minor, D. and E. Isacoff, Electrochemical coupling in the voltage-dependent phosphatase Ci-VSP. Nat Chem Biol, 2010. 6: p. 369-75.

49. Okamura, Y., Lipids: PI couples voltage to catalysis. Nat Chem Biol, 2010. 6: p. 315-6.
50. Jin, L., et al., Single action potentials and subthreshold electrical events imaged in neurons with a fluorescent protein voltage probe. Neuron, 2012. 75: p. 779-85.
51. Ahern, C.A., The secret lives of voltage sensors. J Physiol, 2007. 583: p. 813-4.
52. Cao, G., et al., Genetically Targeted Optical Electrophysiology in Intact Neural Circuits. Cell, 2013. 154: p. 904-913.
53. Villalba-Galea, C.A., et al., Charge movement of a voltage-sensitive fluorescent protein. Biophys J, 2009. 96: p. L19-21.
54. Piston, W.D., Claxton, N. S., Olenych, S. G., Davidson, M. W., The Fluorescent Protein Color Palette. Olympus corporation.
55. McNamara, G., Multi-Probe Microscopy. 2011: The University of Texas MD Anderson Cancer Center.
56. Han, Z., Jin, L., Chen, F., Loturco, J., Cohen, L., Bondar, A., Lazar, J. and V. Pieribone, Mechanistic Studies of the Genetically Encoded Fluorescent Protein Voltage Probe ArcLight. PLoS One, 2014. 9: p. e113873.
57. Han, Z., Jin, L., Platisa, J., Cohen, L., Baker, B. and V. Pieribone, Fluorescent protein voltage probes derived from ArcLight that respond to membrane voltage changes with fast kinetics. PLoS One, 2013. 8: p. e81295.
58. Akemann, W., Sasaki, M., Mutoh, H., Imamura, T., Honkura, N. and T. Knöpfel, Two-photon voltage imaging using a genetically encoded voltage indicator. Sci Rep, 2013. 3: p. 2231.
59. Shcherbo, D., Merzlyak, E., Chepurnykh, T., Fradkov, A., Ermakova, G., Solovieva, E., Lukyanov, K., Bogdanova, E., Zaraisky, A., Lukyanov, S. and D. Chudakov, Bright far-red fluorescent protein for whole-body imaging. Nat Methods, 2007. 4: p. 741-6.
60. Vasileva, A. and R. Jessberger, Precise hit: adeno-associated virus in gene targeting. Nat Rev Microbiol, 2005. 3: p. 837-47.
61. Aschauer, D.F., S. Kreuz, and S. Rumpel, Analysis of transduction efficiency, tropism and axonal transport of AAV serotypes 1, 2, 5, 6, 8 and 9 in the mouse brain. PLoS One, 2013. 8: p. e76310.
62. Cearley, C.N. and J.H. Wolfe, Transduction characteristics of adeno-associated virus vectors expressing cap serotypes 7, 8, 9, and Rh10 in the mouse brain. Mol Ther, 2006. 13: p. 528-37.
63. Goncalves, M.A., Adeno-associated virus: from defective virus to effective vector. Virol J, 2005. 2: p. 43.
64. Bleijs, D.A. Adeno-Associated Viral Vectors. 2013.
65. Zincarelli, C., Soltys, S., Rengo, G. and J. Rabinowitz, Analysis of AAV serotypes 1-9 mediated gene expression and tropism in mice after systemic injection. Mol Ther, 2008. 16: p. 1073-80.
66. Dreyfuss, J.L., Regatieri, C., Jarrouge, T., Cavalheiro, R. Sampaio, L. and H. Nader, Heparan sulfate proteoglycans: structure, protein interactions and cell signaling. An Acad Bras Cienc, 2009. 81: p. 409-29.
67. Kotin, R.M., Siniscalo, M., Smulski, R., Zhu, X.D., Hunter, L., Laughlin, C.A., McLaughlin, S., Muzyczka, N., Rocchi, M. and K.I. Berns, Site-specific integration by adeno-associated virus. Proc Natl Acad Sci U S A, 1990. 87: p. 2211-5.
68. Daya, S. and K.I. Berns, Gene therapy using adeno-associated virus vectors. Clin Microbiol Rev, 2008. 21: p. 583-93.
69. de Backer, M.W., Garner, K.M., Luijedijk, M.C. and R.A. Adan, Recombinant adeno-associated viral vectors. Methods Mol Biol, 2011. 789: p. 357-76.
70. Ferrari, F.K., Samulski, T., Shenk, T. and R.J. Samulski, Second-strand synthesis is a rate-limiting step for efficient transduction by recombinant adeno-associated virus vectors. J Virol, 1996. 70: p. 3227-34.

71. Grieger, J.C., V.W. Choi, and R.J. Samulski, Production and characterization of adeno-associated viral vectors. Nat Protoc, 2006. 1: p. 1412-28.
72. Elektronik, H., Manual 2.4; EPC10 / EPC10 USB, in Patch Clamp Amplifier. 2014, HEKA Elektronik Dr. Schulze GmbH.
73. Lange, W., Transduktion von primären corticalen Neuronen aus der Ratte. 2011, Institute of Bioelectronics: Forschungszentrum Juelich.
74. Addison, C.L., Hitt, M., Kunsken, D. and F.L. Graham, Comparison of human versus murine cytomegalovirus immediate early gene promoters for transgene expression by adenoviral vectors. J Gen Virol, 1997. 78: p. 1653-61.
75. Hong, S., Hwang, D.Y., Yoon, S., Isacson, O., Ramezani, A., Hawley, R.G. and K.S. Kim, Functional analysis of various promoters in lentiviral vectors at different stages of in vitro differentiation of mouse embryonic stem cells. Mol Ther, 2007. 15: p. 1630-9.
76. Bernardi, G. and S.C. Makrides, Gene transfer and expression in mammalian cells. Vol. 38. 2003, the Netherlands: New comprehensive biochemistry, Elsevier.
77. Gold, C., Henze, D.A., Koch, C. and G. Buzsaki, On the origin of the extracellular action potential waveform: a modeling study. J Neurophysiol. 2006. 95: p. 3113-28.
78. Bootman, M.D., Collins, T.J., Peppiatt C.M., Prothero, L., MacKenzie, L. and P. De Smet, Calcium signaling - an overview. Cell & Developmental Biology, 2001. 12: p. 3-10.

7. APPENDIX

7.1. List of Tables

7.2. List of Figures

7.3. Protocols

7.3.1. Standard V-C protocol

A standard V-C protocol starts with the resting membrane potential that is set in TIDA after forming a high resistance in the membrane, a gigaseal. Then, the membrane potential is stepped from resting to holding potential with incensement of 10 mV and then stepped back to resting potential. The written stimulation code for TIDA is saved as .stm file and as such, attached here. It is indicated that there are 26 loops.

```
rem Aufsteigende (-50 bis +50 mV) VC-Pulsserie zur Zellanregung
rem Dateiname: VC-check.stm
rem Beschreibung: - Generierung einer Serie von 20 200 ms Pulsen: -50mV, ... ,
+50mV
rem     - Pause vor den Pulsen jeweils 50 ms
rem     - Pause zwischen den Pulsen jeweils 50 ms
rem     - Anzeige des Stromkanals Channel 2 und Spannungskanals Channel 1
rem     - Über Kanal 5 wird paralell eine die externe Spannung rem aufgezeichnet
rem       (FET Input)
rem     - Die Stimulation erfolgt um den Faktor 10 überhöht da der EPC 9 rem ein
rem       Signalteilverhältnis von 1:10 aufweist.
rem     - Achtung: Spannung ist abhängig vom Haltepotential und wird damit
rem       verrechnet(hier -50 mV)

rem Initialisierung
 channels 3 3 4 5
 pps 25000
 da 1 0
 da 2 0
 da 3 0
 da 4 0

rem Umschalten in Overwrite Mode zur überlagerten Darstellung der Kurven
 owr

rem Beginn der Wiederholungsschleife zur 11-fachen Wiederholung
 for 26
 acq
rem Pulsformung: 50 ms Pause vor Puls

  da 2 0
  wait 50
  da 2 -.50 *
  wait 200
  da 2 0
  wait 50

rem Ende der Wiederholungsschleife mit Erhöhung der Pulsspannung um je 10 mV
 sacq
 next 0.1

end
```

7.3.2. Stimulation V-C protocol

The stimulation protocol, written and adjusted according to the stimulation preferences in the fluorescent cortical neurons, is attached here. There are two active channels here, #2 (voltage) and #3 (current). It is indicated that the trigger gives a signal to start the iteration of 26 loops. The program is adjusted to the exposure time of 100 ms; hereby the duration time of every step is multiplied 6-10x regarding the standard V-C check protocol.

```
rem Aufsteigende (-50 bis +50 mV) VC-Pulsserie zur Zellanregung
rem Dateiname: VC_onetimetrigger_ex100ms_Zeljka.stm
rem Beschreibung: - Generierung einer Serie von 20 200 ms Pulsen: -50mV, ... ,
+50mV
rem     - Pause vor den Pulsen jeweils 50 ms
rem     - Pause zwischen den Pulsen jeweils 50 ms
rem     - Anzeige des Stromkanals Channel 2 und Spannungskanals Channel 1
rem     - Über Kanal 5 wird paralell eine die externe Spannung aufgezeichnet (FET
rem        Input)
rem     - Die Stimulation erfolgt um den Faktor 10 überhöht da der EPC 9 ein
rem       Signalteilverhältnis von 1:10 aufweist.
rem     - Achtung: Spannung ist abhängig vom Haltepotential und wird damit
rem        verrechnet(hier -50 mV)

rem Initialisierung
 channels 2 2 3
 pps 25000
 da 1 0
 da 2 0
 da 3 0
 da 4 0

rem Umschalten in Overwrite Mode zur überlagerten Darstellung der Kurven
 owr

Trigger X

rem Beginn der Wiederholungsschleife zur 11-fachen Wiederholung
 for 26
 acq
rem Pulsformung: 50 ms Pause vor Puls

  da 2 0
  wait 1000
  da 2 -.50 *
  wait 600
  da 2 0
  wait 1000

rem Ende der Wiederholungsschleife mit Erhöhung der Pulsspannung um je 10 mV
 sacq
 next 0.1

end
```

8. ACKNOWLEDGEMENTS

I would like to express my greatest appreciation to Prof. Offenhäusser, the head of the Institute of Bioelectronics, ICS-8, for the given opportunity to become a part of the research team. With his professional support and inspiration, I was able to conduct my very first interdisciplinary research project as a Master thesis. My deep gratitude goes to Dr. Vanessa Maybeck, my research supervisor, for the patient guidance through the project with the constant constructive discussions, suggestions and critics. Besides, for the professional and psychological encouragement while struggling with difficulties in research as well as in private. Hereby, I would like to extend my special thanks to Dr. Wienke Lange, who has supervised me from the early beginnings in the lab, yet as a summer student and motivated me for pursuing the Master thesis here. Just as much I want to thank Prof. Ivančić – Baće for being my on-distance supervisor at the home Faculty of Science, University of Zagreb.

The cell – culture experiments would be impossible without the lab technicians Bettina Breuer and Rita Fricke, who did the neuronal cell preparation every week. Additionally, I would like to thank Prof. Baumann from the Institute of Cellular Biophysics, ICS-4, for the advice in molecular cloning and for finding alternative solutions for many obstacles on the molecular level that have interfered with our work. Also, my grateful thanks belong to Anne Günther and Nadine Gruteser for the virus preparation and the help with the plasmid design.

As one of the two main subjects of this work, plasmid CAG_Butterfly, was originally designed at the Knöpfel Lab. The basic idea of its modification and potential usage has arisen after it was given to ICS-4, as a present. Hence, thank you!

I wish to acknowledge the men's support and every day's life discussions provided by my irreplaceable office mates: Lars, Bernd and Duy. A great appreciation to Wenfang, who has always been here as an older and more experienced student willing to help. To all other members of the IBN-2/PGI-8/ICS-4, thanks for providing a pleasurable working atmosphere (and cakes), where one can find a lot of motivation even during the most difficult days. It was a pleasure to work with you!

For giving me the very first lab experiences and introducing me with the science abroad already during the bachelor study, I am thankful to Sandra Vidak. Conducting this thesis abroad, from the

administrative point of view, would be much more difficult without the immense help of Student office workers, Vlatka Marjan and Sanjica Mihaljević.

As an external support, first I would like to thank my closest family; mom, dad and sis for all the sacrifices they made on my behalf, encouraging my education and understandings they had while raising me as a grown-up, independent and tolerable citizen of the world. I am thankful to all other family members who were also a tail wind, both emotionally and financially. I consider a huge luck to have so many good friends who, although far away, were always achievable as an emotional support. Therefore, Antonela, Barbara, Iva, Ivana, Lara, Marta, Nataša, Petre, Stela, Tihana, hvala! To my molecool friends, nowadays scattered around Europe, a great thank for feeling so close to you, no matter where. Adrijana, Marija, Vesna, Alen, Frane, Goran, Kruno, hvala! Finally, for limitless encouragement, motivation, joyful moments and journeys on our way, as well as for scientific help, heartfelt thanks to Alexey.

9. CURRICULUM VITAE

Zeljka Trepotec

Dubovecki breg 24; 48000 Koprivnica, Croatia +49(0)16092238751; +385(0)99797243 *zeljka.trepotec@gmail.com*

Personal information

Date of birth 01/10/1990
Nationality Croatian

Education

09/2012 – 02/2015 **M.Sc. in Molecular Biology**
University of Zagreb, Faculty of Science, Department of Biology
Master thesis: "*Optogenetic monitoring of neuronal electrical activity using fluorescent protein-based voltage sensors*" conducted at Research Center Jülich at the Institute of Complex Systems/Bioelectronics supervised by Prof. Dr. Andreas Offenhäusser
GPA: 4.5/5.0

09/2009 – 09/2012 **B.Sc. in Molecular Biology**
University of Zagreb, Faculty of Science, Department of Biology
Bachelor thesis: "*Genetic instability in cancer and Telomeres*" supervised by Dr. Inga Marijanovic

Research and work experience

03/2014 – 02/2015 **Institute for Complex Systems/Bioelectronics (ICS-8), Research Center Jülich; Germany**
Master student

- Thesis project "*Optogenetic monitoring of neuronal electrical activity using fluorescent protein-based voltage sensors*"
- Description: novel voltage sensor fluorescent proteins (ArcLight A-242 and Butterfly 1.2) were introduced as a non-invasive method for action potential recordings in cortical neurons
- Experience: voltage-clamp fluorometry, adeno-associated viral (AAV) transduction, molecular cloning and neuronal cell-culture

07/2013 – 10/2013 Research internship

- Worked on the research project "*Genetically targeted optogenetic transduction*"
- Description: achieved temporal and spatial control of neuronal activity of cells expressing light-activated ion channel (Channelrhodopsin-2)
- Experience: patch-clamp and multielectrode array measurements, immunofluorescence staining, fluorescence microscopy, molecular cloning, AAV transduction and neuronal cell-culture

07/2012 – 08/2012 **Max F. Perutz Laboratories, Vienna Biocenter; Austria**
Summer internship

- Participated in the project "*The role of Nucleoplasmic Lamin A/C-Lap2α-pRb Complexes in Hutchinson-Gilford Progeria Syndrome*"

- Description: investigation of potential deregulation of the signalling pathway (of the pRb protein) in the development of cellular progeria phenotypes upon progerin expression
- Experience: cell-culture of human fibroblasts and HeLa cells, PCR, Western blotting and molecular cloning

09/2010 – 02/2011 **University of Zagreb, Faculty of Science, Department of Biology; Croatia**

Student teaching assistant of the Cell Biology course

- Guided students through the practical part and assisted in explaining theory

Scholarships

03/2014 – 02/2015	Erasmus Student mobility Practicum (SMP) and Erasmus+ SMP grant EU Erasmus Program
07/2013 – 10/2013	"IHRS BioSoft Guest Student Programme" Internship Program Scholarship International Helmholtz Research School of Biophysics and Soft Matter
09/2009 – 02/2015	Student scholarship City of Koprivnica

Professional skills

- Knowledge and experience with laboratory animals in biological research
- HPLC course conducted at Ruder Boskovic Institute (Zagreb, Croatia)
- Bioinformatics course (University of Zagreb)

Additional skills

Languages	• English – fluent • German, Italian – basic • Croatian – mother tongue
Computing	• Microsoft Office™ tools (Word™, Excel™ and PowerPoint™) • Molecular Biology software (SerialCloner, GENtle and SnapGene) • Programs for statistical and data analysis (R and Origin, ImageJ)
Management	• Project liaison for the popular scientific manifestation *Biology night* (2009–12) • Leader of Odonatology section of Biology student association BIUS (2 years) • Fieldwork on island Hvar (2011 for 10 days) and island Cres (2013 for 10 days) - inventarisation of dragonflies • Part-time promoter of the food products for Podravka Inc. (a food processing and pharmaceutical company), Koprivnica, Croatia
Licenses	• Driving license (Category B) • Diving license CMAS1*/Open Water Diver PADI

Attendances

9-10/2014	12th Greta Pifat Mrzljak International School of Biophysics (Primosten, Croatia)
10/2014	16th EMBL PhD Symposium (Heidelberg, Germany)
11/2013	10th Forensic Science Symposium (Ankara, Turkey)
06/2013	8th ISABS Conference on Forensic and Anthropologic Genetics and Mayo Clinic Lectures in Individualised Medicine (Split, Croatia)